Master Thesis

Mechanical Engineering
Biomechanical Design Track

Collecting Relevant Environmental Parameters for Surgical Lighting Control

Eda Emirdag

Supervisor Ir. A. J. Knulst
Professor Prof. Dr. J. Dankelman

Delft, 29 August 2011

TU Delft
Faculty of Mechanical, Maritime and Materials Engineering

Abstract

Surgical lighting is an important element in the operation room. When adequate lighting is not provided, the performance of the surgical team can be negatively affected. A major aspects of the proper lighting is the position and orientation of the light beam, which need to be often adapted during the surgery. In current commercial systems, the necessary adaptations are done manually by pushing or pulling the lighting fixture with a sterile handle. However, the manual adaptation may causes loss of concentration, loss of time and increased risk of infections. To improve this, a semi-automated lighting system commanded by the surgeon has been suggested. This system would use a 6DOF infrared tracking system to collect the necessary parameters from the surgical environment.

The purpose of this study was to develop a method to collect the relevant parameters and to evaluate this method using a low-cost tracking system consisting of Nintendo Wii Remotes. First, the parameters related to the surgical lighting were investigated and the relevant parameters were defined. These parameters can be listed as: Wound position, indicated lighting direction, working depth and the wound dimensions and shape. Given that, the data collection method was designed. This design consisted of a pointer device with three active markers and could be used by the surgeon to indicate the required properties. Moreover, a tracking system with four Wii Remotes was developed. The precision and accuracy of the tracking system was evaluated using static markers, dynamic markers and the developed device. Moreover, the wound reconstruction was investigated.

The results showed that the tracking system was sufficiently precise and repeatable. The geometric accuracy was satisfactory $E_{dist_{rms}} = 3.41mm$) and comparable to similar systems. On the other hand, the position accuracy was lower than expectations, especially with the pointer device ($E_{3d_{rms}} = 6.46mm$ for static markers, $T_{3d_{rms}} = 26.75mm$ for pointer tip position). Moreover, it was shown that the use four Wii-remotes, in other words six camera pairs, was useful in eliminating wrong estimations and reducing tracking failures. The data collection with the pointer was successful, also in the wound reconstruction. With a proper mapping of the system coordinates to the real world coordinates, the data collection method with the pointer and low-cost tracking system can be used for surgical lighting control.

Preface

This thesis is submitted to the Faculty of Mechanical, Maritime and Materials Engineering of Delft University of Technology at Delft, the Netherlands in partial fulfillment of the requirements for the degree of Master of Science in the Department Mechanical Engineering with Biomechanical Design Track. The work presented here was conducted within the *Minimally Invasive Surgery & Interventional Techniques (MISIT) Group* and was a part *LIFE-OR* project, which aimed at improving lighting and instrumentation in operating rooms to obtain a flexible and ergonomic working environment for surgical staff.

This document consist of two main parts: A scientific paper and a detailed project report. The scientific paper focuses on the development of a low-cost tracking system to be implemented for surgical lighting control. The project report provides background information and details to the topics mentioned in the scientific paper, including the development of the surgeon-lighting unit interaction and further details on the evaluation of the developed interaction method.

Hereby I would also like to show my gratitude to the people who supported me through my long road. It was a great pleasure to work with Prof. Jenny Dankelman and Arjan Knulst, who provided me invaluable guidance and inspiration.

I would like to thank Arjan van Dijke for using his skills on the electronic equipment; obviously there would be nothing but a bunch of burned-out parts without his help. Many thanks to John van den Dobbelsteen for providing me a precious space in the MISIT Lab. Furthermore, thanks to the employees of "3mE Inloopwerkplaats" for dealing with my machining attempts. Dear Oytun Akman and Gorkem Saygili, thanks for your small but very valuable contribution which helped me just the exact moment when I lost my hope.

During this journey I was lucky to have people around who made my life in Delft enjoyable. My friends from *Board of European Students of Technology*, especially the first ever co-boardies, *Babylon Theater Group* and my dear housemates Erdem Demir, Daniel Swakman and Bastiaan van de Weerd, thank you for all the laughs, games, plays and wines. A very special person for me is dear Esin Isik, who was always there when I needed, of course with a warm pot of tea.

Special thanks go to my family for their continuous support. The last but not least, Panagiotis Afratis, *σε ευχαριστώ για την κατανόηση και την αγάπη σου.*

Contents

Chapter 1

Paper: A low-cost tracking system for surgical lighting control using Nintendo Wii Remotes

A low-cost tracking system for surgical lighting control using Nintendo Wii Remotes

Eda Emirdag · Arjan J. Knulst · Jenny Dankelman

08.08.2011

Abstract Improper surgical lighting may have a negative effect on the performance of the surgical team. During the surgery, the lighting unit often needs to be manually adapted, which can cause loss of concentration, loss of time and increased risk of infections. To improve the adaptation, a semi-automated lighting system commanded by the surgeon via a pointer device is suggested. The pointer device can be tracked in space with an infrared 6DOF real-time tracking system. The purpose of this study is to investigate the precision and accuracy of a low-cost infrared tracking system based on Nintendo Wii-remotes for this application. Four Wiimotes were used in pairs to perform the tracking with stereo vision. The precision and accuracy of the tracking system were investigated using static markers, dynamic markers and the pointer device. Moreover, the wound reconstruction was evaluated. The results showed that the tracking system is sufficiently precise and repeatable. The geometric accuracy was satisfactory as well ($E_{dist_{rms}} = 3.41mm$), where position accuracy was lower than expectations, especially with the pointer device ($E_{3d_{rms}} = 6.46mm$ for static markers, $T_{3d_{rms}} = 26.75mm$ for pointer tip position). Moreover, it was shown that the use four Wii-remotes, in other words six camera pairs, is useful in eliminating wrong estimations and to reduce tracking failures. The low-cost Nintendo Wii-remote tracking system would be promising for the surgical lighting control application with a proper mapping of the system coordinates to the real world coordinates.

Delft University of Technology
Faculty of Mechanical, Maritime and Materials Engineering
Dept. of BioMechanical Engineering
Delft, The Netherlands

Keywords stereo vision · infrared · tracking · surgical lighting

1 Introduction

Surgery is a delicate task requiring precision and caution. During surgery, the vision of the surgeon and other surgical staff members can easily be affected by inadequate and improper lighting [1]. This will highly increase the risk of errors especially while detecting the details and the tissue color, which is an important diagnostic tool[1]. Moreover, the risk of infections may be increased and the comfort of the staff may be reduced due to eye fatigue, additional heat and disturbed airflow caused by the lighting unit [2,3]. To ensure proper lighting during the surgery, the light beam properties such as intensity, the focal length and size, position and orientation of the light beam can be adapted according to needs of the surgeon. In the current systems, the positioning and orientation is done manually by pulling or pushing the lighting fixture with a sterile handle and the adaptations on the light beam properties are done by additional buttons or knobs. A prior research have shown that the type of the adaptation that is required most often is on the position and orientation of the light beam with an average of one adaptation per 7.5 minutes [4]. However, the state of art commercial systems and available literature focus mostly on the improvements of the adaptation of the light beam properties and do not provide any other solution except the manual positioning and orientation. On the other hand, this manual manipulation may cause loss of concentration, loss of time and increased risk of infections. In addition to that, the pendant system requires high forces in certain cases and can even cause the complete immo-

bility of the lighting unit [4]. This difficulty in the use of the surgical lighting system is perceived as source of potential hazards and requires improvements [5].

A semiautomated lighting system is suggested, as a solution to these problems. This system includes a tracking system to gather data from the surgical environment to control the actuators for adapting the position, orientation and other properties of the light beam. The necessary data is provided by the surgeon via a hand-held pointer device which is tracked in real-time with six degrees-of-freedom (DOF) tracking system. The surgeon can use the device to point out the working location and the desired lighting direction so that the light beam is directed on the correct location. Moreover, the device can be used to indicate the wound edges and the wound depth, so that the size, shape and the direction of the wound can be recorded to adapt the light beam properties for optimal illumination. The parameters to be collected by this system are given in Table 1.

Table 1 Environment parameters to be collected by the tracking system

Parameter	Description
Wound location	Position in space (x-y-z coordinates in mm)
Indicated lighting direction	Direction in space (angles in degrees)
Wound size	Wound length and width (in mm)
Wound shape	Closed curve (coefficients of equation)
Working depth	Depth (in mm)

First, available tracking systems in the lighting, surgery and other fields such as virtual reality, entertainment, computer assisted surgery, surveillance et cetera were investigated to select of a suitable tracking system. It was concluded that optical and infrared tracking systems are the most suitable options for working in the operation room during the entire surgery considering the interferences with other surgical equipment. On the other hand, commercially available optical and infrared systems have high costs and provide either high accuracy in a small volume or low accuracy in a very high volume prone to occlusions (Example systems can be found in [6] or [7]). Thus, a low-cost system with ease of adaption and implementation was required. This requirement was satisfied by constructing an infrared(IR) tracking system with Nintendo Wii-Remotes (also known as *Wiimote*) [8].

This paper focuses on the construction and evaluation of the low-cost IR tracking system with four Nintendo Wii-remotes and a pointer device for the purpose of the surgical lighting control. First, the accuracy and precision of the constructed tracking system were evaluated for several single markers placed in the working space. Second, the accuracy and precision performance of the pointer device was explored. Finally, reconstruction of wound properties was performed with the pointer.

2 Methods

2.1 Tracking System Design

2.1.1 Hardware

Nintendo Wiimotes In this work, Wiimotes were used as cameras. To avoid battery life related fluctuations, they were connected to the mains. Although two cameras are sufficient to perform triangulation (see Appendix), four cameras were used in pairs to compensate the occlusions and blockages of the camera view which might occur often in a crowded working environment such as the operation room. The cameras were placed with a cross-shaped configuration with a distance of $0.35m$ to the center and a mounting angle of 50^o. This configuration provided a working volume starting from $0.7m$ away from the camera fixture, covering a conical volume and ending at $1.80m$ distance, which corresponds to the focal properties of common surgical lighting systems [9]. The cross-shaped structure was mounted on the carrier built from aluminum profiles with the cameras facing downwards (Fig. 1). A horizontal support with adjustable height mounted on the aluminum structure provided an experimental platform (see Section 2.2).

The Wiimote contains a CCD camera with an infrared filter and acceleration sensors [10]. The camera has a view angle of 40^o and works the in near-infrared band with a sampling frequency of 100Hz [11]. The native resolution of the integrated camera is 128 x 96 pixels and is interpolated via internally built processor into 8x-subpixel precision [11,12]. The Wiimote returns information about four bright infrared points as interpolated pixel coordinates with a resolution of 1024x768 and size between 0 and 15 [12]. The connection between the host computer and the Wiimote can be established via Bluetooth.

Markers Active markers were preferred for this application since they have a larger working range with a smaller marker size. As active markers, 940nm high

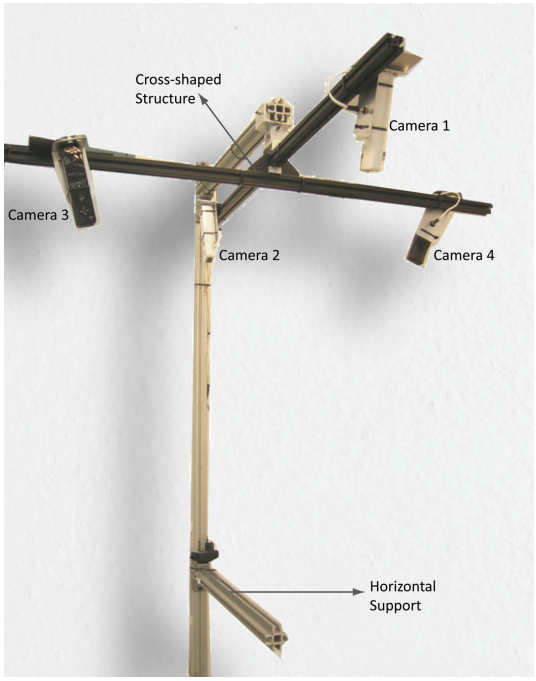

Fig. 1 The experiment setup constructed with aluminium profiles and four Nintendo Wii Remotes

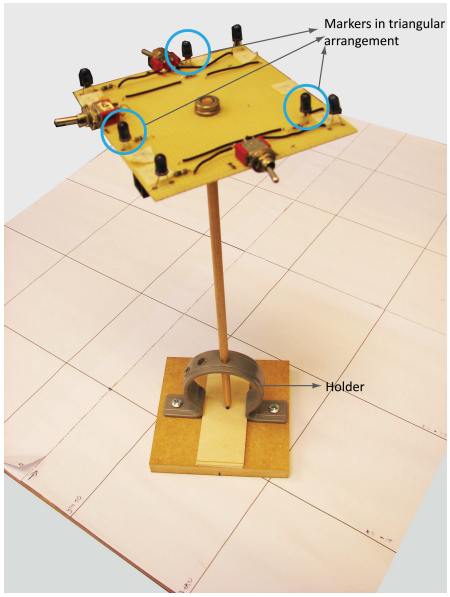

Fig. 2 The model of the pointer. 3 LED's were placed on a circuit board, which was mounted on a wooden rod. In this picture, the model was placed on the holder. The extra four LED's visible on the picture can be ignored.

power infrared emitting diodes from Vishay Semiconductors (Model no: TSAL6400) [13] with a diameter of $5mm$ were used since the Wiimotes have been reported as sensitive to the wavelength of 940nm [11] and this wavelength is out of the operating spectrum of the common surgical lighting systems [14].

Pointer device A simple model of the pointer device was build by mounting a $100x100mm$ circuit board to $250mm$ long wooden rod with a diameter of $6mm$ and tapered end. On the circuit board, 3 LEDs were placed at the corners of an equilateral triangle so that the rod connection is at the center of the triangle. The minimum distance to detect two different markers was measured as $40mm$ at a distance of $1.6m$ from the cross structure. Thus, the distance between the markers was set slightly larger than the double of the minimum distance, as $86mm$. An on-off switch enabled the user to activate or deactivate the LED's. The constructed model can be seen in Fig 2. This construction enabled the calculation of the location of the tip and the orientation of the pointer device using the world coordinates of the three markers.

2.1.2 Software

Connection to the host computer The connection to the host computer was provided via a native C++ Wiiremote library *WiiYourself!* [15]. The demo program distributed with Wiiyourself! was adapted for enabling the simultaneous connection of four Wiimotes and the transfer of the pixel coordinates, point sizes and unique device identification numbers to MATLAB via a shared memory class.

Calibration In the publication from Vader et al. [16], it has been suggested to calibrate the cameras simultaneously instead of using the results of stereo calibration for each pair. Accordingly, the algorithm developed by Svoboda et al. [17] was chosen for multi-view calibration. The method from Svoboda is fully automatic and uses one single bright point to calibrate all cameras simultaneously. A MATLAB compatible code for this algorithm is available on the website of the corresponding author [18]. The first step of the algorithm makes use of a set of captured images as input to extract the point coordinates with subpixel precision. The second step carries out the calibration. On the other hand, the Wiimote does not provide image files and carries out the point extraction with a built-in processor. The output of Wiimote can be used as input of the second step, after correcting for the image origin which is set as left-down corner.

To align the tracking system coordinates with the real world coordinates, the camera coordinates (x,y and z) were entered manually. It was not possible to gather the perfect camera coordinates since there was no information available on the location of the camera sensor within Wiiremote. On the other hand, it has been re-

ported by Svoboda that "an error of a few centimeters does not affect the calibration results significantly" [17]. The origin of the world coordinate system was placed on the middle of the cross-shaped structure at an average level of the Wiiremotes so that the world origin did not change when the cross moves or rotates. This provided flexibility to the system and removed the need of the calibration before each use.

The calibration was done with a single marker traveling in the working volume. The calibration marker was sampled 2500 times while it was moved manually in the working volume and the first and last 10 percentage of samples were left out. Nine different calibration datasets were recorded, run with different configuration parameters and compared to each other to achieve the best performance. Most significant configuration parameters were the initialization and update of nonlinear camera parameters, such as view angle, principal point, radial and tangential distortion. The best calibration results were achieved by leaving out the tangential distortion parameters. This set was selected considering the number of inliers (Fig. 3), uniform distribution of inlier's in space, consistency of camera parameters and finally the system accuracy.

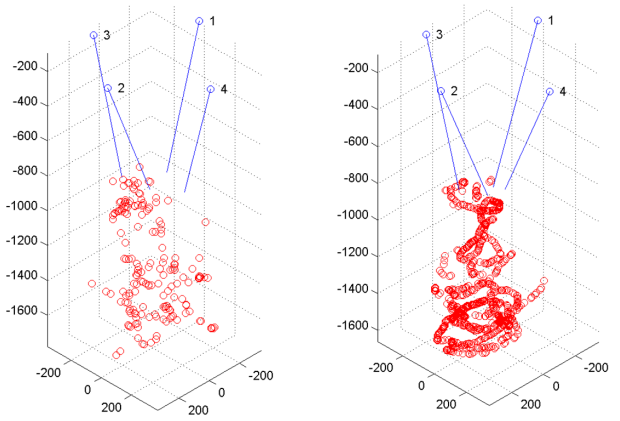

Fig. 3 On the left: A dataset with a low number of inliers with poor distribution. Such a set is discarded. On the right: A dataset with high number of inliers and good distribution. Both of the datasets are achieved with 2500 samples

Camera pair selection The camera pair selection was performed using the principles of the epipolar geometry (see Appendix). In a perfect situation, the epipolar lines constructed using the visible points in one view match with the corresponding points on the other camera view. When disturbances are present, such as time delay, erroneous pixel coordinates or shortcoming of the calibration, this matching can fail and produce poor triangulation results. To prevent this, a global optimization with a cost function was applied to match the points in two camera views. The camera pair with the lowest cost is selected as the most suitable camera pair at each frame.

Triangulation Numerous triangulation algorithms are available in the literature. Considering the performance and target application, three triangulation algorithms were implemented: Midpoint method [19], Direct Linear Transformation (DLT) method [19] and Optimal Poly-Abs method from Hartley-Sturm [20]. The DLT algorithm was selected for its higher precision and low computational cost after comparing all three methods in pilot experiments.

Correction A misalignment between the tracking system and the real world coordinates was observed during pilot experiments. Although the position estimations were precise, their accuracy was low. A linear relationship between the estimated positions and actual positions were observed. The first correction was applied to discard the cases where the epipolar matching fails. The relative distances between the marker were calculated and the cases where distance was above 1.5 times the actual distance were discarded. Two other corrections were employed to correct the alignment of the system coordinates to world coordinates. First, all x, y and z coordinates were plotted versus their expected values and fitted on a linear trend (Fig. 4. The equation of the trend line was used to construct a linear correction equation. Second, x and y coordinates were plotted versus the z-coordinate and again corrected with the help of a trend line. A last correction step was applied only for the measurements with the pointer to correct the dislocation of the origin due to modifications on the experiment setup (see Section 2.2). The first data point at the first level was used to redefine the origin and correct the triangulation results for each camera pair.

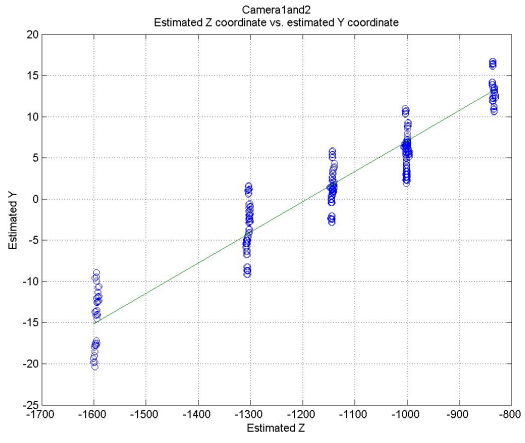

Fig. 4 An example trend line used to correct the y coordinates relative to the estimated z coordinates.

Shape reconstruction The shape reconstruction was applied to gather wound size, shape and orientation information given a set of points following the wound edges. To reconstruct the shape, the set of points were fitted into a plane and projected on this plane. An ellipse was fitted into the projected points. The location and the orientation of the plane and the ellipse equation were used to reconstruct the wound.

2.2 Experiments

Three sets of experiments (*Set A*, *Set B* and *Set C*) were conducted. Set A aimed to measure the accuracy and precision of the tracking system, Set B aimed to measure the accuracy with the pointer and Set C evaluated the wound reconstruction.

2.2.1 Setup and Procedure

Experiment Set A For *Set A.1*, two $100x100mm$ circuit boards with four markers at each corner were constructed (Fig. 5) and mounted on the horizontal bar of the tracking setup with a distance of $100mm$ in between on the horizontal support. 3 times 300 samples were taken at 5 different distance levels of the horizontal support to the cameras (840, 1000, 1140, 1300, 1600mm), covering working volume similar of the common lighting units. For *Set A.2*, one board with only two activated markers at $98mm$ distance was moved with free hand in the working space to collect 1300 samples with dynamic movement.

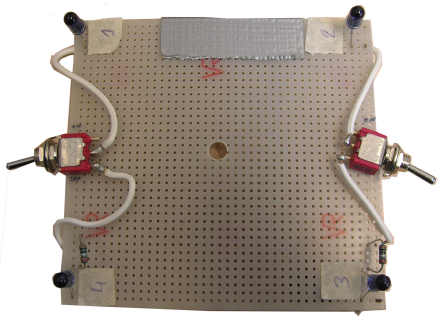

Fig. 5 Circuit board with four active markers

Experiment Set B In this set, the performance of the pointer was evaluated statically. The pointer device was placed on a holder (Fig. 2) and the holder was placed at different locations on a $500x600mm$ horizontal platform with adjustable height. The platform was gridded into $100x100mm$. *Set B.1* was conducted to see the effect of the rotation of the markers around a vertical axis on the calculation of the pointer tip location. The model was placed on a holder vertically and close to the origin ($x = -15, y = 0$) at a fixed level so that the circuit board was approximately 820mm away from the origin vertically (*Level 1*). Three different rotations (0, 90 and 180 degrees) of the board around the vertical axis were executed and sampled 3 x 300 times. *Set B.2* was conducted to determine the tip accuracy and precision at different positions in 3D space. The holder was placed at 16 different locations at four different levels corresponding to the Set A (Fig. 6). The last level (1600mm) was left out due to space limitations. 3 x 300 samples were taken at each location. *Set B.3* was conducted to see the effect of pointer orientation. The pointer was placed at two different angles (16^o and 33^o with vertical) on the holder. The holder was placed in two different orientations (along x and y axes) on different wound locations at Level 1 and 3 x 300 samples were taken.

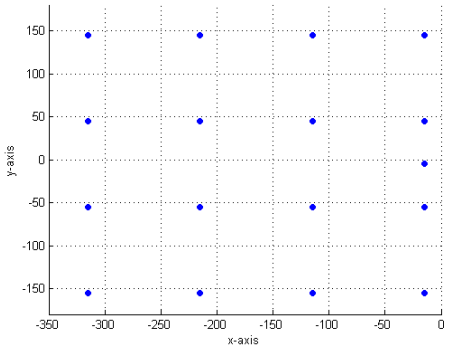

Fig. 6 The coordinates of the targeted points in space, top view. The point $x = -15, y = 0$ was used for Set B.1 and remaining 16 points for Set B.2 and B.3

Experiment Set C The wound reconstruction was evaluated using a two circular metal rings with the diameters of $100mm$ and $220mm$ as wound models. The rings were placed at a fixed position on the platform. The pointer was used to follow the edges of the horizontal surface with free hand movements. The recorded points were used to reconstruct the shape (see Section 2.1.2). Five runs were performed for each ring.

An overview of the experiment structure can be found in Table 2.

2.2.2 Analysis

To evaluate the performance of the system, the following metrics were calculated (Table 3): In Set 1.A, the position of each marker was calculated and compared to the actual position. Moreover, the distance between markers were calculated and compared to the actual

Table 2 The experiment structure and variables

Variables	Experiment Set					
	A.1	A.2	B.1	B.2	B.3	C
Tools	2 Boards	1 Board	Pointer	Pointer	Pointer	Pointer and wound
Samples at each point	3 x 300	1300	3 x 300	3 x 300	3 x 300	5 x 300 for each ring
Points on x-y plane	8	2	1	16	16	2 rings
Height levels (on z axis)	5	-	1	4	1	1
Number of rotations around vertical axis	-	-	3 (0^o,90^o,180^o)	1 (0^o)	1 (0^o)	-
Number of orientations	-	-	1 (0^o)	1 (0^o)	2 x 2 (16^o,33^o; x,y)	-

Table 3 The metrics used in each experiment set

Exp.	Metric	Description
Set A	E_{3d}	Distance of the estimated point to the actual marker position
	E_x (E_y or E_z)	Difference between the x (y or z) coordinates of the estimated and actual marker position
	E_{dist}	Error of the estimated distance between two markers
Set B	C_{3d}	Distance of the estimated centroid to the actual centroid
	C_x (C_y or C_z)	Difference between the x (y or z) coordinate of the estimated and actual centroid position
	T_{3d}	Distance of the estimated tip to the actual tip
	T_x (T_y or T_z)	Difference between the x (y or z) coordinate of the estimated and actual tip position
	E_{dist}	Error of the estimated distance between two markers
	E_{ang}	Angular error of the estimated pointer orientation
Set C	z ,a , b and α	Coefficient of the ellipse equation $X = z + \begin{bmatrix} \cos\alpha & -\sin\alpha \\ \sin\alpha & \cos\alpha \end{bmatrix} \begin{bmatrix} a*\cos\theta \\ b*\sin\theta \end{bmatrix}$ with $0 \leq \theta < 2\pi$
	W_{ang}	Angular error of the estimated wound orientation
	W_z	Difference of the z coordinate for the estimated and actual wound position

values. In Set 2.A, only the distance between two markers were evaluated. For Set B and C, the positions of three markers were estimated and their centroid was calculated. Moreover, the orientation of the plane containing these markers was determined as the orientation of the pointer. The tip position was estimated using the centroid position and the pointer orientation. In Set C, the position data was used for shape reconstruction (See 2.1.2). For Set A.1 and B.2, the calculations were performed for each camera pair separately and using the camera selection algorithm. For each metric, root-mean square error (RMSE) and standard deviation (STD) were calculated and the boxplot was created to evaluate the precision and the accuracy of the tracking system. The standard deviation (STD) gave information about the repeatability of the measurements and the precision of the results whereas the RMSE and boxplot gave information about the accuracy of the system.

3 Results

Experiment Set A.1 The RMSE and the standard deviation of the marker positions (E_{3d}) and marker distances (E_{dist}) for all volume is given Table 4. As seen in the table, the camera pairs produced similar results for both error. The measurement of the marker distances produced smaller errors compared to the marker positions.

Table 4 The RMSE and standard deviation of the marker position and distances for each camera pair and using the selection algorithm

Camera Pair	E_{3d}		E_{dist}	
	RMSE *(in mm)*	STD *(in mm)*	RMSE *(in mm)*	STD *(in mm)*
1 and 2	5.78	2.32	3.45	2.12
1 and 3	6.03	2.68	3.86	2.19
1 and 4[1]	6.81	2.94	3.75	2.12
2 and 3	6.74	2.63	4.17	2.51
2 and 4	6.32	3.80	3.30	2.31
3 and 4	5.73	3.35	3.52	2.41
Selection	6.46	3.20	3.41	2.01

[1] Excluding the measurements at 1m distance

The results at $1m$ distance for the camera pair 1 and 4 were excluded due to results with a very high error at this particular level. For neither any other level nor any other pair a similar behavior was observed. The selection algorithm showed slightly higher RMSE and STD for marker positions. On the other hand, the selection provided superior results for the marker distances. From the histogram of the selected camera pairs in Fig 7, it can be concluded that different camera pairs were employed through the process. The Camera Pair 2&3 is never selected.

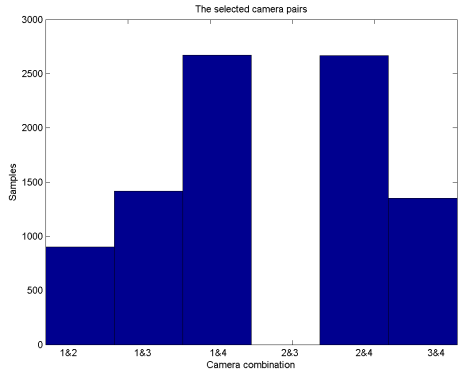

Fig. 7 The histogram of the selected camera pairs at the Experiment Set A.1.

As in Fig 8, the error at the x and y coordinates were similar whereas the error in z coordinate was slightly higher with a larger deviation.

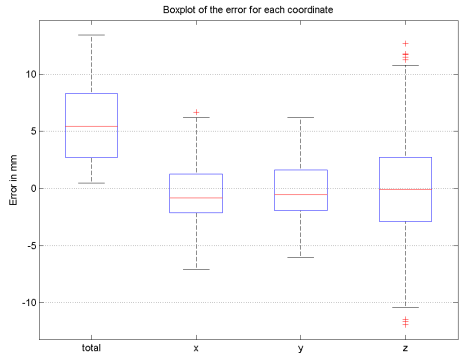

Fig. 8 The contribution of the errors at each coordinate to the total error.

Although above described errors provided a general overview about the system performance, it was also important to see the error distribution within the working volume. The highest deviation was observed with the increasing vertical distance to the cross-structure. This effect was less visible for marker positions and more obvious for marker distances (Fig. 9).

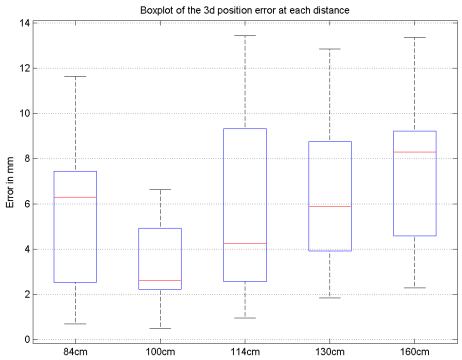

(a) Marker positions

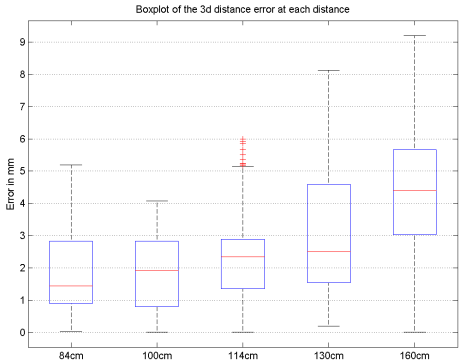

(b) Marker distances

Fig. 9 The error distribution at each level (distance to the cameras)

Experiment Set A.2 For the dynamic situation with a moving board, the camera selection algorithm was employed. 1217 samples (out of 1300) survived after discarding the miscalculated cases with the first correction algorithm (see Section 2.1.2). The RMSE was $3.26mm$ and the standard deviation was $3.06mm$ for total E_dist. The E_dist for each sample can be seen in Fig. 10.

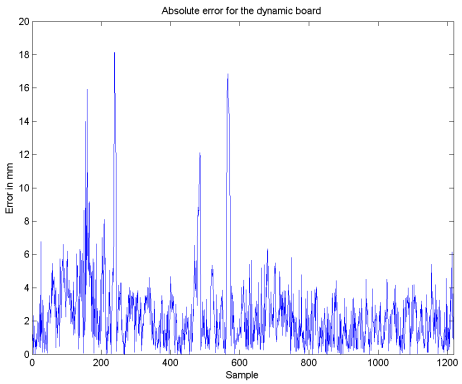

Fig. 10 The distance error E_dist for each sample of the dynamic measurement

Experiment Set B.1 Fig. 11 shows that the results of different rotations were very similar to each other. On the other hand, the median of the error for the tip position was remarkably higher than for the centroid position. The deviation, in other words the size of the boxplots, was small for all cases, but the number of outliers was higher for the tip measurements. Another important measure was the angular error for the orientation of the plane formed by the three markers, which also indicates the lighting direction. For all rotations, the indicated lighting direction was expected to be perpendicular to the horizontal platform. Again, the angular error deviated slightly from expected results, but it showed similar behavior for all rotations (Fig. 12).

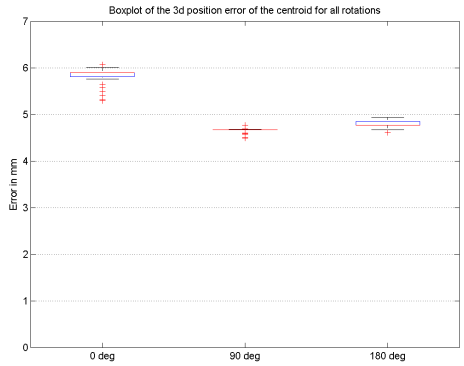

(a) Boxplots for centroid position

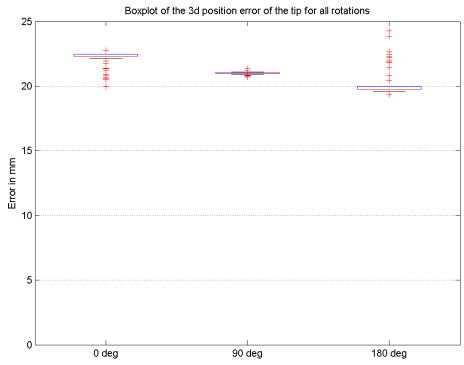

(b) Boxplots for tip position

Fig. 11 The effect of three different rotations of the model around its vertical axis.

Experiment Set B.2 Fig. 13 shows that the median error for the tip position was almost two times larger than the median error for the centroid. Similarly, the deviation of the error was higher for the tip position, even some instances with very high errors (50 to 80 mm) were observed. Furthermore, both RMSE and standard deviation of C_{3d} and T_{3d} were remarkably higher than E_{3d} in Experiment Set A. In Table 5 it can be seen that the RMSE and STD for C_{3d} and T_{3d} were highly

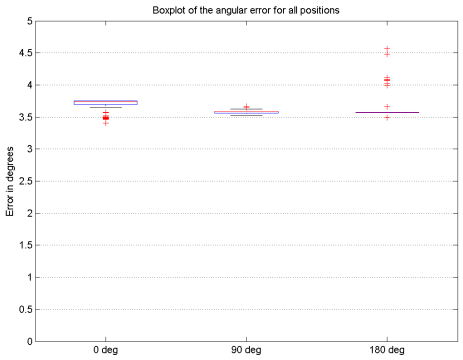

Fig. 12 The boxplot of the angular error of the plane formed by the three markers at each rotation.

varying among the camera pairs, especially high values were observed for camera pairs 2&3 and 2&4. On the other hand, the angular orientation errors (E_{ang}) were similar to each other. The selection algorithm managed to provide results with low RMSE and STD compared to some pairs.

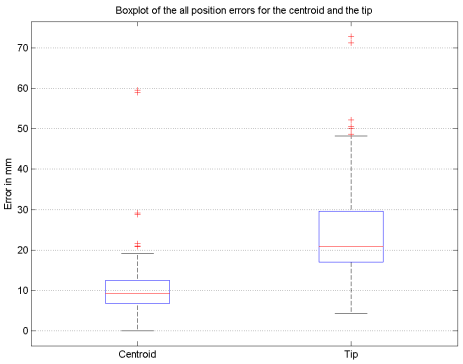

Fig. 13 The boxplot of the centroid and tip positions for all measurements.

Table 5 The RMSE and STD of the error for centroid and tip positions and the orientation of the pointer

	RMSE			STD		
	C_{3d}	T_{3d}	E_{ang}	C_{3d}	T_{3d}	E_{ang}
Pair	*mm*	*mm*	*deg*	*mm*	*mm*	*deg*
1&2	10.27	25.40	4.26	4.08	9.93	1.55
1&3	16.88	34.75	5.53	9.50	12.33	1.72
1&4	20.00	31.97	5.30	9.25	10.19	1.54
2&3	47.52	59.22	6.80	22.27	20.06	2.21
2&4	19.32	31.70	4.69	11.35	12.84	1.94
3&4	33.50	47.48	6.09	16.47	15.65	1.35
Selec.	13.23	26.75	4.36	7.93	11.77	1.65

When RMS and STD of the distance error E_dist between the three LED markers are calculated, it was seen that they were comparable to the marker distances in Experiment Set A, except the higher RMSE and STD for camera pair 1 & 4 (Table 6).

Camera Pair	RMSE	STD
1 and 2	4.65 mm	2.10 mm
1 and 3	3.38 mm	2.15 mm
1 and 4	6.38 mm	2.43 mm
2 and 3	4.26 mm	2.15 mm
2 and 4	2.00 mm	1.19 mm
3 and 4	2.98 mm	1.31 mm
Selection	4.62 mm	2.12 mm

Table 6 The RMSE and standard deviation of the distance between the marker LEDs

Both the centroid and tip position error (C_{3d} and T_{3d})increased slightly with the increasing distance to the cameras (Fig. 14). The increase in deviation of the position error was more obvious for the tip. An increase in the median error was not observed for the angular error E_{ang}, but the deviation again increased with increasing distance (Fig. 15).

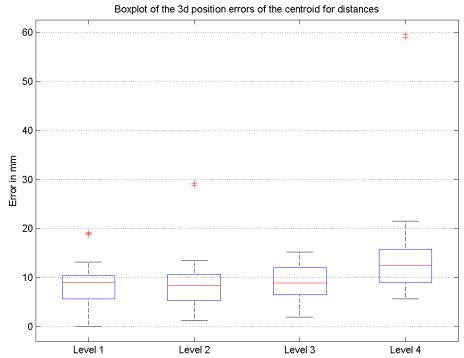

(a) Boxplots for the centroid position error C_{3d}

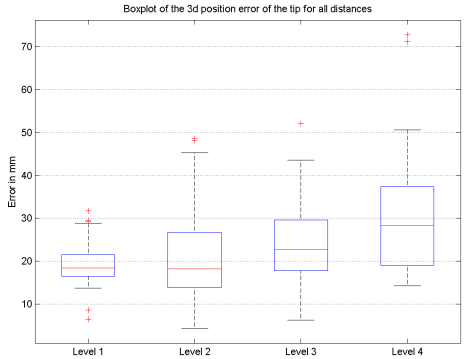

(b) Boxplots for the tip position error T_{3d}

Fig. 14 The error distribution for each level (distance to the cameras)

Experiment Set B.3 Fig. 16 shows that the orientation of the pointer, in other words its angle with the vertical axis, did not have a significant effect on the tip position error T_{3d}. On the other hand, several measurements with high position errors were present. The high position errors was indicated by higher angular deviation.

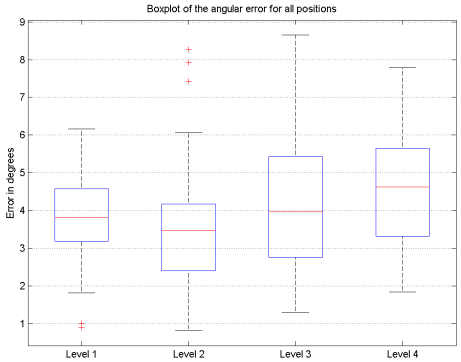

Fig. 15 The boxplot of the angular error of the plane formed by the three markers at each level.

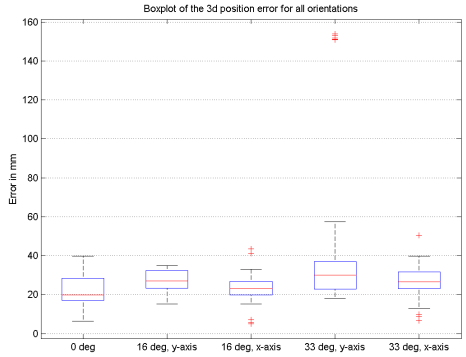

(a) Boxplot of the tip position error

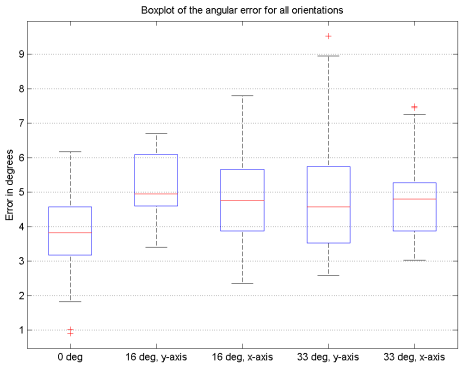

(b) Boxplot of the angular error

Fig. 16 Tip position and angular error at each orientation.

Experiment Set C Fig. 17 and 18 show two example reconstructions of the rings representing wound. Large ring (220mm diameter) was reconstructed larger than actual size (shown with red circle) and shifted on its location. The shape is close to a circle. On the other hand, the small ring (100mm diameter) had the dimensions close to the actual diameter, but in an elliptical shape and again shifted on location. On both figures, the start and end point of the pointer device was recognized with a high number of localized points.

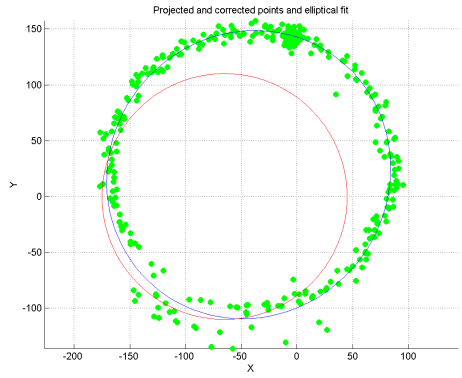

Fig. 17 The reconstructed shape for the ring with a large diameter (220mm).

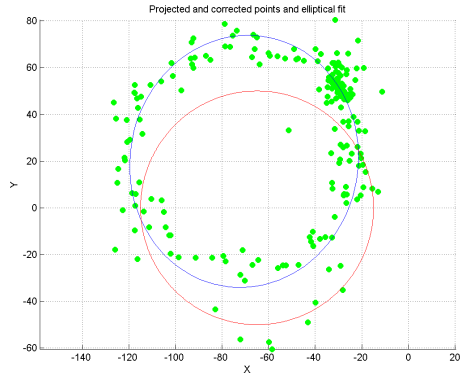

Fig. 18 The reconstructed shape for the ring with a small diameter (100mm).

4 Discussion

The aim of this study was to investigate the accuracy and precision of the Nintendo Wiimote tracking system. The outcome of Set A.1, $E_{dist_{rms}} = 3.41mm$ for marker distances showed similar results to other Wiiremote tracking systems found in the literature [10,11, 16]. The position error E_{3d} was higher than distance error E_{dist}. On the other hand, there were no other studies found which investigated the position error in a similar way. The low standard deviation, which was between 2 and 3 millimeters both for distance and position errors, proved that the measurements with the Wiiremote system were repeatable and precise. The standard deviation of the single position measurements was even lower, less than 1mm in most cases. For Set A.1, the results from camera pair 1 & 4 at 1m distance to the cameras were excluded. It was observed that epipolar matching of the camera views failed for the measurements at this particular distance. This behavior is hypothesized as a shortcoming of the tracking system due to camera calibration. Set A.2 showed that the dynamic tracking was also successful with a good accuracy $E_{dist_{rms}} = 3.06mm$ and alow number of excluded samples.

Set B provided less satisfactory results compared to Set A. The position error for the tip and centroid (T_{3d} and C_{3d}) was higher than expected. On the other hand, the angular error E_{ang} for the pointer was $4.36mm$. One interesting result was the distance error between the markers. This error $E_{dist_{rms}}$ was remarkably lower than the position error and was comparable to the results from Set A.

The main reason of the high differences between these two sets was anticipated as the erroneous alignment of the tracking system coordinates to the real world coordinates. The same effect was also observed between the camera pairs in Set B.2. The preliminary results from Set A.1 were used to create the correction algorithms. These algorithms performed poorly for Set B, even with an additional correction for the origin. A solution would be to improve the calibration step for the alignment to the world coordinate system. A proper alignment can even make the correction algorithms redundant. Another observation on calibration was that a calibration set covering the entire working volume and taken with slow movements of the calibration marker provided better calibration results.

Another reason for high error rates with the pointer device might be the inaccuracies introduced by the construction of the pointer device. The model was assumed to be perfectly orthogonal with a straight rod, which might not be correct in practice. During the measurements, the tip of the model was located at the target so that the centroid might not be in the expected position due to misalignments. When the tip position was calculated, this misalignment was extrapolated creating a higher error. This was illustrated by the tip errors depending on rotation around own axis.

It was also shown that the camera pair selection algorithm performed well to select the camera pairs providing the best results at each instance. One shortcome of this algorithm, which is visible as outliers in the boxplots Fig. 8 and 13, was the markers were in the view of only the camera pairs with poor performance. In that case, a result with lower accuracy was produced. This problem can be solved by introducing a maximum cost threshold to the camera selection algorithm.

The slight offset in the coordinates was also observable by the wound reconstruction as well. The reason for this estimation error was anticipated as the employment of different camera pairs through the free hand movement. Moreover, large shape was more circular due to high number of points. The balance between the number of samples, computational load and time for use can be achieved by introducing a sampling rate which

captures sufficient points without over-increasing the computational load. Moreover, the algorithm for elliptical fit is open for improvements.

5 Conclusion

The results of this study showed that the pointer device and the Wiimote tracking system are promising for the surgical lighting control application. Compared to the commercially available optical tracking systems, the Wiiremote tracking system provided acceptable accuracy ($E_{dist_{rms}} = 3.41mm$) and precision ($E_{dist_{std}} = 2.01mm$) for lower costs (around 250€). To improve the performance of the tracking system, it can be suggested to employ another strategy to align the system coordinates to the real world coordinates. Moreover, the implementation of this system into an actuated lighting unit would be beneficial to investigate the user-lighting unit interaction further.

References

1. Beck, W.: Operating room illumination: the current state of the art. Bulletin of the American College of Surgeons **66**(5), 10–5 (1981)
2. Jesurun, D.: Led technology provides enlightening solution for surgical areas. Emlen Publications, Inc. **6**(1) (2008)
3. Scott, C., Sanderson, J., Guthrie, T.: Choice of ventilation system for operating-theatres. comparison of turbulent versus laminar-linear flow systems in operating-rooms and industrial clean rooms. Lancet **1**(7712), 1288–91 (1971)
4. Knulst, A., Mooijweer, R., Jansen, F., Stassen, L., Dankelman, J.: Indicating shortcomings in surgical lighting systems. Minimally Invasive Therapy & Allied Technologies **0**(0), 1–9 (0). DOI 10.3109/13645706.2010.534169
5. Matern, U., Koneczny, S.: Safety, hazards and ergonomics in the operating room. Surgical Endoscopy **21**, 1965–1969 (2007)
6. A.R.T. GmbH: Infrared optical tracking systems. Website (01.08.2011). `http://www.ar-tracking.de`
7. Northern Digital Inc: Polaris. Website (08.01.2011). `http://www.ndigital.com/`
8. Nintendo : Wii remote controller. Website (01.08.2011). `http://www.nintendo.com/`
9. Illuminating Engineering Society: Lighting for hospitals and health care facilities. Manual (1995)
10. Hay, S., Newman, J., Harle, R.: Optical tracking using commodity hardware. In: Proceedings of the 7th IEEE/ACM International Symposium on Mixed and Augmented Reality, ISMAR '08, pp. 159–160. IEEE Computer Society, Washington, DC, USA (2008)
11. De Amici, D., Sanna, A., Lamberti, F., Pralio, B.: A wii remote based infrared-optical tracking system. Entertainment Computing **1**(3-4), 119 – 124 (2010)
12. WiiBrew: Wiimote - wiibrew. Website (21.07.2010). `http://wiibrew.org/wiki/Wiimote`
13. Vishay Semiconductors: Tsal6400. Website (04.08.2011). `http://www.vishay.com/`
14. Knulst, A.: Prestatiemetingen aan led-operatielampen. Delft University of Technologyi Department of Biomechanical Engineering Internal report (2008)
15. gl.tter: WiiYourself! Native C++ Wiimote Library v1.15 RC3 (2007-2011). `http://wiiyourself.gl.tter.org`
16. Vader, M., Chadda, A., Zhu, W., Leu, M., Liu, X., Vance, J.: An integrated calibration technique for multi-camera vision systems. ASME Conference Proceedings **2010**(49088), 267–274 (2010)
17. Svoboda, T., Martinec, D., Pajdla, T.: A convenient multi-camera self-calibration for virtual environments. Teleoperators and Virtual Environments **14**(4), 407–422 (2005)
18. Svoboda, T.: Multi-camera self-calibration. Website (08.08.2011). `http://cmp.felk.cvut.cz/~svoboda/SelfCal/`
19. Hartley, R., Zisserman, A.: Multiple View Geometry in Computer Vision, second edn. Cambridge University Press, ISBN: 0521540518 (2004)
20. Hartley, R., Sturm, P.: Triangulation. Computer Vision and Image Understanding **68**(2), 146 – 157 (1997)
21. Wikipedia: Triangulation. Website (21.07.2010). `http://en.wikipedia.org/`
22. Manintveld, B., Hogerwerf, E.: Nintendo wiimote 3d tracking using reflective optical markers. TU Delft Haptics Lab, Biomedical Engineering Minor final assignment (2010)

Appendix: Background on stereo vision

As a CCD camera, the Wiimote can be approximated with the pinhole camera geometry, so that a point in space can be mapped on the image plane through a line joining the camera center and the point [19]. In practice, factors like off-set between the image origin and principal point of the camera, non-square pixels, skew between image axes and distortions shall be taken also in account. All these intrinsic parameters are included so called *calibration matrix*. Besides the intrinsic parameters, there are also extrinsic parameters which define the relation between the camera position and orientation and the world coordinate frame. The intrinsic and extrinsic parameters can be combined in a *camera matrix* as following [19]:

$$\mathbf{x} = P\mathbf{X} \qquad P = K\left[\mathbf{R}|\mathbf{t}\right] \tag{1}$$

where $\mathbf{x}$ is the image point, $\mathbf{X}$ is the world point and P is the camera matrix. P matrix consist of the calibration matrix K (3x3), which describes the intrinsic parameters and rotation matrix $\mathbf{R}$ (3x3) and translation vector $\mathbf{t}$ (3x1), which describe the extrinsic parameters. K matrix is a product of the "camera calibration" process, whereas P matrix is the product of a "system calibration" process.

With the two view geometry from two cameras, it is possible to determine the position and orientation of a marker in 3D space via triangulation. In triangulation, the location of a point is determined by measuring angles from two known points at both ends of a fixed line [21]. The position for the point is calculated as the third point of a triangle with one known side and two known angles. For applying the triangulation, the relationship between the two camera views shall be known. This relationship can be expressed with the *epipolar geometry*, which provides a set of constraints to describe this relationship [19].

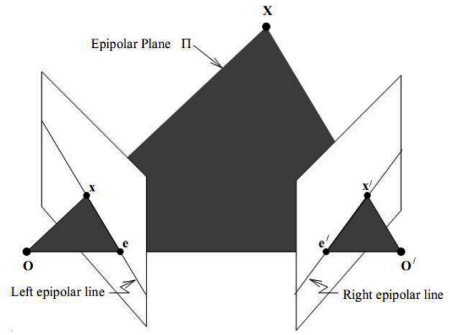

Fig. 19 Epipolar geometry: The camera centres and the space point X form a plane, called epipolar plane. The image points x and x' lie on the same plane. (From [22])

In the epipolar geometry (Fig. 19) it is assumed that the point in space (Point X), and the points on the image planes (Point x and Point x') lie on the same plane, called *epipolar plane*. The camera centers C and C' lie on this plane as well. The line where the epipolar plane intersects with an image plane is called *epipolar line*. The relationship between the two image planes are expressed with the *fundamental matrix F*, using the constraints defined by the epipolar geometry. The two corresponding image points (Point x and Point x') are related to each other satisfying the following equation:

$$\mathbf{x'^T} F \mathbf{x} = 0 \tag{2}$$

The fundamental matrix F can be computed using the camera matrices P and P'. A camera pair defines an unique fundamental matrix F, but the converse is not valid [19]. There are various methods and algorithms available in the literature to compute the fundamental matrix F and the camera matrices.

Chapter 2

Detailed Project Report

2.1 Introduction

Vision results from visible light falling on the retina in the human eye. The light activates photoreceptive cells and neural signals are created to be processed in the brain (Figure 2.1). Thus, a good light level is crucial for a good vision. An adequate lighting is needed especially for delicate tasks requiring precision and caution, such as medical operations. During surgical operations the vision of the surgeons and other surgical staff members can be easily affected by inadequate and improper lighting [5]. In that case, the risk of errors during the surgery can be highly increased especially while detecting the details and the tissue color, which is an important diagnostic tool [5]. Moreover, the risk of infections may be increased and the comfort of the staff may be reduced due to eye fatigue, additional heat and disturbed airflow caused by the lighting unit [15, 31].

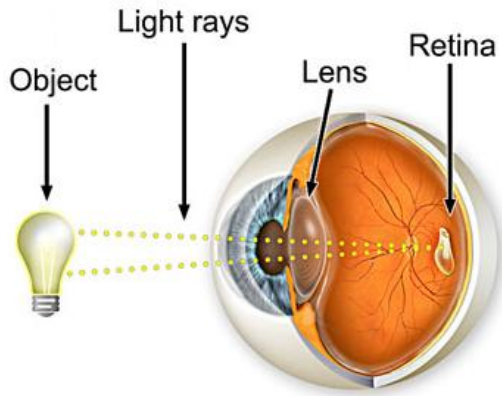

Figure 2.1: Anatomy of the eye. Light falling on the retina activates photoreceptive cells and creates neural signals [16].

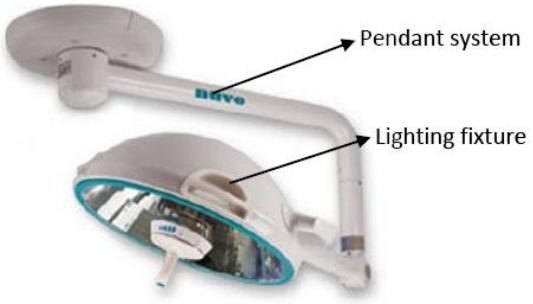

Figure 2.2: Lighting Unit. It consists of a lighting fixture and a pendant system. (Adapted from [28])

High illuminance lighting focused around the wound area is used as task lighting to provide better lighting during the surgery. The lighting unit basically consists of a lighting fixture carrying the bulbs and reflectors, and a pendant system to carry the fixture (Figure 2.2). The unit can also include handles and control buttons to enable the user interaction or additional units like video cameras, light sensors etc. The fixture may contain different types of bulbs. In Figure 2.3(a), fixtures with High-Performance HID, LED and Halogen bulbs, respectively, are shown.

Numerous surgical lighting systems with different properties are commercially available. Most common systems are the ceiling mounted systems with one or two main fixtures optionally combined with smaller *satellite* fixtures to provide desired level of illimunation and to achieve maximum shadow elimination (Figure 2.3(b)). Occasionally the lighting system is combined with cameras and monitors and offered as a multi purpose surgical system.

Surgical lighting systems have gone through numerous improvements through the history, but little academic research have been conducted in this field. These improvements have generally focused on the implementation of the new lamp types such as LED lamps. The adaptation of the light beam properties have been another popular field where numerous systems have been invented. However, there are only a few documentation about adaptations for the position of the lighting fixture, which might happen numerous times during the surgery, with an average of in every 7.5 minutes [20]. The possible reasons for the repositioning have been reported as following: shadows, change in the wound depth, repositioning of the staff or patient, required changes in the illumination level and area size, glare and heat production, and most significantly, change in the work location of the surgeon [20]. Commonly, the repositioning of the light beam is done manually by the surgeon or resident by pulling or pushing the light fixture with handles [5]. This action may create following problems [20, 24]:

(a) Chromophare Series by Brechtold

(b) Harmony by Steris

Figure 2.3: Some commercially available lighting units

1. The surgeon needs to apply force on the lighting unit, which can reach on high values in 10% of the cases.

2. The location of the lighting fixture is usually above the head of the surgeon, which limits the movements to reposition the fixture in terms of ergonomics and the amount of force he or she can apply.

3. The pendant system of the lighting fixture can be locked or blocked by other instruments, which does not allow manipulations or requires time and effort from the surgeon.

4. The attention of the surgeon moves from the working area to the lighting fixture, which is usually located above his head.

5. There is only one sterile contact point with the fixture (middle handle), which limits the movement possibilities, since the surgeon cannot use handles placed on the sides or above the lighting fixture.

6. Although the middle handle of the lighting unit is covered with a sterile cover, the contact with a device outside of the working area increases the risk of infections.

7. The manual manipulation causes loss of time and concentration.

As a solution to these problems, a semi-automated lighting system was suggested. This system includes a tracking system to gather data from the surgical environment. This data can will be used to control the actuators for changing the position and orientation of the lighting fixture and the properties of the light beam (Figure 2.4).

First, available tracking systems in the lighting, surgery and other fields such as virtual reality, entertainment, computer assisted surgery, surveillance et cetera were investigated to select of a suitable tracking system. There were four main categories of interest: Optical tracking, infrared tracking, acoustic tracking and electromagnetic tracking. The properties of these tracking systems were evaluated with a set of criteria to determine the most suitable system. It was concluded that the optical and infrared systems are the most suitable options for

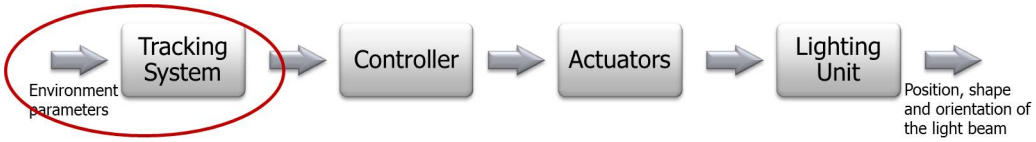

Figure 2.4: Overview of the general lighting system. Only the input parameters and the tracking system was the focus of this project.

working in the operation room during the entire surgery considering the interferences with other surgical equipment. On the other hand, commercially available optical and infrared systems have high costs and provide either high accuracy in a small volume or low accuracy in a very high volume prone to occlusions (Example systems can be found in [4] or [27]). This requirement was satisfied by constructing an infrared(IR) tracking system with Nintendo Wii-Remotes (also known as *Wiimote*) [26].

This project focused on the development of a data collection method for the low-cost six-degrees-of-freedom (6DOF) IR tracking system consisting of Wiimotes. This method shall enables the user to control the lighting in a semi-automated way, so that the lighting system actuation shall be initiated, guided and stopped by the user input or actions via a handheld device. Accordingly, the problem definition and the goal of this project were formulated as following:

Problem Definition

Which parameters in the surgical environment are required to control the lighting system and how can these parameters can be collected by an IR 6DOF tracking system?

Goal

To define the environmental parameters for controlling the lighting unit, to find a method to acquire these parameters and to test this method using the Wiimote IR Tracking System.

2.2 Defining Relevant Parameters

Although surgical lighting have not been a popular research area, some required properties can be found in the literature and related regulations. The fundamental properties of the surgical lighting can be divided into following topics: Basic illumination parameters, area of illumination and focus, color appearance, glare, shadow elimination, heat production, airflow, ease of positioning and maintenance. Most of the parameters related to these topics are regulated by the IES and CIE standards, but some variation possibilities are left up to personal preferences and application needs. Thus, the parameters can be divided into two main categories considering their use through the surgery process: Constant parameters and variable parameters (Table 2.1). Constant variables are desired to be set on a specific level during the operation and are not subjective. These can be listed as color rendering index, unified glare rating, heat dissipation, airflow type, uniformity of the lighting beam, setup time, maintenance time and electromagnetic compatibility. Variable parameters such as illumination level, size and shape of the illumination area, position and orientation of the light beam, depth of focus and correlated color temperature depend on the preferences of the surgeon and the requirements of the operation. Required values for these variable parameters might also change during the surgery.

Table 2.1: Constant and variable parameters defining the surgical lighting systems. The constant variables desired to be fixed during the operation, whereas the variable parameter might change due to needs and preferences.

Constant parameters	**Variable parameters**
Color rendering index	Illumination level
Unified glare rating	Position of the illumination area
Uniformity of the light beam	Orientation of the light beam
Heat dissipation	Size of the illumination area
Airflow type	Shape of the illumination area
Setup time	Depth of focus
Maintenance time	Correlated color temperature
Electromagnetic compatibility	Number of units needed

Table 2.2: Parameters expected to change during an operation and their units

Variable Lighting Parameters	**Units**
Illumination level	*in lux*
Position of the illumination area	*x,y,z coordinates in mm*
Orientation of the light beam	*Euclidean angles in degrees*
Size of the illumination area	*Diameter(s) in mm*
Shape of the illumination area	*Circular or elliptic*
Depth of focus (Figure 2.5)	*Distance from the lighting fixture in mm*
Correlated color temperature	*in Kelvin*
Number of units needed	*1 or 2 (3 and more for uncommon systems)*

The focus of this project was on the variable parameters and specifically to define a method to gather parameters from the environment. A more detailed description of the variable parameters is given in the Table 2.2.

These variable lighting parameters tend to change according to the events during the surgery, e.g. incision, change of working area, blockages, and sometimes due to personal preferences, e.g. preferred color temperature or visual contrast. The question to investigate was how these variable parameters are related to the surgical environment and to the changes during the surgery. The parameters in the surgical environment related to the lighting system are listed in Table 2.3. The relationship between the environmental parameters and the variable lighting parameters can be seen in Table 2.4. Since the variable parameters are affected by the environmental parameters, they will be mentioned as *affected lighting parameter*. The environmental parameter *personal preferences* was left out, since it has effect on all the lighting parameters to some extent.

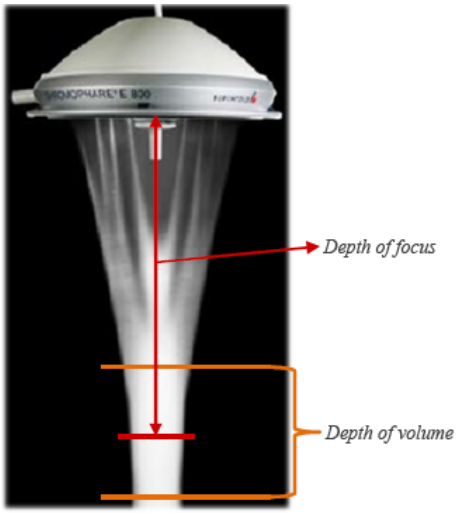

Figure 2.5: The working area of the surgeon shall locate within focal field for proper lighting.(Adapted from [1])

Table 2.3: Environment parameters related to the surgical lighting system

Source	Environment	Units
Wound related	Wound position	*x, y, z coordinates in mm*
	Wound orientation	*Euclidean angles in degrees*
	Wound length	*Length in mm*
	Wound width	*Width in mm*
	Wound shape	*Closed curve or narrow-linear*
Surgeon related	Surgeon position	*x, y, z coordinates in mm*
	Surgeon orientation	*Euclidean angles in degrees*
	Working depth	*x, y, z coordinates in mm*
	Personal preferences	-
Other	Location of the obstacles	*x, y, z coordinates in mm*
	Additional lighting	*Environment, head lights etc...*
	Operation type	*Laparotomy, minimal invasive etc...*

The environmental parameters give information about the state of the operation room (Figure 2.6 and 2.7). According the these parameters, the need for change in the affected parameters can occur. For example when the surgeon changes his working depth, the depth of focus needs to be rearranged or when the surgeon starts to work on another wound, the illumination area and light beam direction, shape and size needs to be set again.

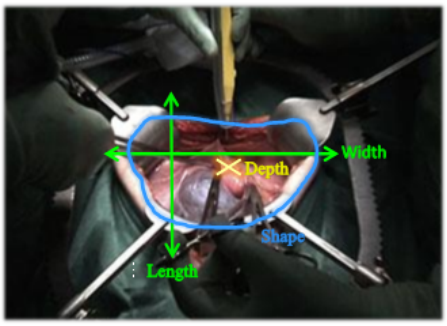

Figure 2.6: Wound properties: Wound width and length (green), wound shape (blue) and working depth (yellow). (From [12])

Table 2.4: The relation between the environmental parameters and variable lighting parameters (affected parameters).

Environment Parameter	**Affected Lighting Parameter**
Wound position	Illumination area position Light beam orientation
Wound orientation	Light beam orientation
Wound length	Illumination area size Illumination area shape
Wound width	Illumination area size Illumination area shape
Wound shape	Illumination area shape Depth of focus
Surgeon position	Light beam orientation
Surgeon orientation	Light beam orientation
Working depth	Depth of focus Illumination area size Illumination area shape
Location of the obstacles	Number of units needed Light beam orientation
Additional lighting	Illumination level Number of units needed
Operation type	Illumination level Correlated color temperature

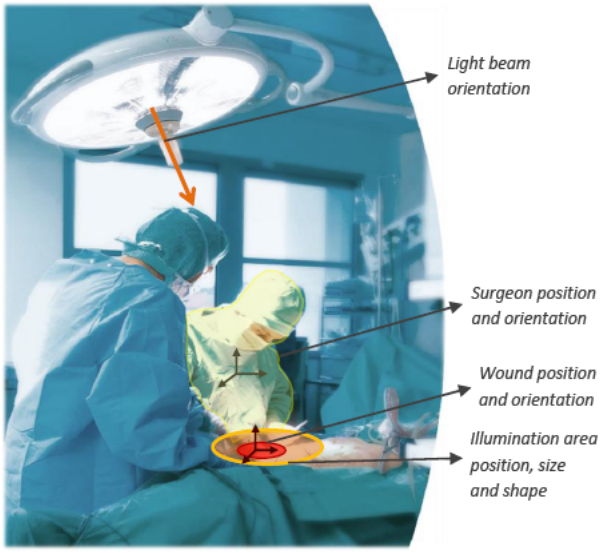

Figure 2.7: Some environmental and affected parameters. The environmental parameters such as surgeon position & orientation and wound position & orientation affect light beam orientation and illumination area position, size and shape. Other environmental parameters and affected parameters do exist, but not shown in the figure.(Adapted from [22])

Basically three mechanisms are available on the lighting unit to change its properties: The pendant mechanism to change the position and orientation of the lighting fixture, the mechanisms within the lighting fixture to change the position and orientation of the lamps or reflectors and a voltage regulator to decrease or increase the voltage input to the lamps (Table 2.5).

Table 2.5: Variable parameters for the surgical lighting system and control mechanisms

Mechanism	**Effect**	**Primarily changed lighting parameter**	**Secondarily changed lighting parameter**
Pendant system	Change in the position and orientation of the lighting fixture	Illumination area position	Illumination level
		Light beam orientation	Illumination area size and shape
Actuators inside the lighting fixture	Change in the position and orientation of the lamps and/or reflectors	Illumination area size	Illumination level
		Illumination area shape	
		Depth of focus	
Voltage regulator	Change in the voltage input	Illumination level	Illumination area size and shape
		Correlated color temperature	
		Number of units employed	

1. **Pendant mechanism and related parameters:**
   The parameters related to the pendant mechanism depend on the position and orientation of the lighting fixture. These parameters are the position of the illumination area and orientation of the light beam. On the other hand, changing the position and orientation of the lighting fixture can also change the parameters related to the light beam, such as illumination level, illumination area size and shape. This effect can be described as secondary and it is observed due to the non-uniformity of the light beam, where the illumination level and beam size is not constant through the light beam volume.

2. **Mechanisms in the lighting fixture and related parameters:**
   The parameters related to the the mechanisms in the lighting fixture depend on the inner structure of the lighting fixture. The fixture may contain several lamps and reflectors, whose position and orientation can be controlled by an actuation system. The parameters that can be changed with such a mechanism are the size of the illumination area, the shape of the illumination area and depth of focus. In addition, illumination level is changed as a secondarily effect.

3. **Voltage regulator and related parameters:**
   The parameters in this category are the parameter which can be controlled by regulating the voltage input. These parameters are illumination level, correlated color temperature and number of units needed. Increasing or decreasing the voltage input, the illumination level can be increased or decreased. Similarly, by turning on/off the individual lamps, the correlated color temperature or the number of employed units can be changed.

Given that, it was concluded that each environmental parameter affects one or more lighting parameter, which can be changed by a mechanism present in the lighting system. For this

study, the secondarily effects of the mechanisms were left out and it was only focused on the primary effects. On the other hand, these relationships may be relevant for other projects in the future, such as design of a lighting control system. The relationship between the environmental parameters, affected lighting parameters and the mechanisms can be seen in Figure 2.8. Accordingly, the and affected parameters form separate clusters for each mechanism.

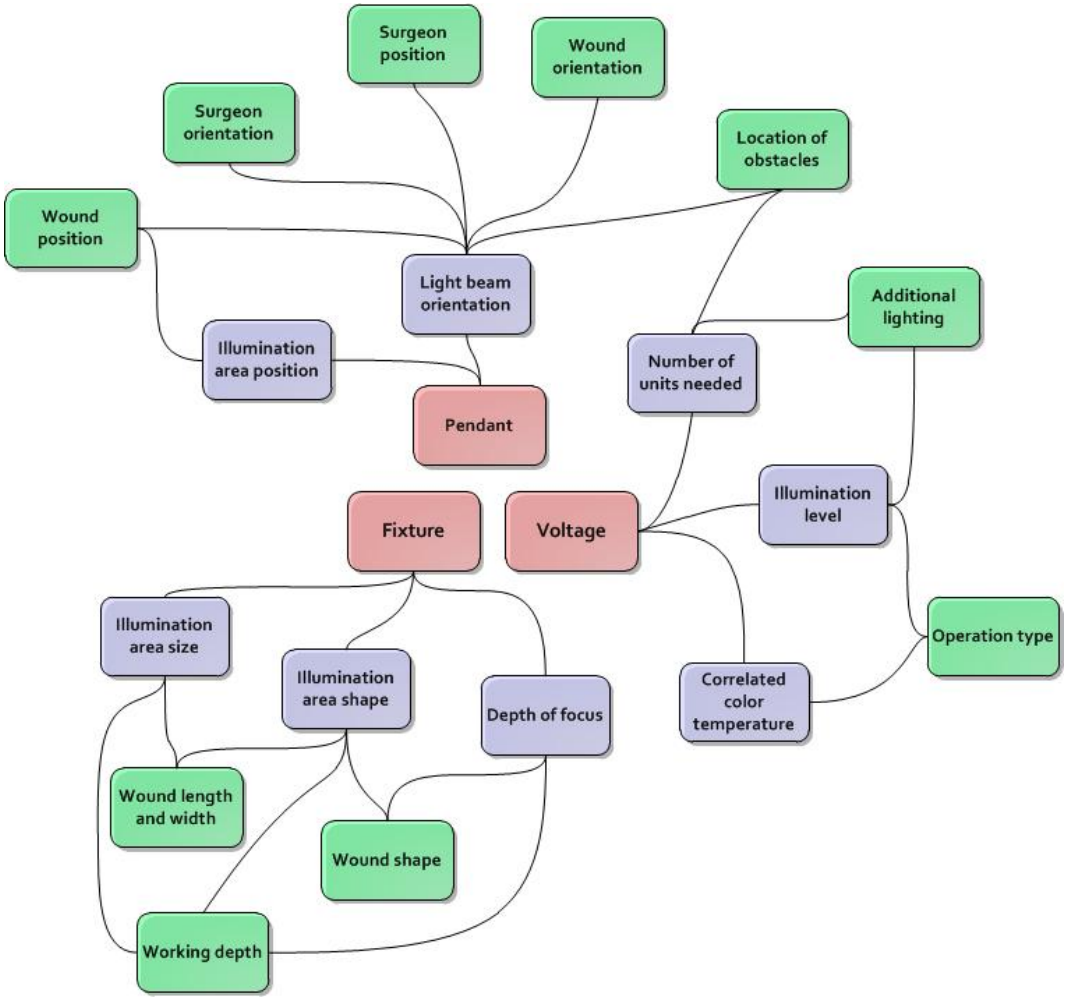

Figure 2.8: Environment parameters (green), affected parameters (blue) and mechanisms (pink) and their relations.

This study only was targeting the collection of parameters a 6DOF IR tracking system for a semi-automated lighting system. The environmental parameters "additional lighting" and "operation type" were not suitable to be detected with such a system. In addition, the affected parameters "number of units needed", "illumination level" and "correlated color temperature" are highly dependent on surgeon preferences, so that the automation could not provide a significant added value. Thus, the voltage mechanism and related parameters were left out for this project.

Another parameter depending on the surgeon was the light beam orientation, as it can be seen in the Figure 2.8. Besides the surgeon position and orientation data, the surgeon preferences play an important role for this affected parameter, such as some surgeons prefer to work with light behind their heads, whereas some surgeons work with a light beam directly above the wound. Thus, these two parameters and the wound orientation were combined into another parameter for a semi-automated system, namely: *indicated lighting direction*. The updated parameter-mechanism figure is given in Figure 2.9. A flowchart for the parameters in the semi-automated lighting system can be seen in Figure 2.10.

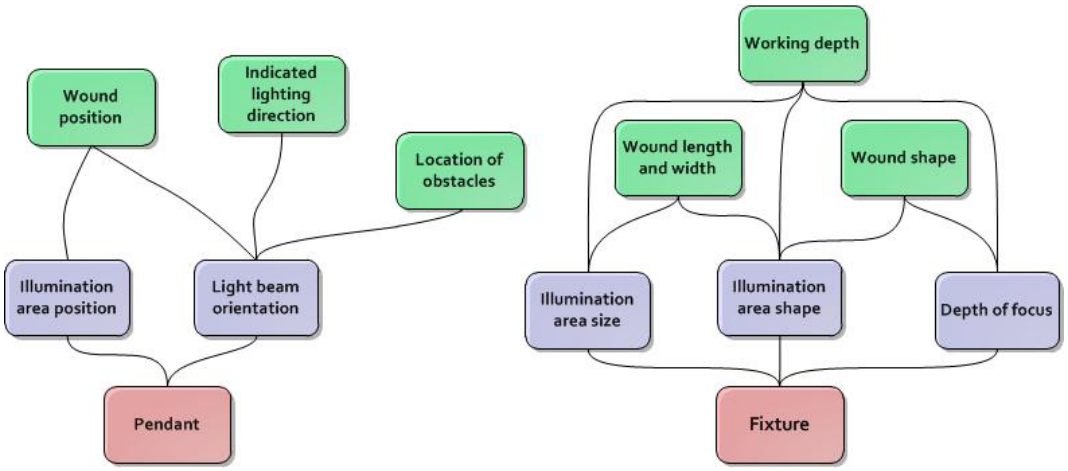

Figure 2.9: Relevant relationships of the environmental parameters (green), affected parameters (blue) and mechanisms (pink), updated for the 6DOF tracking system for the semi-automated lighting system.

Detailed description of the environmental parameters to be included

1. ***Wound position:*** This parameter describes the position of the wound in 3D space. The position of the wound can be used to determine the desired location of the illumination area. This parameter is given as x, y and z coordinates of the wound edges in mm relative to a pre-defined reference coordinate frame.

2. ***Indicated lighting direction:*** The indicated lighting direction is determined by the surgeon to change the light beam orientation considering his or her own position, orientation and the wound orientation. It is given in Euclidean angles alpha, beta, gamma in degrees.

3. ***Wound length:*** Wound length is a parameter used to determine the illumination area size and shape. It is given in millimeters.

4. ***Wound width:*** Similar to the wound length, wound width is used to determine the illumination area size and shape and given in millimeters.

5. ***Wound shape:*** Wound type describes the entrance of the wound. It is a closed curve, commonly circular or elliptical. In case of narrow wounds, a linear form can be defined instead of a curve.

6. ***Working depth:*** The working depth describes the location where the surgeon is performing his/her operation. The operation is not necessary performed near the wound edges, or at the deepest part of the wound, but it can also be a location in between. Thus, having the working point in the focal area of the lighting unit is important. This can be tricky to satisfy when the wound entrance is small or narrow, and the working point is deep below the skin.

7. ***Location of obstacles:*** The light beam shall not be blocked and create shadows on the working area on the surgeon. In addition, an actuated system has the risk of collapsing into other surgical equipment or surgical team members during operation. Thus, the location of obstacles and the coordinated of the occupied area shall be given as x, y and z coordinates in mm.

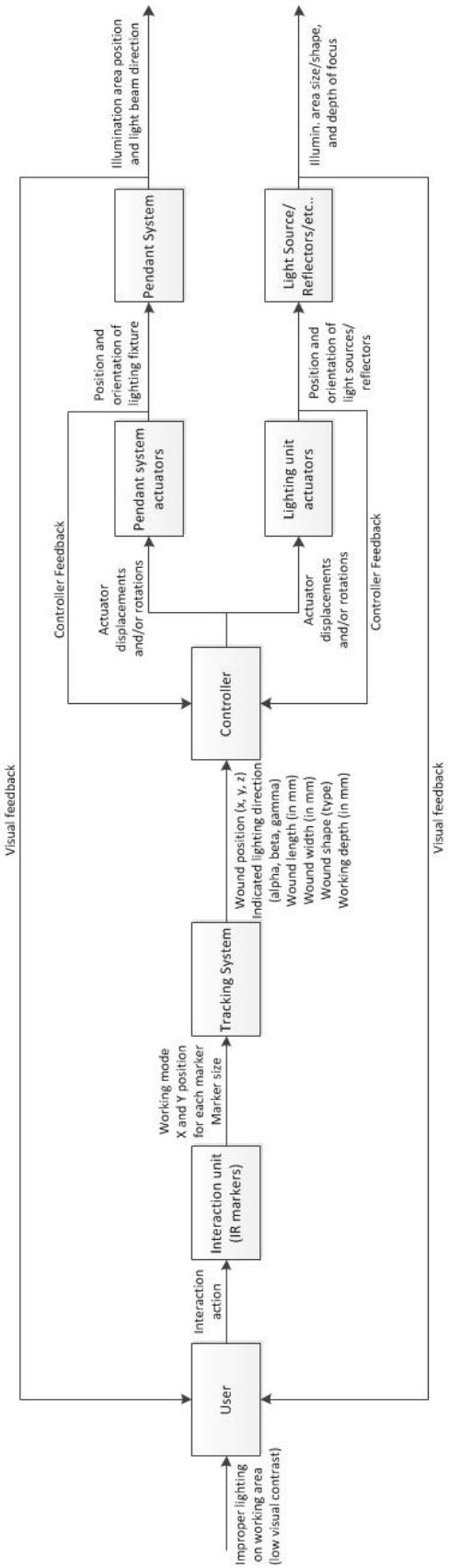

Figure 2.10: Flowchart for the system parameters.

2.3 Conceptual Design of a Method to Collect Relevant Parameters

A method was designed to collect previously defined environmental parameters in the operation room, where the data collection would done with a 6DOF IR tracking system with Wiimotes, which can detect simultaneously up to 4 markers. The first step was to define the requirements and criteria for the design, then to list the functions to be included in the design. For each function, available solutions was listed and promising solutions was be combined into a final design.

2.3.1 Design requirements and criteria

1. ***Shall enable the data collection of environmental parameters***
   The design should be able to collect the previously defined parameters from the surgical environment: Wound position, indicated lighting direction, wound length, wound width, wound shape, working depth and location of obstacles.

2. ***To be operated in the current working area of the surgeon***
   During the surgery, the surgeon works on an area where the wound is located. This area is usually located just above the operation table, in front of the surgeon. To adapt the light manually in current systems, the surgeon shall move his hand to the lighting unit hanging overhead, so outside of his actual working area. The design should be a solution to this problem by keeping the manipulation action for the lighting unit in the actual working area of the surgeon (Figure 2.11).

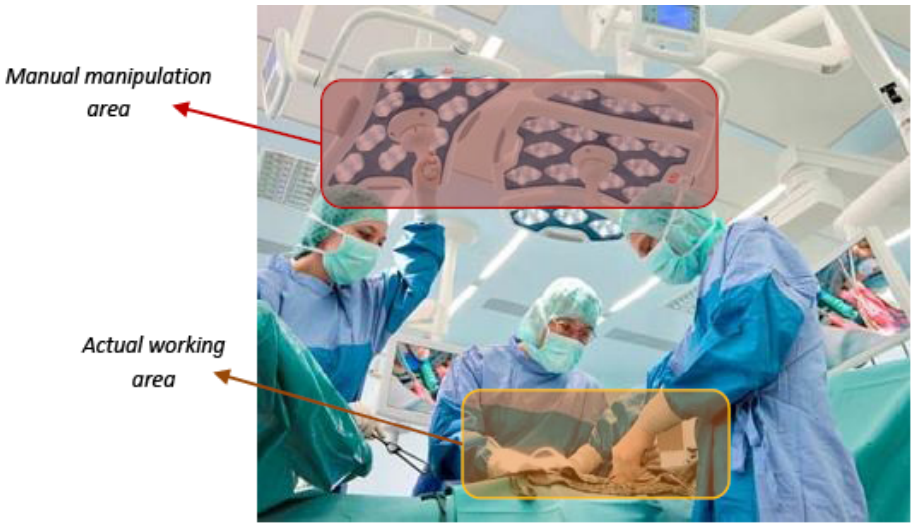

Figure 2.11: Actual working area of the surgeon and the area where the manual adaptation of the lighting unit takes place (here is done by the scrub nurse, but it is common that the surgeon does the adaptation action). The goal was to keep the lighting unit manipulations within the actual working area. (Adapted from [25])

3. ***Requiring short operation time***
   The observations done by R. Mooijweer [20] have shown that most of the lighting unit manipulation action take 5 to 10 seconds. There exist also extreme cases, where the action takes 20, 25 or even above 35 seconds. One criterion for the design was to eliminate the need of these extreme cases and keep the time required for the manipulation action below 10 seconds.

4. ***Suitable to be used in the sterile area***
   The design should be suitable to be used in the sterile area, so it should be either suitable for sterilization or can be covered with a sterile cover.

5. ***Low cost***
   The design should be low cost, either for reusable and disposable options. Since the tracking system already adds a cost to the surgical lighting system, the costs added by the design should be as low as possible. A reasonable cost was defined as below 50€.

6. ***Accurate***
   The design should provide accurate measurements for control parameters. This accuracy was defined as 6 mm in the previous literature study. It was not defined for each specific parameter, but for the output data of the tracking system.

7. ***Reliable***
   The design should be reliable in terms of robustness, minimum down time, occurrence of errors. It should provide sufficient parameter measurements in a single run. During the surgery, the time is very limited and being occupied for a long time to provide accurate measurements for the lighting system is not desired.

8. ***Comfortable for the surgeon***

   (a) **Lightweight**

   (b) **Easy to use**

   (c) **Simple**

   Surgeons are already accomplishing a high precision task during surgeries and work under pressure. Thus, the design should not cause any additional discomfort to the surgeon and should not create any complexities. This required accomplished by a lightweight, easy to use and simple design.

9. ***Safe in the surgical environment***
   Since the design will be used in an environment involving high risk, it should be safe to use, both for the surgical team and the patient. The factors related to the safety in that sense are numerous, but some examples can be listed as compatibility with the surgical equipment, following safety classifications such as for lasers, risk of temporary or permanent damage due to failures etc...

2.3.2 Functions to be included in the final solution

In this section the functions to be included in the design are listed. This list was created using the previously defined environmental parameters and some other required functions in addition to them, e.g. activation of the system. The list includes two categories: data collection functions and other functions. These functions are listed in the Table 2.6.

2.3.3 Possible solutions for each function

For each function, all possible solutions were listed and some preliminary concepts were created using these solutions. In this section, these solutions will be investigated further.

As mentioned before, these solutions aimed to provide a method to be used with a 6DOF IR tracking system, which can be used with active or reflective markers. The tracking system calculates 3D position by the triangulation method. The triangulation method makes use of the locations of the two known points to calculate the location of a third point. This third point can be a marker or a camera, depending on the configuration.

Table 2.6: The functions to be included in the design

No	Function	Data output
Data collection functions		
1	Wound location	Position in space (x-y-z coordinates in mm)
2	Indicated lighting direction	Direction in space (angles in degrees)
3	Wound size	Wound length and width (in mm)
4	Wound shape	Closed curve (diameter(s) in mm)
5	Working depth	Depth (in mm)
6	Detecting obstacles	Occupied areas (x-y-z coordinates in mm)
Other functions		
7	Activate command mode	Enable data use (start command)
8	Deactivate command mode	Disable data use (end command)
9	Change command mode	Detect different types of commands

System configuration options

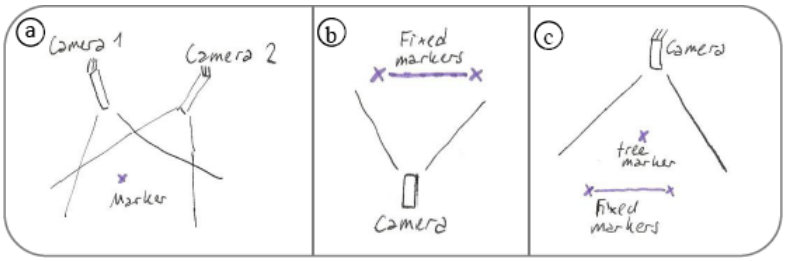

Figure 2.12: System configuration options. In the Option A, two fixed cameras and one free marker is used. In the Option B, the camera is free moving and two markers are fixed in space, whereas as in Option C, one fixed camera, two fixed markers and a free marker is used.

Option A Free moving single marker + 2 cameras in fixed positions: One option to do this process is to locate 2 cameras in fixed known points to calculate the location of a free moving marker, e.g. on a tracked item (Figure 2.12.a). In this case stereovision is used by gathering 2 views of the marker from different viewpoints (camera locations) and to calculate the location of the marker in 3D.

Option B 2 fixed markers + one camera on a tracker: Again, the principle is to use two known points for calculating the position of a third point. In this method, two markers are fixed in space and a free moving camera is used (Figure 2.12.b). Knowing the positions of the markers and the distance between them, the position of the camera can be calculated. This method is the working principle of the Nintendo Wii Console.

Option C 2 fixed markers + one fixed camera + one marker on the tracker: Similar to previously described two solutions, this solution uses the triangulation with 2 fixed markers. A camera located somewhere in space can see these 2 fixed markers and one free moving marker (Figure 2.12.c). In that way, the location of the free moving marker can be calculated.

One of these three configuration options should be selected for the next steps of the design. The Option B, with two fixed markers and one free moving camera, was eliminated due to the additional weight and sterilization difficulties, which occur

when the camera is placed in a handheld device. Moreover, including the camera in a handheld device requires wireless connection with the processing computer and increases the cost for replacements. The Option C, with one fixed camera and two markers, was eliminated since it was more prone to the line-of-sight problem by the blockage of the fixed markers. Thus, Option A, with two fixed cameras and a single marker, was chosen. With this configuration, the weight of the handheld device could be kept low. To reduce the problems due to line-of-sight blockage, the number of cameras was increased to four, so that two cameras having the marker in the view were selected for measurements at each frame. The placement of the cameras was another issue. Since the placement on the ceiling or side walls would increase the occurrence of the line-of-sight problem, the cameras was be placed on the lighting unit itself, so that they have a close view on the working area and less undesired objects on their view angle.

Solutions for each function

1. ***Wound position***

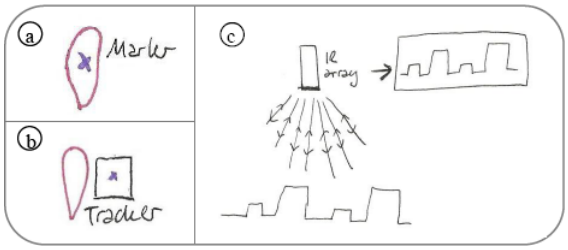

Figure 2.13: The solutions for the wound position In a, a single marker is placed on the wound. In b, the marker is placed on the tracker. The solution c, makes use of the IR reflectance to detect the position of the wound.

   (a) **Single marker on the wound:** The position of an object in 3D space can be calculated with at least one marker placed on the object using triangulation method. In this solution the marker is placed on the wound, preferably at the center at the center of the desired illumination area (Figure 2.13.a).

   (b) **Single marker on the tracker:** In this case, the marker is placed on a handheld device (or tracker) and the tracker is used to indicate the position of the wound (Figure 2.13.b).

   (c) **Time-of-travel:** Time-of-travel method makes use of reflectance property of IR arrays to create a depth image of the environment. Using this information, the working depth can be subtracted from a depth image. It is not possible to create a depth image with Wiimote system, but this principle is being used in the Kinect sensor (Figure 2.13.c) [18].

2. ***Indicated lighting orientation***

   (a) **3 points on the wound to build a plane + perpendicular to the wound plane:** The orientation of an object in 3D space can be calculated with at least 3 markers placed on the object. The location of each single marker can be calculated using triangulation, and the orientation can be derived from the relative position information. In this solution 3 markers are located on the edges of the wound to build a plane (as edges of a triangle, Figure 2.14.a). The orientation of the wound can be found as a direction vector perpendicular to this plane and the indicated lighting direction is assumed to be same as the wound orientation.

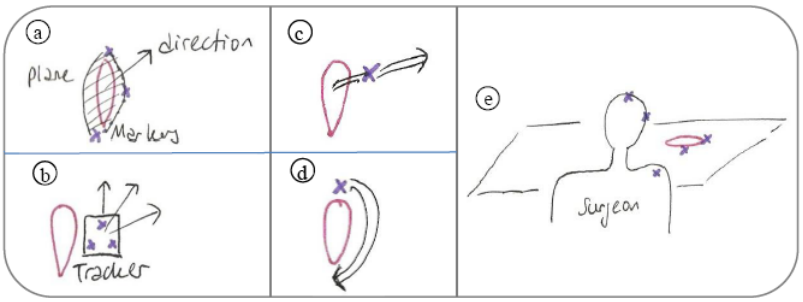

Figure 2.14: The solutions for the indicated lighting direction. In a, three markers are placed on the edges of the wound and the direction of the plane is formed by these markers. In b, the markers are placed on a tracker instead of directly on the wound. In c, a marker is moved perpendicular to the wound plane. In d, one marker follows the wound edges to construct its plane virtually. In e, markers are placed on the surgeon to determine his or her location and orientation.

(b) **3 fixed points on a tracker + tracker orientation:** Similar to the solution 2.a, here are 3 markers are used, this time not directly on the wound, but on a tracker device (Figure 2.14.b). The tracker is pointed on the direction of the desired lighting direction and the orientation of the tracker is calculated.

(c) **Virtual direction:** This solution uses a single marker to indicate the direction of the light. One marker is moved with free hand in the desired direction for the lighting and the formed path is used to derive a vector for the direction (Figure 2.14.c).

(d) **Virtual path with one marker:** Similar to the solution 2.d, a marker is used to indicate the direction of the lighting. By free hand, the marker is moved following the edges of the wound, as close as possible, and the direction is calculated as perpendicular to the plane drawn with this path (Figure 2.14.d).

(e) **Using the surgeon position and wound location information:** In the literature, it is described for the proper lighting, the light beam shall pass through the right ear of the surgeon pointing his right index finger tip. When the location of the wound is known and the right ear of the surgeon is marked, the orientation of the surgeon can be found (Figure 2.14.e) and the light beam can be directed accordingly.

3. ***Wound size***

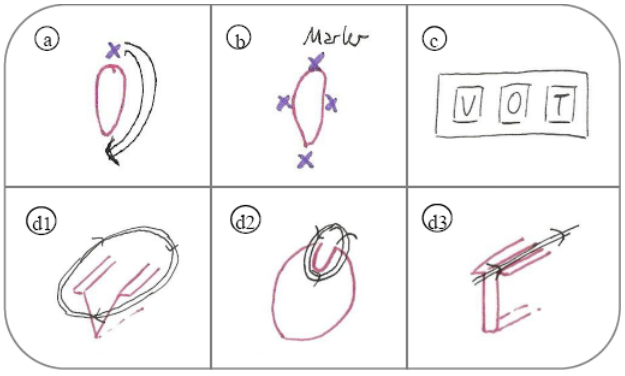

Figure 2.15: Solutions to determine the wound shape and in some cases the size. In a, one marker is travelling on a path over the wound edges. In b, several markers are placed on the wound edges. In c, the wound type is entered via buttons. In d, several gestures to determine the wound shape are shown: A large circular move (d1), a small circular move (d2) and a linear move (d3).

(a) **One marker travelling on a path:** Similar to solution 3.a, a marker travelling on the edges on the wound can indicate its size (Figure 2.15.a). The marker position is captured the tracking system and the longest and widest distances of the wound can be derived from the path shape.

(b) **One marker activated on wound edges:** In this solution, a marker is activated at least 4 points of the wound: two corners at largest length and width. The distances between these points can be calculated to have the length and width information.

(c) **Several markers on wound edges:** In this case, several markers are located at the wound edges and the relative distances are calculated (Figure 2.15.b).

(d) **User input:** The length and width information will be entered manually by the surgeon via a number pad.

4. ***Wound shape***

(a) **One marker traveling on a path:** A marker traveling on the edges of the wound can indicate the shape (Figure 2.15.a). But this solution fails to give information about the depth of the wound.

(b) **Several markers on wound edges:** Several markers can be placed on previously defined points of the wound, e.g. the widest point, at the ends of the incision etc... (Figure 2.15.b). The positioning of these markers can indicate the shape of the wound, but again there is no information about the shape in depth.

(c) **User input via a selection button:** The wound shape can be selected via a button by the user (Figure 2.15.c).

(d) **Gestures:** The surgeon can indicate the wound shape by using different gestures: e.g. a large circular move for a large open wound, a small circular move a small wound, a linear movement for a narrow but long wound etc. (Figure 2.15.d).

5. ***Working depth***

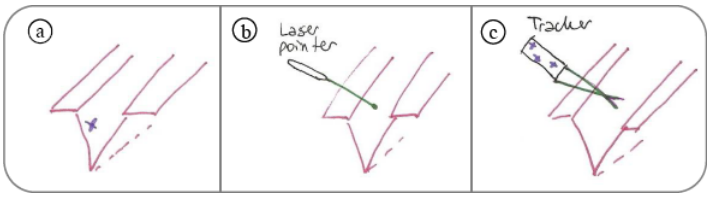

Figure 2.16: Solutions to collect the working depth data. In a, a marker is placed on the operation point. In b, a laser point is used to indicate the operation point. In c, two converging laser beams are used. The convergence point corresponds to the operation point.

(a) **Single active marker on the location:** One marker can be temporarily placed of on the location of the operation to mark the depth. This is often inside the wound (Figure 2.16.a).

(b) **Laser pointer:** This solution makes use of a pointer to be used as a marker. In this case, a device does not need to be placed inside the wound, but the surgeon can point out the operation location without contact (Figure 2.16.b). One disadvantage of this solution is that it requires modifications on the Wiimote tracking system. When the IR filter of the Wiimote is removed, it can detect any bright light source, including the common cheap laser pointers. But the system becomes sensitive to environmental light, which is not useful under high illuminance lighting. IR pointers are also available on the market, but they are not visible with naked eye, classified

as risky for health (level 2 or 3 lasers) and more expensive (commonly above several hundred Euros).

(c) **Converging laser beam:** To provide a solution without contact with the wound, two laser beams can be used. These laser sources are placed on a tracker device, so that the beams converge. The surgeon points out the operation location with the convergence point (Figure 2.16.c). If the tracker position and the location of the convergence point relative to the tracker are known, the location of the operation can be calculated.

(d) **Navigation arrows:** Another solution is to enter the desired working depth manually to the system by means of navigation arrows.

(e) **Time-of-travel:** Time-of-travel method can also be used to detect the depth or the wound and the working depth of the surgeon, since the Kinect sensor can provide a depth-image.

6. ***Detecting obstacles***

(a) **Markers on surgeon:** A major obstacle for the lighting is the heads and shoulders of the surgeons. These can be detected by placing markers, but again there is a limit to the number of markers tracked simultaneously.

(b) **Time-of-travel:** The time-of-travel method can be very useful for detecting obstacles, by means of providing a map of the environment.

7. ***Activate command mode***

The command mode activation is used to start to control the lighting unit. In other words, to start the use of the data collected by the tracking system. This can be done using different principles depending on the system properties: e.g. turning on tracking system, turning on markers, turning on IR array, recording the data collected etc...

(a) **Start button:** The activation is done by a start button placed on the tracker or somewhere nearby the surgeon.

(b) **Movement activated:** The data collection is activated by movement: E.g. use of a tracker, a startup gesture etc...

(c) **When predefined working range is violated:** The activation is done when the operation point is outside of a predefined range. This solution is suitable for a system with continuous information flow, e.g. time-or-travel method.

8. ***Deactivate command mode***

The command mode deactivation is used to stop the manipulations on the lighting unit. In other words, to stop the use of the data collected by the system. Again, this can be done using different principles: e.g. turning of the system, turning off markers, turning off IR array, disposing collected data etc...

(a) **Stop button:** The deactivation is done by a stop button placed on the tracker or somewhere nearby the surgeon.

(b) **Deactivated when no movement is present:** The deactivation takes place when there are no control movements are present: e.g. no markers to be tracked, stationary tracker etc...

(c) **When the light actuation is finished:** The system goes into the inactive mode after each actuation action.

9. ***Change command mode***

   As can be seen in the Step 2 Section 1, the collected data is used to control two different parts of the lighting system: The pendant system and the actuators inside the fixture. The data transfer for these two parts can be defined as two command modes: Positioning mode and light beam properties mode.

   (a) **Command mode change button:** The command mode can be changed by a button on a tracker or near the surgeon.

   (b) **Different gestures for different modes:** Different gestures can be assigned to different modes, so that the system recognizes what kind of data shall be processed.

   (c) **Marker properties:** Markers with different properties can be employed to indicate different modes: e.g. large/small markers, placement of markers, combinations of markers etc...

   (d) **Number of active markers:** The number of active markers can be selected differently for each mode. For example for the positioning task, where the wound position and orientation is needed, usually 3 markers are required, whereas one marker can be sufficient for controlling light beam properties.

	Function	Solutions				
1	Wound position	Single marker on wound	Single marker on tracker	Time-of-travel		
2	Indicated lighting direction	3 points on the wound to build a plane + perpendicular to the wound plane	3 fixed points on a tracker + tracker orientation	Virtual direction	Virtual path with one marker	Using the surgeon position and wound location information
3	Wound size	One marker travelling on a path	One marker activated on wound edges	Several markers on wound edges	User input	
4	Wound shape	One marker travelling on a path	Several markers on wound edges	User input via a selection button	Gestures	
5	Working depth	Single active marker on the location	Time-of-travel	Converging laser beams	Navigation arrows	Laser pointer
6	Detecting obstacles	Markers on surgeons	Time-of-travel			
7	Activate command mode	Start button	Movement activated	When predefined working range is violated		
8	Deactivate command mode	Stop button	Deactivated when no movement is present	When the light actuation is finished		
9	Change command mode	Command mode change button	Different gestures for different modes	Marker type/size	Number of active markers	

Figure 2.17: Summary of the solutions for each function

2.3.4 Preliminary concepts

Before creating preliminary concepts, the previously provided solutions were evaluated considering the requirements and criteria determined in Section 2.3.1. The evaluation was not done quantitatively, but the solutions that would not perform well in one or more aspects are eliminated. The eliminated solutions can be seen in the Figure 2.24 as gray areas.

For the wound position and indicated lighting direction function, the placement of the markers on the wound was eliminated since they provide additional difficulty to the surgical team. The solution virtual direction was eliminated due to the lower accuracy and increased difficulty of drawing a direction path on air. Similarly, the accuracy and reliability of the virtual

path is low, since a plane needed to be calculated from a closed path drawn with free hand. Another solution eliminated was the use of the surgeon and wound location information. The number of markers can be used simultaneously is limited to four, so that it was not feasible to place many markers on a surgeon. In addition, the available places which does not create sterilization problems or hinder the actions of the surgeon are very limited, such as the back of the ear, head, back of the shoulders. Moreover, the theoretical approach is not followed by every surgeon and in each operation. So, it was more preferable that the surgeon actively indicates the lighting direction.

For the wound shape, size and working depth solutions, the solutions requiring on-place markers were eliminated again due to the additional difficulty to the surgical team, but similar principles could be used when the markers are placed on a tracker. The solutions where the user needs to give an input manually, such as type, size or navigation arrows were also eliminated, since they added complexity to the process and were not easy to use in many cases, such as giving a numerical input for the size. The laser pointer solution for the working depth was promising by means of providing accurate data without an on-place marker, but serious modifications need to be done on the Wiimote system and the system would be highly sensitive for lighting level changes. Thus, it was concluded that it did not worth the effort to try-out this solution.

Using the rest of the solutions given for each function, numerous preliminary concepts were created as below. Some of the eliminated solutions were included in a few preliminary concepts, considering they could be replaced or improved at later stages. Each preliminary concept and the included solutions are given in the Figure 2.24.

Preliminary Concept 1: Carpenter's rule with markers
Functions included: 1, 2, 3, 4 (as given in Figure 2.17)

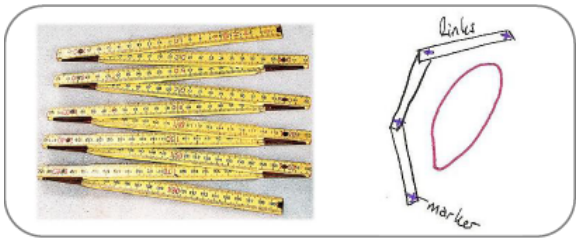

Figure 2.18: Carpenter's ruler (on left) and the links with markers (on right).(Adapted from [12])

This preliminary concept consists of links connected to each other by means of a revolute joint, like a carpenter's ruler (Figure 2.18). The markers are placed on the revolute joints, so that the distance between each marker is constant. The interconnected links are placed on the edges of the wound (or hold above), so that the location, orientation, type and size of the wound can be recorded. This concept is simple and easy to use, but requires time to shape and place the links. In addition the device might have problems with the sterilization. Moreover, it might be problematic during the calculations to determine which marker is connected to which one, since only the markers will be visible on the IR image, not the links.

Preliminary Concept 2: Non-contact manipulation
Functions included: 1, 2, 5 and 7

In this concept, several markers are placed on the lighting unit and a camera is included in a handheld device (Figure 2.19). When the surgeon wants to move the lighting unit, he points the camera to the lighting unit and pushed a button. The button activated the system to record the distance and orientation between the lighting unit and the handheld device. Then, the surgeon can move the handheld device in space and the lighting unit will follow its movement

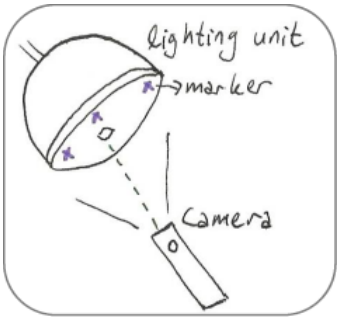

Figure 2.19: The distance between the handheld device and the lighting unit is set to constant when the button on the device is pressed. When the handheld device with the camera moves in space, the lighting unit will follow.

by trying to keep the distance and orientation to the device constant. This concept enables the surgeon to stay his or her working area and minimizes the force required to manipulate the lighting unit. One disadvantage can be that the process will require slightly longer time. On the other hand, the occurrences of the extreme cases requiring long manipulation time are minimized. Even though the surgeon position, orientation and working depth parameters are not measured directly, these data is included in the manipulation action from the surgeon, so that he coordinated the lighting unit in a position where the light beam orientation and focal depth is suitable for this use.

Preliminary Concept 3: Room mapping with IR arrays
Functions included: 1, 3, 4, 5 and 6

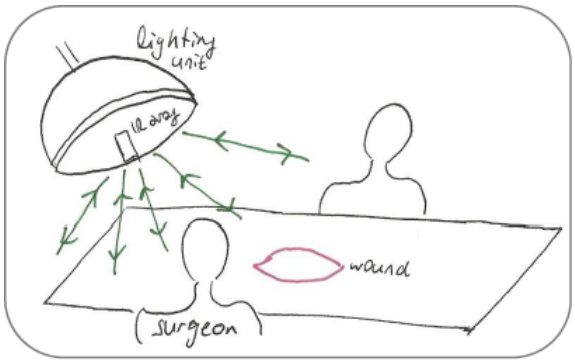

Figure 2.20: The reflectance property of the IR array is used to map the surgical environment and detect the position and orientation of the surgeons, the wound and the wound properties.

As mentioned in the previous section, the time-of-travel method with IR reflectance properties can provide a depth map of the environment. In this concept, an IR sensor working with reflectance properties is placed on the lighting unit (Figure 2.20). By sending and receiving signals, a map can be created. Using this map, the position, orientation, shape and size of the wound can be determined. Moreover, the operation point of the surgeons can be detected without disturbing the surgeon. In addition to that, the position and orientation of the surgeon and other obstacles can be detected. This solution provides many advantages such as containing various functions in one sensor, working without input from the surgeon, data collection without disturbing the surgery et cetera. One disadvantage can be the range limitations (which is given as 1.5 - 3.5 meters for the Primesense sensor in the Kinect system [30]) and lower accuracy with increasing distance, which result in failure for working depth recognition. Another disadvantage is the possible tissue drying effect due to the IR arrays on the open wound, which shall be tested clinically. One more difficulty associated with the system is that is requires image

processing algorithms to isolate the wound information from the depth image. The recognition of the human body is already common for such a system, but it is more challenging to detect the wound in the image, since it might vary highly in shape, depth, orientation and location.

Preliminary Concept 4: Range sensor for operation depth detection
Functions included: 1, 2, 5

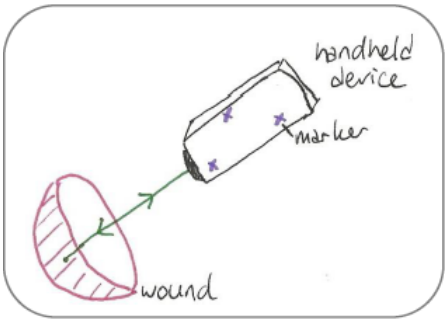

Figure 2.21: The handheld device with a laser range sensor.

Some range sensors make use of the time-of-travel method, similar to the IR array reflectance systems described before. A laser range sensor attached to a handheld device can be used for this purpose. The surgeon points the operation point with the laser and the distance to the handheld device can be calculated (Figure 2.21). For this system, the risks of using laser in the surgical environment and on an open wound shall be investigated. Similarly ultrasound range sensors can be used, but a pointer shall be incorporated to make it visible where the surgeon points.

Preliminary Concept 5: Handheld device with converging laser beams (A&B)
Functions included: 1, 2, 5

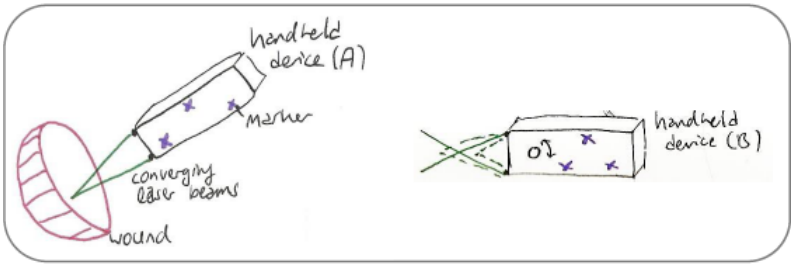

Figure 2.22: The handheld device with the converging laser beams. In version A, the beams converge on a known point. In version B, the convergence point can be adapted by means of a revolute button.

As described in the previous section, two converging laser beam can be used to determine the working depth (Figure 2.22). The laser sources are placed on a handheld device, so that they converge on a known point relative to the device (Version A). The three markers placed on the device provide information about the position and orientation of the device, so that the coordinates of the convergence point can be calculated. In version B, the convergence point can be changed by means of a revolute button, so that it is easier to manage the distance between the handheld device and the operation point. The relation between the revolution angle of the button and the convergence point is known, so that the coordinates can be calculated similar to the Version A. This solution is simple to use and does not gets into direct contact with the wound. It is useful especially for the narrow wounds, where a direct placement of the marker is difficult.

Preliminary Concept 6: Line-of-sight
Functions included: 1, 2, 6, 7 and 8

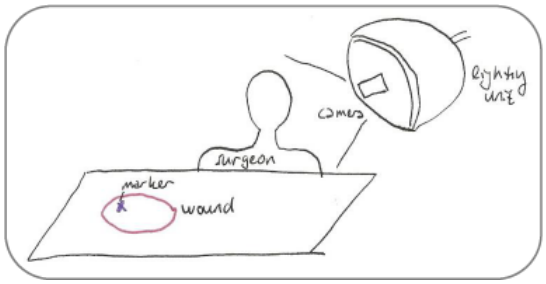

Figure 2.23: A camera is place in the lighting unit and a marker is placed on the wound location. The actuation system is activated when the marker disappears from the camera view.

In this concept, a marker is placed on the operation point, either on the wound, on the tools or on the hand of the surgeon (Figure 2.23). A camera is placed on the middle of the lighting unit, whose angle and orientation is similar or larger than the view angle of the light beam. When the line-of-sight is blocked, e.g. by the surgeon, obstacles or due to change of the operation point, the marker disappears from the camera view, so that the tracking system activates the actuation of the lighting unit to reposition. The repositioning stops when the marker is again in the view. This system works without an input from the surgeon and aims to provide appropriate lighting during the all surgery. One problem related to this solution is how to decide to which direction to move for the search of the marker. In the cases where the marker moves out of the working area, a camera with wide angle can be used, so that the marker stays in the camera view even if moves out of the light or out of a predefined working area. When the marker exists the working area, the lighting unit moves following the violated border of the working area. But this method does not provide a solution to the cases where the line-of-sight is suddenly blocked. Another problem is, a marked attaches to the tools or the on the hand of the surgeon tend to exist and enter the working area very often and a placement of a marker on the working point is not desirable. In this case, a reaction time can be defined, so that the system react the disappearance of the marker after a time period. Even with such a solution, the system is very prone to *false activation*.

2.3.5 Concepts

From the Figure 2.24, it can be easily seen the preliminary concepts did not include all the required functions. Thus, the missing functions were added to these preliminary concepts to develop a complete method satisfying the requirements. Unfortunately, this was not possible for all the six preliminary concepts due to the limitations of the principles employed. Three concepts out of six stood out by their potential for further developments. In this section, these three concepts are discussed. The functions and solutions included in each final concept can be found on Figure 2.24 as well.

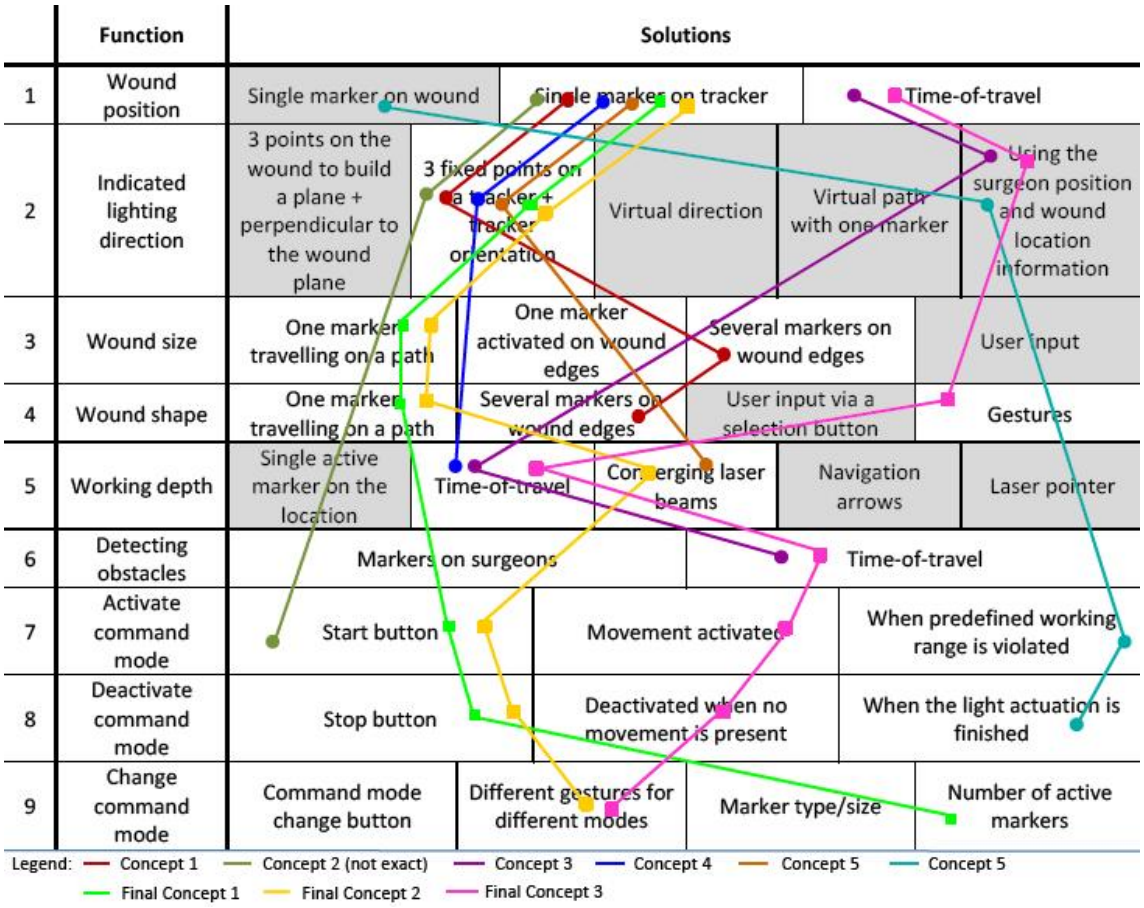

Figure 2.24: Concepts and related solutions. The solutions not included in the concept creation are marked as gray areas. Preliminary concepts are shown with a different color for each and with a circular marker. Final concepts are shown again with color codes and a rectangular marker.

Concept 1 - Virtual handle

This concept was modified from the Preliminary Concept 2: Non-contact manipulation. In the preliminary concept, the camera was placed on a handheld device and the markers were placed on the lighting unit. In this concept, the placement is done on the other way around: Two (or four) cameras are placed on the lighting unit, and three active markers are placed on the handheld device (Figure 2.25).

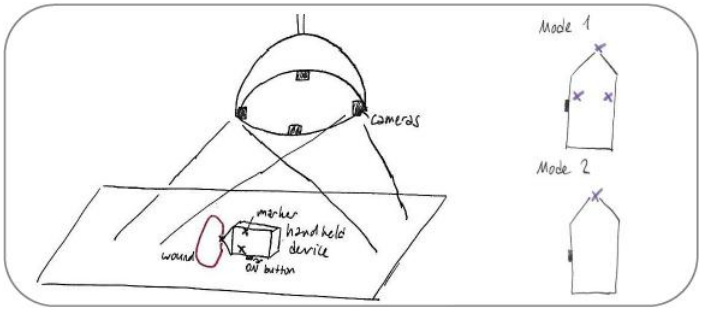

Figure 2.25: The handheld device with three markers and the cameras placed on the lighting unit (on the left). On the right, the two working modes of the handheld device is shown: Mode 1 is with three active markers and used for positioning task and Mode 2 is with one marker and used for determining the light beam properties.

The tracker can work with 2 modes: Positioning mode and light beam properties mode. The modes are indicated by the number of active markers: Activating three markers puts the system into the positioning mode and activating only one marker puts the system into light beam properties mode (Figure 2.25).

When the surgeon wants to manipulate the light, he or she follows these steps:

1. Pick up the handheld device.
2. Move the device on a position within the light beam, in free air (not on the patient).
3. Press to ON button. Three markers are activated and the position relative to the lighting unit is calculated.
4. Move the handheld device, so that the light beam falls on the desired location with the desired angle. The lighting unit follows the handheld device.
5. When desired location is reached, press the ON button once again to switch mode or twice to turn of the tracking. When the button is pressed once, only one marker is active.
6. Move the handheld device above the wound so that it forms a closed path. The wound type and size will be calculated from this path.
7. Press the ON button once to turn of the device or twice to go back to the positioning mode.
8. Put down the device or pass to the scrub nurse.

In this concept, the location of the obstacles and the working depth is not measured directly, but this information included when the surgeon decides where to place the lighting unit. The concept provides accurate and reliable manipulations on the light with low force input and within the working area of the surgeon. The handheld device is easy to use, simple and lightweight. One disadvantage is that the entire process takes time (estimated as 20 sec), but during the surgery it is expected use the positioning mode more often, which requires same or less time

as manual manipulation, assuming that a fast reacting actuation system is available. Another problem is the sterilization of the device, which can be solved by using a sterile cover. The cost of the handheld device is expected to be low (3 LED's, a battery, switch and case).

Another option can be using passive markers instead of active markers and giving the same ON/OFF effect by covering the markers. The passive markers are cheaper and more suitable for sterilization. Since passive markers are not as bright as active markers, the system might have smaller range or the system can be get disturbed other tools in the environment reflecting IR. The latter is a less likely problem for active markers, since the Wiimote system detects the brightest spots. To investigate the passive marker option, the range for the passive markers and their interaction with other tools in the surgical environment shall be investigated.

The key property of this system is that it reacts on the user input in real-time and the user observes the manipulations on the light immediately. Unfortunately, this requires an actuated lighting unit within the experiment setup. Since the controller and actuation of the system is beyond the goals of this project, such a system cannot be built for experimenting. Thus, only the tracker device and the placement of the cameras will be included in the experiment setup. Further detail on the experiment setup will be given in the following sections.

Concept 2 - Tracker with converging laser beams

This concept is modified from the Preliminary Concept: Handheld Device with Converging Laser Beams. In this concept, again two or four cameras are placed on the lighting unit and three markers are placed on a handheld device (Figure 2.26). In addition to the markers, two laser beams are placed at the end of the device, converging at 80-120 mm distance and on the same plane as the markers.

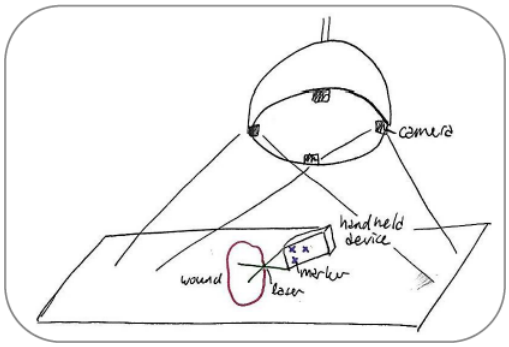

Figure 2.26: The handheld device the converging laser beam. The hotspot of the laser beam can be used to point the working spot and the wound edges.

The device is operated as following:

1. Pick up the handheld device.
2. Activate the device via pressing a button.
3. Point the operating point with the laser spot, similar to the desired orientation for the light. The position and orientation of the markers on the device is collected and the position of the laser hotspot is calculated. The light beam will follow the same direction as the handheld device.
4. Follow the wound edges with the laser spot. The path will be calculated and recorded for type and size information.
5. Turn off the device via a button.

6. Put down the device or pass to the scrub nurse.

This concept provides a good solution to get the working depth information minimizes the force input and keeps the action in the working area of the surgeon. Again, it is simple and easy to use. One disadvantage is the surgeon shall have an insight on the directing the light beam, since he needs to show the direction with the handheld device before the action takes place. In the Concept 1, the surgeon is able to see the manipulations on the light immediately and can react accordingly, but in this case he or she needs to give the correct input and expect it to be good. Another disadvantage is that there is no clear change between the pointing the depth and pointing the edges modes. A solution to that can be deactivating the device between different modes (pointing vs. drawing closed path) or assigning gestures for each mode. In addition, the accuracy might depend on the action for the following the edges: e.g. keeping the device in one location and rotating it slightly can provide lower accuracy than moving the device just above the edges. Another point worth to investigate is the safety of the use of laser beams on the patient. Moreover, the cost of the handheld device is higher than Concept 1, the sterilization is not possible except the sterile cover option and the use of passive markers does not provide a remarkable improvement on these two issues.

The implementation of the converging laser beams is not easy for an experiment setup. In addition, it might be difficult to target with laser beams. Thus, the concept in developed into a simpler version. The laser beams are replaced with a rod with a known length. The user touches the wound edges and the working point by the end of the rod and the end position can be calculated when the position and orientation of the tracker is known. Moreover, it can be used also to create a virtual volume of the wound, by marking both the wound edges and the walls deep inside the wound. This method can be used also for narrow and deep wounds, since the end of the rod does not need to be at the view angle of the tracking system. Again, further details are available in following sections.

Concept 3 - IR depth mapping with Kinect

This concept is a modified version of the Preliminary Concept 3: Room mapping with IR arrays. It works with the same principle as described before as mapping the environment with IR reflectance. The required information shall be extracted from the depth image.

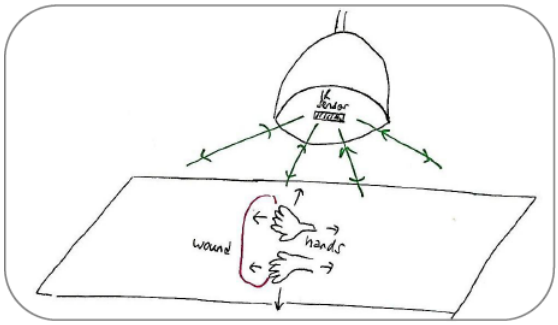

Figure 2.27: The IR sensor is placed in the middle of the lighting unit. The surgeon can use his hands to operate the lighting unit.

In this concept, there are two possibilities to gather the necessary data from the depth image. The first possibility is to use reflectance markers in a particular shape, such as cross, triangle etc, so that they can be detected in the image easily. This marker can be placed next to the wound or on a handheld device. The movements of the marker in space can be recorded and used to control the lighting unit, similar to the previous two concepts. Another possibility is to make use of the hands of the surgeon, so that he can control the light with gestures (Figure

2.27). For each manipulation of the light, e.g. bring light closer, go left, go right, widen the area, make the area smaller etc... a different gesture can be defined.

A sample operation flow can be as following:

1. Open your fingers and raise your hand above the wound to start the light manipulation process.

2. Move your open hand in space (left, right etc...). The lighting unit will follow your hand. Move your hand closer to the wound to bring the lighting unit closer, and away from the wound to move away the lighting unit. Form a fist with your hand when the lighting unit is at the desired position.

3. Open both of your hands to change the diameter of the lighting unit. Move your hands away from each other to increase the diameter and closer to each other to decrease the diameter.

4. To change the focus, again with use two open hands. When the hands are moved closer to the wound, the focus will move deeper into the wound. When the hands are moved away from the wound, the focus will move to an upper position.

5. Form a fist to stop the system.

This concept is simple and easy to use for the surgeon. It does not create any problems due to sterilization, since no additional devices are introduced into the sterile area. The system is also able to recognize the position and orientation of the surgeons and other obstacles in the environment. One disadvantage is the need of the use of two hands for manipulating the light beam properties, since in many cases the surgeon has one hand busy with holding clamps, suction or other tools. Another disadvantage is that higher computational and processing power is required for analyzing the depth image compared to the Wiimote system and this may also result in increased lag times.

The reflectance property of IR arrays is being used on the Xbox Kinect sensor, which has been on the market since November 2010. When this project was in progress, various groups and people were investigating the use of Kinect sensor in non-gaming applications, such as controlling computers, virtual reality and 3D reconstruction. Some drivers and applications to connect the Kinect to a computer and acquire depth mapping and RGB camera outputs were shared on the Internet, but they were in development stage, not stable and difficult to operate. At this level, advance level coding skills were required for working with the Kinect sensor on a different environment than Xbox. Although Kinect sensor provided a low cost and good solution to the problem, it needed extensive research.

Out of these three concepts, only Concept 2 was selected for further experiments. Although the Kinect sensor was very promising, but still on an early stage of developments and required extensive computer programming experience. The main difference between Concept 1 and Concept 2 was the user-interaction: In the first concept, the user guides the lighting unit actively and can see the results of the action immediately. On the second concept, the user gives the necessary commands to the lighting unit and expects it to act on the desired way and can only interfere after the action is finished. Although the working principles of these two concepts were different, the both concepts included a handheld device with three active LED markers mounted on, which was used in a similar way. So, one single model of the handheld device could be used to evaluate both concepts. On the other hand, a major difficulty was the lack of an automated lighting unit. Such a system requires extensive research and some additional costs, and was beyond the focus of this project. Thus it was not possible to be evaluate the main principles of Concept 1. Given that, only Concept 2 was constructed.

2.4 Realization of the Final Concept on a Model

The constructed model for Concept 2 can be seen in Figure 2.28. A $10x10cm$ circuit board with LED's was mounted on a wooden rod o $6mm$ diameter. The wooded rod ended with nail-head. The circuit board was connected to the mains via an 3V adapter. The on-off switch enabled the user to activate or deactivate the LED's.

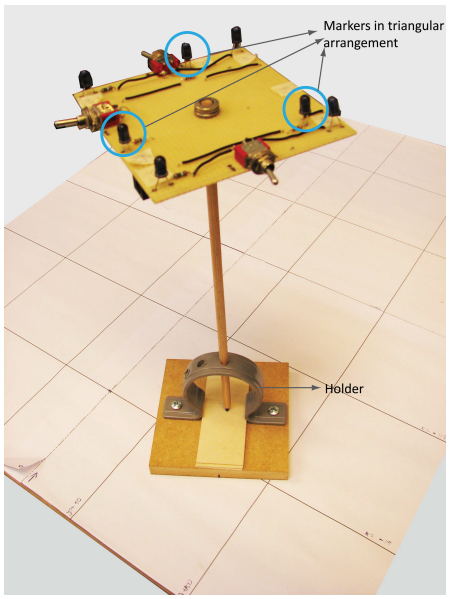

Figure 2.28: The model of the pointer. 3 LED's were mounted on a circuit board, which is placed on a wooded rod. Here, the model is seen on the holder. The extra four LED's visible on the picture can be ignored.

2.4.1 Important aspects of the model

Even though the model seems to be simple and straightforward, some important decisions were made during the construction:

Pointer rod length: The length of the pointer rod was an important parameter for the user comfort and tracking accuracy. The pointer should enable the user to reach even to the points deep in the wound and provide sufficient space for a good grip. On the other hand, the accuracy was expected to be reduced with increasing rod-length due to the extrapolation of the end-point position. To determine this parameter, other surgical instruments used during the surgery were investigated. Most similar instrument to this concept was found as the *coagulator pencil* [17]. Different lengths of the coagulator pencils are available on the market. A middle size pencil was chosen as representative and the rod length was set to $250mm$.

Marker type and size: For this application, active markers were preferred, since they have a larger working range with a smaller marker size. As active markers, 940nm high power infrared emitting diodes from Vishay Semiconductors (Model no: TSAL6400) [37] were used, since the Wiimotes are reported as sensitive to on the wavelength of 940nm [6] and this wavelength is out of the operating spectrum of the common surgical lighting systems [19]. On the other hand, this IR LED's have a limited view angle (25 degrees) and thus prone to the line-of-sight issues. LED's have a diameter of $5mm$ and can easily be placed on a circuit board together with a resistor.

Number of markers and their placement: It has been reported that the accuracy increases with the increased number of the markers and with the increasing distance between the markers [29, 33]. On the other hand, the maximum number of markers tracked simultaneously was limited to four for each Wiiremote (add ref). Moreover, a high distance between the markers is difficult to be handled by the user [14]. Thus, a balance between the accuracy and usability should be found. Another important point was the occurrence of occlusions. As a result of occlusions, the tracking system could recognize one or more markers as a single marker and fail to perform the tracking. To prevent the occlusions, the distance between two markers should be greater than two times of the minimum recognized distance. This distance was determined as $4cm$ for the Wiiremote tracking system (See Section 2.5.5, so that the minimum distance between each marker was set as $86mm$.

Another issue was the choice of 2D or 3D spread for the markers. There are no guidelines found in the literature to prefer one method over to another in a case similar to us. Usually 3D spread has been used to prevent occlusions and often for passive spherical markers [29]. In our case, the view angle of the LED's was too small (25 degrees) to make use of this principle, so that 2D spread was preferred for ease of calculations.

One last point to consider was the placement of the markers on the 2D spread plane. One strategy in the literature [14] suggests to choose the marker distances as multiples of the minimum allowable distance. This strategy is useful to distinguish the markers based on the distances in between, so that the orientation of the circuit board can be calculated correctly. When we apply this strategy to our case, the marker distances increased beyond reasonable measures (more than 340mm for four marker case). Thus, another strategy should be employed which did not require to distinguish the markers for orientation calculations. The solution was to place three markers as a equilateral triangle and to locate the pointer rod perpendicular to the triangle at the center of gravity (See Figure 2.28). This method eased the calculation of the position of the pointer tip.

2.5 Experiments

The previously developed concept was investigated further using an experiment setup and the developed model. The setup consisted of two main parts: the surgical environment and the tracking system. In the surgical environment, an environment resembling the surgery was created, such as surgical table, wound, and the lighting unit. The second part consisted of the Wiimote tracking system and the constructed model.

2.5.1 Goals of the experiments

The first step for preparing the experiment setup was to define the goal of the experiments and the data to be measured for the analysis. The first goal was to demonstrate the functionality and suitability of the selected concept. This was done by evaluating the performance the using following aspects:

i. Precision

ii. Accuracy

iii. Fail cases

iv. Wound reconstruction

The second goal was to test the concepts under different conditions in various scenarios. These can be listed as following:

A. On different wound locations (Directly under the light, near the boundaries, etc...)

B. With different indicated lighting directions (Vertical or at different angles)

C. With different wound shapes and dimensions

2.5.2 Requirements for the experimental setup

The experimental setup should satisfy following requirements:

- Providing reliable and repeatable quantitative data for analysis
- Realistic in terms of resembling the surgical environment
- Low cost
- Easy to construct
- Portable
- Easy to calibrate

2.5.3 Surgical environment

The first part of the experiment setup was the surgical environment, which is investigated in this section in details. The surgical environment includes many devices and instruments, as well as surgical team members, but not all of these elements was integrated in the experiment setup. In this section, the relevant elements was selected and realized as following.

2.5.3.1 Elements in the surgical environment

1. **Surgical team:**

   (a) *Surgeon:* The medical staff performing the surgery. She or he is the main user for the surgical instruments and dressed up in sterile scrubs.

   (b) *Second surgeon or surgical assistant (Optional):* It is common to have another surgeon or surgeon-on-training assisting the primary surgeon through the process, again dressed up in sterile scrubs. For complex procedures, the surgery can be performed as a dual task with two surgeons. In rare cases, more surgeons can join the team, e.g. operations with incisions in different body locations.

   (c) *Scrub nurse:* The scrub nurse assists the surgeon(s) through the process. She or he delivers surgical tools from the sterile table to the surgeon(s) and uses some tools if necessary, e.g. clamps, suction etc... She is again dressed in sterile scrubs.

   (d) *Circulating nurse:* Circulating nurse works in non-sterile field and assists the procedure by providing tools to the sterile area, monitoring the patient, filling out paperwork etc

   (e) *Anesthesiologist:* Anesthesiologist is responsible for putting the patient under anesthesia and monitoring his or her status.

2. **Operating table:** Operating table is where the patient is placed safely during the operation. The average dimensions can be given as 2000x500mm with an adjustable height from 500 to 1000mm ([3, 32]). Commonly it consists of sections which can be moved or tilted, so the patient can be placed in a position suitable for the surgery (Figure 2.29).

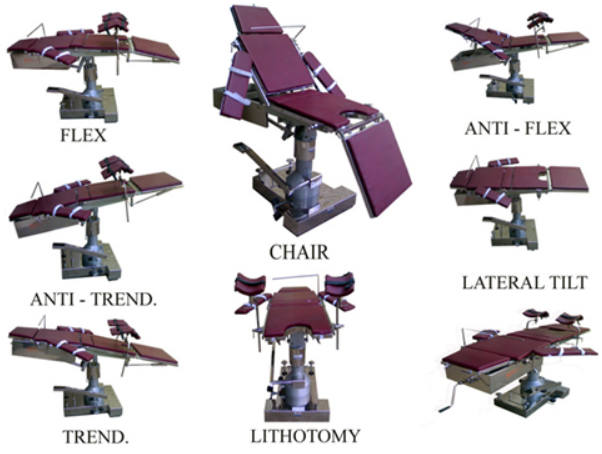

Figure 2.29: Operation table in different positions.(From [32])

3. **Surgical instruments:** Surgical instruments are the tools used by the surgeon to manipulate tissue and perform the surgery. The surgical instruments have a high variety from classical scalpels, scissors and clamps to high-tech laser cutters, endoscopes or drills. Surgical instruments shall be sterile to be used on an open wound. The instruments are kept on the instrument table during the operation and given to the surgeon by the scrub nurse.

4. **Surgical equipment:** Surgical equipment is the relatively larger sized devices used during the operation, e.g. monitors, X-ray or CT scan, suction pumps etc These are commonly placed in the non-sterile area, but can be brought closer to the patient when they are in use.

5. **Surgical lighting:** Surgical lighting is placed above the operation table. It provides high illuminance light on the working area of the surgeon. It consists of one or more lighting fixtures hanging on a pendant system fixed to the ceiling. The lighting fixtures can be moved and tilted above the table to the desired position.

6. **Surgical drapes/sterile clothing:** Surgical drapes are sterile cloths placed on the patient's body and fixed around the wound usually with a tape. It covers all the area on the patient besides the operation area (Figure 2.30). It reduces the risk of contamination, provides a clear working area for the surgeon and protects the patient. The drapes are also used to cover the instrument table and to provide a sterile place to placing instruments. The surgeons and the scrub nurse wear sterile scrubs, sterile gloves and cover their mouth and hair. The hands, arms and chest of the scrubbed person are *most sterile* areas and they are not allowed to get into contact with *less sterile* areas in the body, such as head, face, shoulders, back etc...

Figure 2.30: Surgical drapes placed on the patient.(From [2])

7. **Patient:** The last but not least element in the operation room is the patient. He or she is placed on the operating table according to the type and location of the surgery, put under anesthesia and covered with surgical drapes except the incision area. During the surgery, while the surgeon works on the wound, the anesthesiologist and circulating nurse follow the condition of the patient and his or her stats.

2.5.3.2 Elements to be included in the experiment setup

From a practical point of view, it was not possible to include all the previously described elements in the experiment setup. On the other hand, the setup should be as realistic as possible. Thus, a selection of most important elements was done for constructing the setup. The selected elements was listed in two categories: Basic setup and scenarios.

Elements in the basic setup

The elements included in the basic setups were as following (Figure 2.31):

1. **Operating table:** A white, flat surface with minimum size of 500mm width and 500mm length. It should be lightweight for ease of repositioning and its height should be variable within at least 500mm.

2. **Surgical lighting:** A simple model of the surgical lighting. A circular fixture with a diameter of 700mm to 1000mm was needed, which was comparable to the current systems. This fixture should be placed minimum 700mm, maximum 1700mm away from the operating table, since in current systems the volume of depth is usually placed between these distances [13]. In addition to that, the fixture should be able to turn around its central

axis and can be tilted up to 60 degrees around its horizontal axis. In addition to that, the fixture cannot be mounted on a ceiling or wall like in the real case, so that it should have a support either with adjustable height or leaving sufficient space for changing the elevation of the operation table.

3. **Work field of the surgeon:** Another important element of the surgical environment was the patient, in other words the work field of the surgeon. For the basic setup, a point close at the center of the operating table was set as the target of the surgeon and to represent the wound. The area around this point should be under room lighting and free of any obstacles. The basic wound direction was set as vertical. The work field is approximated as a single point.

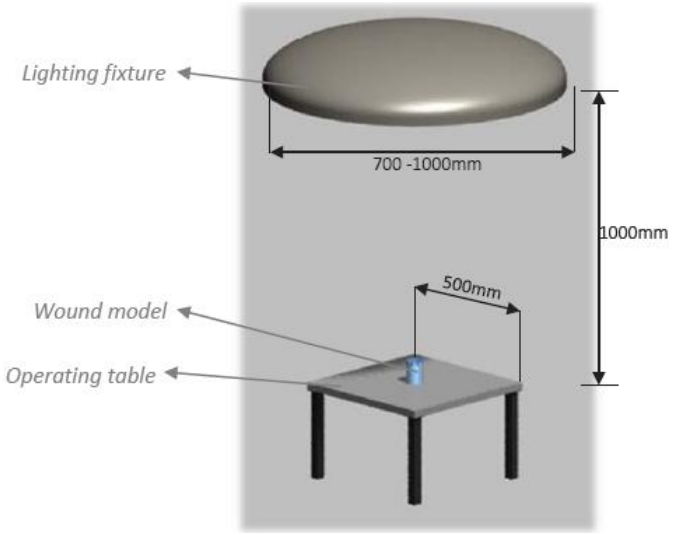

Figure 2.31: Basic configuration for the experiment setup. The lighting fixture was placed directly above the wound model, which was placed at the center of the operating table.

Elements in the scenarios

A. **Different wound locations:** In the basic setup, the wound was placed directly at below the lighting fixture at a distance of 1000mm. But this is not the case for many operations. In this scenario, the target of the surgeon was changed on the operation table within the range of the tracking system. The exact locations used for experiments is given in the *Expriment procedure* (Section 2.5.5).

B. **Different indicated lighting directions:** The indicated lighting direction was defined as the direction of the plane formed by the markers on the model. In the basic setup, the direction was vertical. On the other hand, this case is not common, and the surgeons might prefer other directions [8]. Thus, it was worth to experiment with different directions.

   (a) The indicated lighting directions was 16 degrees to the vertical axis.

   (b) The indicated lighting directions was 33 degrees to the vertical axis.

C. **Different wound shapes and dimensions:** In the basic setup, the wound was approximated as a single point. This approximation was not suitable for evaluating the wound reconstruction. A metal structure in shape of a truncated cone with the diameters of 100mm and 220mm was used for this purpose.

2.5.3.3 Materials and methods to construct the setup

The experiment setup was constructed using $50x50mm$ and $25x25mm$ aluminum profiles. $50x50mm$ aluminum profiles were used for the main body, which was a suspender of $2m$ high with a horizontal $600mm$ support mountable at different heights (Figure 2.32(a)).

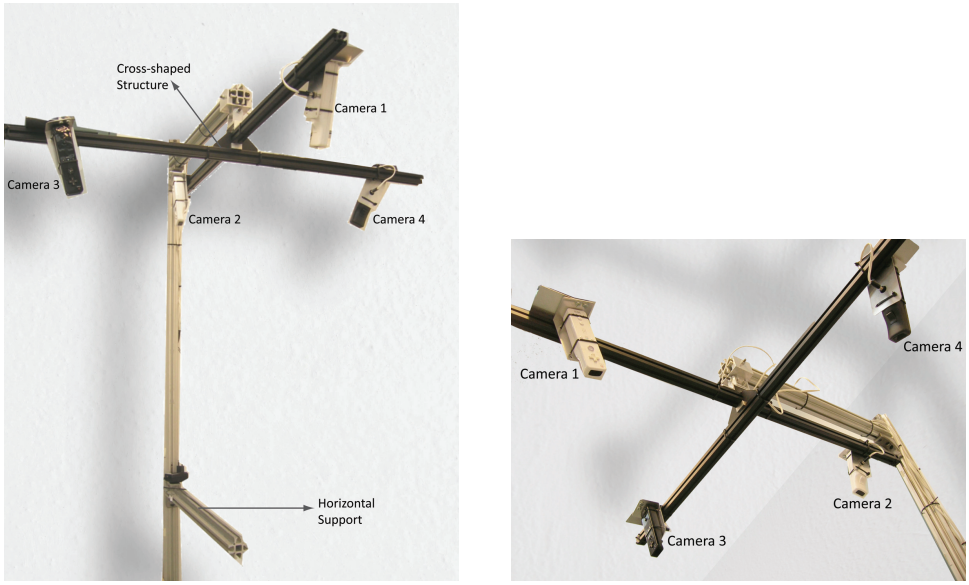

(a) The setup with the horizontal platform (b) Cross configuration of the Wiimotes

Figure 2.32: The experiment setup constructed with aluminum profiles and four Wiimotes as cameras

The $25x25mm$ aluminum profiles were fastened as a cross. The aluminum cross was connected to the suspender via a self-produced joint with two degrees-of-freedom, so that the cross shaped structure could be fully rotated around its vertical axis and can be tilted up 60 degrees around its horizontal axis. The joint parts were processed from aluminum blocks on milling and drilling machines.

Wiimotes were mounted at the four ends of the cross with an self-produced aluminum connector inclined at 20 degrees (Figure 2.32(b)). The aluminum connectors were cut and bended from $1mm$ plates. The average height of the Wiimotes was $1.8m$ above the ground. The battery compartment of the Wiimotes was canceled and the Wiimotes are connected to the mains via a 4V adapter to provide continuous and reliable use without the dependence on the battery levels. More information on the placement of the Wiimotes is given in the section about the construction of the tracking system. Besides that, all the technical drawings of self-produced parts can be found in the Appendix A.

2.5.4 Tracking system

The tracking system used for the experiments was a modified version of the Wiimote Tracking System constructed previously in the Haptics Lab [21]. This system was improved by introducing two extra Wiimotes, a new calibration algorithm and implementing camera pair selection. In this section, the detailed process of the tracking system construction can be found.

2.5.4.1 Optical tracking theory

Mathematical model for a single Wiimote camera

The IR camera within the Wiimote can be represented with the pinhole camera model similar to the CCD cameras [21]. According to the pinhole camera model, a point in space (Point X) can be mapped to the point on the image plane (Point x) through a line joining the camera center (Point C) and the Point X (Fig. 2.33, [10]). As a result of this, the coordinates of the point on the image plane is a function of its coordinates in space, related by the similarity of triangles:

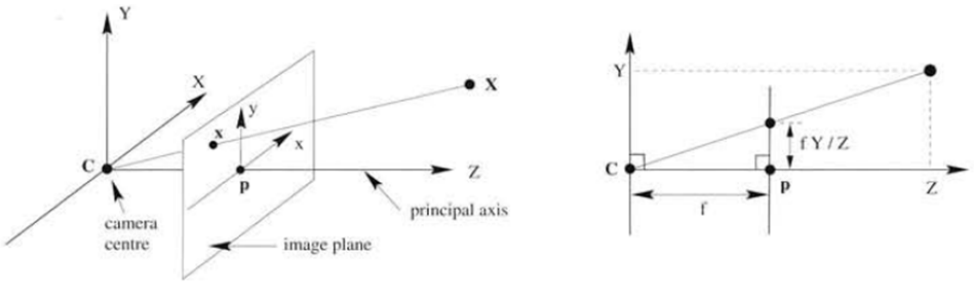

Figure 2.33: Left: Pinhole camera geometry. The Point X and the camera center C is connected with a line through the image plane. The projection of the point lies on the intersection of this line and the image plane (given as Point x). Right: The coordinates of the image Point x is a function of the coordinates in space [10]

$$\mathbf{X} = (X, Y, Z)^T \tag{2.5.1}$$

$$(X, Y, Z)^T \mapsto \left(f\frac{X}{Z}, f\frac{Y}{Z} \right)^T \tag{2.5.2}$$

The equation (2.5.2) describes the perspective (central) projection from real world coordinates to image coordinates [10]. The camera center is the center of the projection as well. The line from camera center perpendicular to the image plane is called principal axis and it intersects the image plane at the principal point [10]. The equation (2.5.2) can be written in form of a matrix multiplication using homogeneous vectors as following:

$$\begin{pmatrix} fX \\ fY \\ Z \end{pmatrix} = \begin{bmatrix} f & 0 & 0 & 0 \\ 0 & f & 0 & 0 \\ 0 & 0 & 1 & 0 \end{bmatrix} \begin{pmatrix} X \\ Y \\ Z \\ 1 \end{pmatrix} \tag{2.5.3}$$

The equation (2.5.3) is also known as projection matrix [10]. In this equation it is assumed that the origin of the image coordinate system lies on the principal point and the principal axis aligned with the camera axis. This is not always valid in practice, thus the offset between the principal point and the image origin can be expressed as following:

$$\begin{pmatrix} fX + Z \cdot p_x \\ fY + Z \cdot p_y \\ Z \end{pmatrix} = \begin{bmatrix} f & 0 & p_x & 0 \\ 0 & f & p_y & 0 \\ 0 & 0 & 1 & 0 \end{bmatrix} \begin{pmatrix} X_{cam} \\ Y_{cam} \\ Z_{cam} \\ 1 \end{pmatrix} \tag{2.5.4}$$

where p_x and p_y are the coordinates of the principal point P. The equation (2.5.4) can be rewritten as

$$\mathbf{x} = K \begin{bmatrix} 1 & 0 & 0 & 0 \\ 0 & 1 & 0 & 0 \\ 0 & 0 & 1 & 0 \end{bmatrix} \begin{pmatrix} X_{cam} \\ Y_{cam} \\ Z_{cam} \\ 1 \end{pmatrix} \qquad K = \begin{bmatrix} f & & p_x \\ & f & p_y \\ & & 1 \end{bmatrix} \tag{2.5.5}$$

where $\mathbf{x}$ is the vector of the coordinates of Point x on the image. The matrix K is called as camera calibration matrix [10]. Another assumption of the pinhole camera model is square pixels, which might not be valid for CCD cameras. Thus scaling factors m_x and m_y, defined as the number of pixels in the given direction, are introduced for x and y directions, respectively, and the K matrix is rewritten as following [10]:

$$K = \begin{bmatrix} \alpha_x & & x_0 \\ & \alpha_y & y_0 \\ & & 1 \end{bmatrix} \tag{2.5.6}$$

where $\alpha_x = fm_x$ and $\alpha_y = fm_y$ represent the focal length of the camera and, $x_0 = m_x p_x$ and $y_y = m_y p_y$ represent the coordinates of the principal point in terms of pixel dimensions. Another parameter which can be added to this matrix is the skew parameter, s. This parameter is equal to zero for most cameras, but can be non-zero in certain cases where the x and y axes of the image plane is not perpendicular [10].

$$K = \begin{bmatrix} \alpha_x & s & x_0 \\ & \alpha_y & y_0 \\ & & 1 \end{bmatrix} \tag{2.5.7}$$

where $s = \tan\theta$, and θ as the angle between the image axes. This matrix K gives information about the intrinsic camera parameters, which represent the relationship between the pixel coordinates of the image point to the camera coordinate frame.

Besides the intrinsic camera parameters, there are also extrinsic parameters, which relate the world coordinate frame to the camera coordinate frame and include the rotation and translation of the camera. In that case, a $3x3$ matrix R can represent the rotation of the camera, and a $3x1$ vector t can represent the translation.

$$\begin{pmatrix} X_{cam} \\ Y_{cam} \\ Z_{cam} \\ 1 \end{pmatrix} = \begin{bmatrix} \mathbf{R} & \mathbf{t} \\ 0 & 1 \end{bmatrix} \begin{pmatrix} X \\ Y \\ Z \\ 1 \end{pmatrix} \tag{2.5.8}$$

When we combine the equations (2.5.5) and (2.5.8), it results in:

$$\mathbf{x} = K \begin{bmatrix} 1 & 0 & 0 & 0 \\ 0 & 1 & 0 & 0 \\ 0 & 0 & 1 & 0 \end{bmatrix} \begin{bmatrix} \mathbf{R} & \mathbf{t} \\ 0 & 1 \end{bmatrix} \begin{pmatrix} X \\ Y \\ Z \\ 1 \end{pmatrix} \tag{2.5.9}$$

or in short form:

$$\mathbf{x} = K \left[\begin{array}{c|c} \mathbf{R} & \mathbf{t} \end{array} \right] \mathbf{X} \tag{2.5.10}$$

This can also be expressed as following, where P is defined as the camera matrix:

$$\mathbf{x} = P\mathbf{X} \qquad P = K \left[\begin{array}{c|c} \mathbf{R} & \mathbf{t} \end{array} \right] \tag{2.5.11}$$

Usually gathering the K matrix information is called as calibration for a single camera. But in case of multi-camera systems, not only the calibration of single cameras is important, but also the relationship between the multiple cameras shall be known.

Two view geometry with two Wiimotes

With the two view geometry from two cameras, it is possible to determine the position and orientation of a marker in 3D space via triangulation. The camera matrices are given as following [10]:

$$\mathbf{x} = P\mathbf{X} \quad \text{for Camera 1 and} \qquad \mathbf{x}' = P'\mathbf{X} \quad \text{for Camera 2} \tag{2.5.12}$$

At first the relationship between the two camera views shall be investigated. This relationship can be expressed with the *epipolar geometry*, which provides a set of constraints to describe this relationship [10].

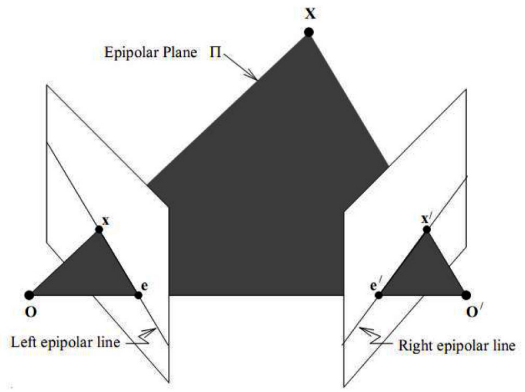

Figure 2.34: Epipolar geometry: The camera centres and the space point X form a plane, called epipolar plane. The image points x and x' lie on the same plane.(From [21])

In the epipolar geometry (Figure 2.34 it is assumed that the point in space (Point X), and the points on the image planes (Point x and x') lie on the same plane, called epipolar plane. The camera centers C and C' lie on this plane as well, connected by a line, also known as baseline. The baseline intersects the image plane at the epipole. The line where the epipolar plane intersects with an image plane is called epipolar line. Epipolar line contains both the image point (x or x') and the epipole (e or e'). This information is very useful to find the corresponding points on both image planes and to calculate the 3D position of the Point X. The relationship between the two image planes are expressed with the fundamental matrix F, using the constraints defined by the epipolar geometry. The two corresponding image points (Point x and x') are related to each other satisfying the following equation:

$$\mathbf{x'^T} F\mathbf{x} = 0 \tag{2.5.13}$$

Since the image point x' lies on the epipolar line l', the following relationship is also valid:

$$\mathbf{l}' = F\mathbf{x} \tag{2.5.14}$$

The fundamental matrix F can be computed using the camera matrices P and P'.

$$F = \left[\mathbf{e}'\right]_x P' P^{+} \tag{2.5.15}$$

where P^+ is the pseudo-inverse of the camera matrix P, $\mathbf{e}' = P'\mathbf{C}$ with $\mathbf{C}$ as the camera center, and $[\mathbf{e}'_x]$ is the matrix notation for the vector product, where

$$\left[\mathbf{e}'\right]_x = \begin{bmatrix} 0 & -e'_z & -e'_y \\ e'_z & 0 & -e'_x \\ -e'_y & e'_z & 0 \end{bmatrix} \tag{2.5.16}$$

A camera pair (P and P') defines a unique fundamental matrix F, but the converse is not valid: Several camera pairs can define the same fundamental matrix [10]. Nevertheless, the fundamental matrix F is sufficient to describe the projective relationship between the two cameras [10]. In that case the camera matrices can be chosen as following:

$$P = \left[\ I \ \middle|\ 0\ \right] \quad \text{and} \quad P' = \left[\ [\mathbf{e}']_x F \ \middle|\ \mathbf{e}'\ \right] \tag{2.5.17}$$

or in general canonical form as

$$P = \left[\ I \ \middle|\ 0\ \right] \quad \text{and} \quad P' = \left[\ [\mathbf{e}']_x F + \mathbf{e}'\mathbf{v}^{\mathbf{T}} \ \middle|\ \lambda\mathbf{e}'\ \right] \tag{2.5.18}$$

where v is any 3x3 vector and λ is any non-zero scalar [10]. There are various methods and algorithms available in the literature to compute the fundamental matrix F and to construct the camera matrices using the fundamental matrix.

Triangulation

If the camera matrices P and P' and the image points x and x' are known, the coordinates of the Point X in space can be calculated using the Equation (2.5.12), assuming that the Point X does not lie on the baseline of the cameras. Even this process seems straightforward; it might end in erroneous results in case of noise in the measurements and calculation of camera matrices. Thus, various methods and algorithms are suggested in the literature to acquire more accurate results.

Multiple view geometry

The two-view approach can be extended to multiple views by employing more cameras. In the case of multiple views, the fundamental matrix F is replaced by a tensor to express the relationships between the image points, e.g. a quadrifocal tensor Q^{pqrs} for four camera views [10]:

$$Q^{pqrs} = \det \begin{vmatrix} \mathbf{a^p} \\ \mathbf{b^q} \\ \mathbf{c^r} \\ \mathbf{d^s} \end{vmatrix} \tag{2.5.19}$$

In this notation, the camera matrices are shown as A, B, C and D instead of P, P' and similar. Accordingly, $\mathbf{a^p}$ represents the p-row of the camera matrix A, $\mathbf{b^q}$ the q-row of the matrix B, $\mathbf{c^r}$ the r-row of the matrix C and $\mathbf{d^s}$ the s-row of the matrix D. Using more cameras, in other words more views, provides stability to the system, but it is more difficult to compute, especially in case of four or more views. On the other hand, introducing redundant cameras is promising to reduce the line-of-sight issues, e.g. a third camera can replace one of the stereo vision cameras with blocked view.

Keeping these in mind, one of the following strategies could be employed for this project:

1. *Use of N-number of cameras for calibration and tracking calculations:* The system is calibrated by using all the cameras and the target should visible in all views simultaneously.

This method can provide more stable and accurate results. On the other hand, it requires complex algorithms and high computational power, and is prone to failures if the marker is not present in all cameras views.

2. *Use of stereo-view for tracking calculations, where the cameras are calibrated in pairs:* This solution is an combination of two or more two-view approaches. In the publication from Vader et al. [36], it has been reported that this approach may result in low accuracy, since the inaccuracies in the camera calibration tend to add up while combining the stereo-systems.

3. *Use of stereo-view for tracking calculations, where all the cameras are calibrated together:* In this case, the system is calibrated using all the cameras and later camera-pairs are chosen for triangulation. This approach had been employed by Vader et al. [36] using the algorithms developed by Svoboda [35] and Zhang [38]. A similar approach was selected for our project as the most suitable approach.

2.5.4.2 Prior Wiimote tracking system

The start up point for the construction of the tracking system was a prior system constructed in the Haptics Lab with 2 Wiimotes to calculate the 3D position and orientation in space [21]. The Wiimotes had been connected to a processing computer via Bluetooth with 100Hz using an modified version of the open source Native C++ Wiimote Library *WiiYourself!* [7]. The modified version had been called *WiiYourself! Matlab* and had used a shared memory class to transfer the Wiimote data to MATLAB. Each Wiimote had returned 2D coordinates (between 0 and 1) and the size (between 0 and 15) of four bright IR spots simultaneously with a resolution of 1024x768 pixels. The Wiimotes had been placed on a frame 0.5m above the ground, with a distance of 1m in between. They had been mounted with an angle of 40 degrees with the vertical and 9 degrees with the horizontal.

For the tracking, 8 mm passive spherical markers had been used in combination with 940nm IR arrays. The arrays had been mounted around the Wiimote, facing the same direction. For calibration, a square plate with 4 active markers on the corners had been used and the fundamental matrix had been calculated by the Normalized 8 Point algorithm given by Hartley et al. [10], where 8 image points in two stereo images had been matched. The extrinsic camera parameters, such as rotation and orientation of the cameras, had been measured and entered manually. The triangulation had been done by using Midpoint and Direct Linear Transformation (DLT) methods, and it had been reported that the Midpoint method provided better results. The MATLAB environment had been used to develop the code for the application of these algorithms and to realize the calculations.

To use this system in our application, three factors were important: The range, the precision and the accuracy. There were no data provided about range and precision, but this system had a lower accuracy than desired: $3 \pm 13mm$ geometrical error in place of $6mm$. It was reported that, an improvement in the determination of the extrinsic camera parameters is required to improve the accuracy of the system. Another improvement point was to reduce the line-of-sight issues. A system consisting of two cameras was prone to the tracking failures if one of the cameras or markers is blocked or if the markers align with each other. Thus, two additional Wiimotes were added to the system to reduce the occurrence of tracking failures.

2.5.4.3 Implementation of 4 Wiimotes

The use of four Wiimotes required modifications on the application enabling the connection of the Wiimotes to the host computer (WiiYourself! Matlab), on the calibration process and on the tracking algorithm. The similar principle employed by Vader et al. [36], is used: all four cameras were calibrated simultaneously and a camera pair was is selected at each frame for

the triangulation calculations. The details of these modifications are covered in the upcoming subsections.

2.5.4.4 Positioning and orientation of the Wiimotes

The camera positioning and orientation should be modified to satisfy the needs of the surgical lighting application. These requirements can be listed as following:

- 4 Wiimotes should be placed on a circular base.
- The diameter of the base should be between 0.7 to 1m.
- The tracking area should be as large as possible.
- The tracking depth should be at least 1m.
- The tracking volume should start 0.7 away from the cameras.
- The angle between the Wiimotes should be large to improve the triangulation [21].

Given the above defined constraints, it was aimed to achieve the maximum tracking volume with the proper positioning of Wiimotes. The remotes are placed on the ends of a cross-shape, with the same distance to the centre, which is set as 0.35m. The mounting angle for each remote is used to adjust the tracking volume. The Wiimotes has been reported to have a viewing angle of 40 degrees in and 30 degrees in vertical [21]. Thus, the goal is set the as to maximize the overlapping view area using the horizontal viewing angle (α) of a camera pair opposing each other. This process results in a non-optimized area on the plane perpendicular to the optimized plane, but this plane is already covered with the second pair. Besides achieving the maximum tracking area, another requirement was that a considerable portion of this area should stay above the 1m distance line from the fixture, since the focal distance of most of the available lighting units lay on this distance. The details of this calculation can be found in the Appendix B. The maximum tracking area was achieved at mounting angle $x = 55^\circ$, but this configuration left a small area above the 1m focal distance line. Thus, the mounting angle was $x = 50^\circ$ chosen to have more tracking volume above the line. With this configuration, the tracking volume started at a distance of $h_{min} = 417mm$ from the fixture, which satisfied the 0.7m distance requirement.

2.5.4.5 Data transfer to the host computer

The previous WiiYourself! Matlab application supported only two Wiimotes. For this project, it is modified for four Wiimotes. Also the reading of unique device identification numbers (device ID's) and timestamps for frame captures were implemented. The normalized pixel coordinates are converted back to the actual pixel coordinates. Moreover, the timing of the frame captures was improved by re-ordering the algorithm and reducing the steps between the data collection from different Wiimotes. It was decided to keep the Wiimote data acquiring and MATLAB calculations on separate programs, so that slow calculations did not effect the data transferred from the Wiimotes. Still, the enhanced WiiYourself! Matlab application is open to further improvements to provide better synchronization between the Wiimotes.

2.5.4.6 Calibration

The calibration process provides the information about the camera locations, orientation (extrinsic parameters) and the mapping from the pixel coordinates to the camera coordinates (intrinsic parameters). In the previous system, the camera locations and orientations have been

entered manually and the mapping had been done by a calibration algorithm, namely Normalized 8 Point algorithm. There were three reasons to improve this step: First, the camera location and orientations was changed for the target application. Second, this method did not result in accurate measurements and third, four cameras was be used instead of two cameras.

After reviewing the literature for the calibration processes and algorithms, it was concluded that the algorithm from Svoboda et al. [35] was the most promising option for the calibration of the multi-view systems. For this algorithm, a minimum of three cameras is required, but there is no upper limit. This method is fully automatic and uses one single bright point to calibrate all cameras simultaneously. The calibration process had been described as following on the abstract of publication from Svoboda:

> *The projections of the point is found with subpixel precision and verified by a robust RANSAC analysis. The cameras do not have to see all points; only reasonable overlap between camera subgroups is necessary. Projective structures are computed via rank-4 factorization and the Euclidean stratification is done by imposing geometric constraints. This linear estimate initializes a postprocessing computation of nonlinear distortion, which is also fully automatic.*

Theory of Svoboda's Algorithm [35]

In the Svoboda's algorithm, the cameras are represented with the pinhole camera model from Hartley as following [10]:

$$\mathbf{X_j} = [X_j, Y_j, Z_j, 1]^T \tag{2.5.20}$$

where $j = 1, ..., n$ with n as the number of object points. These object points are projected on camera coordinates

$$\mathbf{x_j^i} = P^i \mathbf{X_j} \tag{2.5.21}$$

where $i = 1, ..., m$ with m as the number of cameras. Between the camera coordinates and the pixel coordinates, a scaling factor $\lambda \in \Re^+$ exists

$$\mathbf{x_j^i} = \lambda_j^i \begin{bmatrix} u_j^i \\ v_j^i \\ 1 \end{bmatrix} \tag{2.5.22}$$

where u and v are the pixel coordinates. The points from all cameras can be combined into the *scaled measurement matrix* $\mathbf{W_s}$ as

$$\mathbf{W_s} = \begin{bmatrix} \lambda_1^1 \begin{bmatrix} \mathbf{u_1^1} \\ \mathbf{v_1^1} \\ 1 \end{bmatrix} & \cdots & \lambda_n^1 \begin{bmatrix} \mathbf{u_n^1} \\ \mathbf{v_n^1} \\ 1 \end{bmatrix} \\ \vdots & \vdots & \vdots \\ \lambda_1^m \begin{bmatrix} \mathbf{u_1^m} \\ \mathbf{v_1^m} \\ 1 \end{bmatrix} & \cdots & \lambda_n^m \begin{bmatrix} \mathbf{u_n^m} \\ \mathbf{v_n^m} \\ 1 \end{bmatrix} \end{bmatrix} = \begin{bmatrix} \mathbf{p^1} \\ \vdots \\ \mathbf{p^m} \end{bmatrix} [\mathbf{X_1} \cdots \mathbf{X_n}] \tag{2.5.23}$$

When sufficient points are collected (u and v) and the scaling factors λ_j^i are calculated, the $\mathbf{W_s}$ can be divided into $\mathbf{P}$ and $\mathbf{X}$ to obtain the P-matrices of the cameras containing the intrinsic and extrinsic parameters. The collected points are verified by RANSAC analysis to exclude the wrongly detected points [10]. The scaling factors are calculated by Sturm and Triggs' method [34], which is based on the principles of the epipolar geometry described before. The missing image points are filled in with the method of Martinec and Pajdla [23] and optimized, which

replaces the previously excluded points and also gives the flexibility that the calibration marker does not need to be visible in every single image from each camera. The methods 4-factor optimization and Euclidean stratification described by Hartley are used to get the P-matrices [10].

Application of Svoboda's Algorithm for the Wiimote system

This algorithm was available as source code based on MATLAB for Linux-systems. For our application, the MATLAB code was implemented on a Windows-system. The main task was to redefine the *paths* containing necessary documents, since the path definition methods for Windows and Unix-like systems did not match and caused errors while running the code. Another task was to change the format of the output files, so they can be viewed on Windows.

Another problem related to the implementation of the calibration process was the format of the input files. The algorithm from Svoboda makes use of a set of captured images (e.g. 500 images) as input information. The algorithm extracts the point coordinates from these images with subpixel precision. At the end of this process, three output files are created: The coordinates of the bright point on each image as a matrix with size *Number of points x Number of cameras x 3*, where the first two columns correspond to x, y coordinates and the last column represents the existence of the point in the image by value *1*. If there is no point detected in the image, all three columns are valued as *NaN*. The second file gives the presence of the points as a matrix *Idmat* with size *Number of cameras x Number of points*, where the existence of a point is denoted with *1* and the non-existence with *0*. The last file contains a matrix *Res* with size *Number of cameras x 2* to represent the resolution of each camera. These three files are used on the consecutive steps of the calibration process. On the other hand, the Wiimotes do not provide image files. Only the coordinates of the bright points (from 0 to 1024 and 0 to 768, for x and y respectively) and the size of the point (from 0 to 15) are reported to the host computer. The point extraction process by the Svoboda algorithm is already covered by the built-in processor of the Wiimote. Wiimote data is corrected for the origin and converted in a suitable format to carry on with the Svoboda algorithm.

Another required step was the alignment of the tracking system coordinates with the real world coordinates during the calibration. In the algorithm from Svoboda, this step is implemented with an additional file. In this file, the conditions of the real world system are presented to the calibration algorithm. There were several strategies available for this step e.g. using planar placed markers, using a calibration object, defining the world coordinates of several cameras and calculation the remaining camera positions and orientations etc. The most suitable strategy for our application was to enter the camera coordinates manually. In this strategy, it was not possible to gather the perfect camera coordinates since there was no information available on the location of the camera sensor within the Wiiremote. On the other hand it has been reported by Svoboda that an error of a few centimeters do not affect the calibration results significantly [35]. The origin of the world coordinate system was placed on the middle of the cross-structure at an average level of the Wiiremotes so that the world origin did not change when the cross mount was moved or rotated. This provided flexibility to the system and removed the need of calibration before each use.

The calibration was done with a single marker traveling in the working volume. The calibration marker was sampled 2500 times while it was moving in space and the first and last 10 percentage of samples was left out. Nine different calibration datasets are recorded and compared to each other to achieve the best performance. For the comparison, the following criteria is used:

- **The number of inliers after the calibration process:** The calibration process is an optimization to achieve the minimum pixel error with a camera parameter set. The resulting parameter set from the iterations was used to detect the inliers and outliers of

the calibration set. A parameter set determined with a low number of inliers tended to be less accurate to one with a higher number of inliers. Thus, the datasets with low number of inliers was discarded (Figure 2.35).

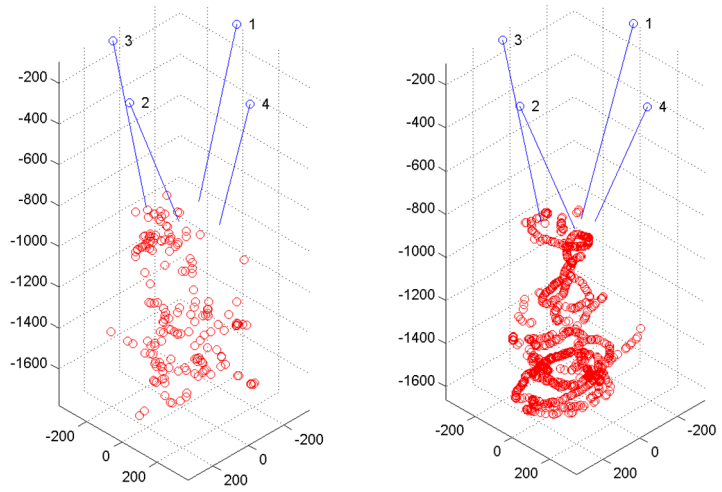

Figure 2.35: On the left: A dataset with a low number of inliers with poor distribution. Such a set was discarded. On the right: A dataset with high number of inliers and good distribution. Both of the datasets were recorded with 2500 samples

- **The distribution of the inlier's in space:** Similar to the number of the inliers, their distribution was also important. The calibration set tended to give better accuracy results for the areas where a high number of inliers was present, so that an uniform distribution of inliers was required (Figure 2.35).

- **The principal point and focal length for each camera:** All the Wiimote cameras were assumed to be identical. Some variations between the camera parameters may occur, but the parameters such as principal point and focal length should have similar values for all four cameras. These parameters were visible after the calibration progress. The calibration datasets, where high variation on these parameters are observed, can be discarded. The camera parameters of the selected algorithm can be found in Appendix C

- **Accuracy results:** The last criteria was to compare the accuracy results using each calibration set. These criteria was applied simultaneously with experiments to determine the tracking system accuracy. More details can be found on Section 2.5.5.

Moreover, different configuration parameters were tested to achieve the best results. Some important parameters were given in Table 2.7. The criteria to evaluate the calibration resulted from different configuration parameters was same as described above.

From the configuration parameters mentioned in Table 2.7, only two of them were tested with different values: initialization and update of nonlinear parameters. After trying out different combinations, and comparing the results, it was concluded that the two tangential distortion parameters can be left out since they were equal to zero. So, the last two digits of each configuration parameter was set to 0. In further investigations, the best accuracy results were achieved with default initialization of the camera view angle. Moreover, the camera view angle, principal point and radial distortion parameters needed to be updated through the optimization.

2.5.4.7 Camera pair selection

The reason to use four cameras was to compensate the instances of the occlusions and blocked views by selecting a camera pair where a proper view is possible. The first strategy was to

Table 2.7: Important configuration parameters for the calibration algorithm

Parameter	**Value**	**Explanation**
Initial tolerance	10 pixel	Valid for epipolar geometry verification. Iteratively decreased.
Number of cameras for reconstruction	3	Suggested value for most cases
Default initialization for nonlinear parameters	[45,0,0,0,0,0]	Camera view angle, principal point, radial and tangential distortions
Update of nonlinear parameters	[1,1,1,1,0,0]	Same as above
Global iteration limit	1 pixel	The input is already in subpixel level
Number of iterations	max 10	Suggested value for most cases

consider only the existence of markers in the camera views. During the tracking accuracy experiments (See Section 2.5.5), it was observed that some camera pair might provide better results depending on the epipolar geometry.

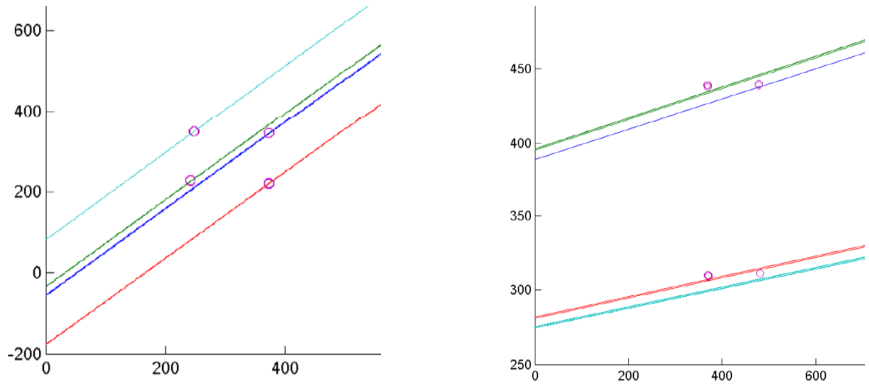

(a) Correct epipolar matching

(b) Poor epipolar matching

Figure 2.36: It is expected that the points on a camera view lie on the epipolar lines created using the camera matrices and the visible point coordinates of the pairing camera.

Ideally, the epipolar lines constructed using the visible points in one view match perfectly with the pair camera view (Figure 2.36(a)). In some cases, the match can be not perfect (Figure 2.36(b)). When the matching error was high, the triangulation also performed poorly. To deal with this issue, a global optimization with a cost function was applied to match the points in two camera views and the camera pair with the lowest cost was selected as the best camera pair for each instance. The selected camera pair was used in triangulation.

2.5.4.8 Triangulation

Again, in the previous system, it was shown that the Midpoint algorithm had performed better than DLT algorithm, but the accuracy was still below the desired values. On the other hand, Hartley and Sturm described the Midpoint method as [9], "This is not a method that one could recommend in any circumstances.". Other triangulation algorithms was considered for improved accuracy and more stable system.

In the literature, several other triangulation algorithms are available. Considering their performance and target applications, it was decided to implement the *Optimal Poly-Abs algorithm* from Hartley-Strum [9]. This algorithm has been reported as with superior 2D performance to

the Midpoint and DLT methods with a slightly higher computation cost. When the accuracy results from all three algorithms were compared, it was seen that Midpoint and DLT methods performed very similar and the Optimal performed slightly poorer for 3D position calculations. Thus, the DLT method was selected.

2.5.4.9 Post-processing

As a result of experiments on the tracking system accuracy (see Section 2.5.5), it was observed that the triangulation results need to be processed further to achieve better results. Especially in the dynamic measurements, the epipolar point matching step failed and calculations with very high errors were performed. These cases were rare but easy to filter out. For this purpose, the known distances between the marker points were calculated and the cases above a certain threshold were discarded. This step was applied as the correction in the post-processing.

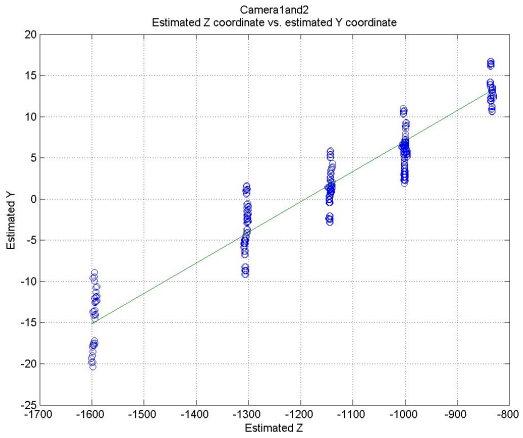

Figure 2.37: An example trend line used to correct the y coordinates relative to the estimated z coordinates.

A second observation was that the alignment of the system coordinates to world coordinates included some errors, which could be fixed using a linear correction. To determine these correction parameters, all x, y and z coordinates were plotted versus their expected values and fitted on a linear trend (Figure 2.37. The equation of the trendline was used to construct the linear correction equation. Another observation was the increased position error with increased distance from the system origin. Again, linear trend lines were used to correct the x,y and z coordinates relative to the z coordinate values. An additional correction for the origin was applied for Set B, since the origin redefined by Set A was shifted during the installation. For this correction, the first measurements for each camera pair was used. The numerical values of these post-processing parameters are given in the Appendix D.

Another post-processing setup was applied for wound reconstruction. In this algorithm, the collected point coordinates are fitted on a plane and the plane direction was calculated. After that, the points are projected on the plane. The projected points are rotated using the plane direction so that the plane including the points is parallel to the $z = 0$ plane. After that, an ellipse is fitted to the projected points to get the coefficients of the ellipse equation.

2.5.5 Procedure

To evaluate the final concept, three sets of experiments (*Set A*, *Set B* and *Set C*) were conducted. Set A aimed to measure the accuracy of the tracking system, Set B aimed to measure the accuracy with the pointer and Set C evaluated the wound reconstruction. An overview of the experiment structure can be found in Table 2.8.

2.5.5.1 Set A: Experiments to evaluate the tracking system

Exp. A.1: In this set, two $100x100mm$ circuit boards with four markers at each corner were constructed (Figure 2.38(a)) and mounted on the horizontal bar of the tracking setup with a distance of $100mm$ in between (Figure 2.38(b)). Two switches were used to activate the markers in pairs. 3 times 300 samples were taken at 5 different distance levels of the horizontal support to the cameras (840, 1000, 1140, 1300, 1600mm), covering working volume similar of the common lighting units.

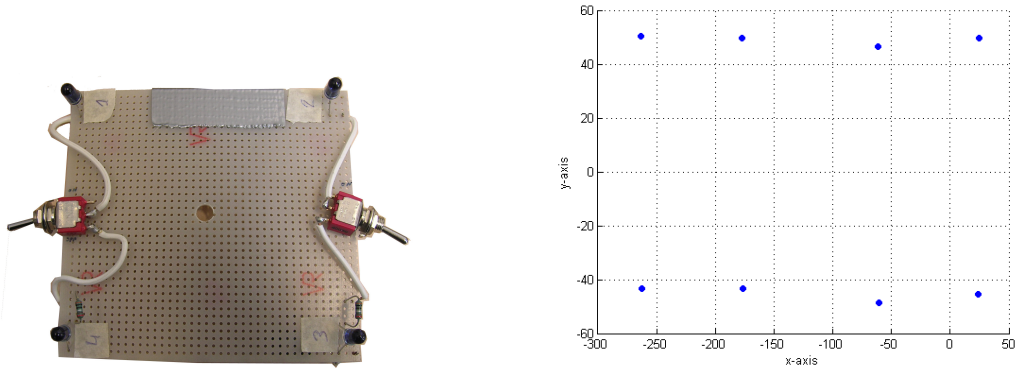

(a) Circuit board with four active markers

(b) The marker location in space, top view

Figure 2.38: The measurement points for Set A.1

In pilot experiments, this set was repeated several times to achieve best tracking results. The raw data gathered with the two boards was used several times to calculate the system accuracy and precision with different calibration sets and configurations, as well with different point matching and triangulation algorithms (see Section 2.5). This data was also used to create the correction algorithms.

Exp. A.2: In Experiment Set A.2, one board only two activated markers at $98mm$ distance was moved with free hand in the working space to collect 1300 samples with dynamic movements. This measurements were used to determine the accuracy in dynamic situation.

Exp. A.3: In Experiment Set A.3, some minor experiments are conducted to measure the minimum allowable distance between two markers. For this purpose, one marker is fixed below the origin of the system and another marker is brought closer till two markers disappear from the camera view and recognized as one. This experiment was performed at two distances: 1600mm and 840mm.

2.5.5.2 Set B: Experiments to evaluate the final concept

In this set, the performance of the pointer was evaluated statically. The pointer device was placed on a holder (Figure 2.28) and the holder was placed at different locations on a $500x600mm$ horizontal platform with adjustable height. The platform was gridded into $100x100mm$.

Exp. B.1: This experiment set was conducted to see the effect of the rotation of the markers around a vertical axis on the calculation of the pointer tip location. The model was placed on a holder vertically and close to the origin ($x = -15, y = 0$) at a fixed level so that the circuit board was approximately 820mm away from the origin vertically (*Level 1*). Three different rotations (0, 90 and 180 degrees) of the board around the

vertical axis were executed and sampled 3 x 300 times. This provided three different marker placements in space for the same pointer tip location.

Exp. B.2: This set was conducted to determine the tip accuracy and precision at different positions in 3D space. The holder was placed at 16 different locations at four different levels corresponding to the Set A (Figure 2.39). The last level (1600mm) was left out due to space limitations. 3 x 300 samples were taken at each location.

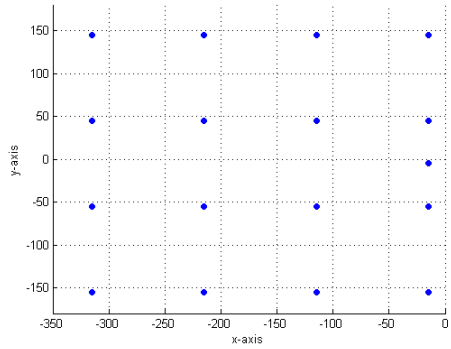

Figure 2.39: The coordinates of the targeted points in space, top view

Exp. B.3: Another set of experiments was conducted to see the effect of different pointer orientation. The pointer was placed at two different angles (16^o and 33^o with vertical) on the holder. The holder was placed in two different orientations (along x and y axes) on different wound locations at Level 1 and 3 x 300 samples were taken.

2.5.5.3 Set C: Wound reconstruction

The wound reconstruction was evaluated using a two circular metal rings with the diameters of $100mm$ and $220mm$ as wound models. The rings were placed at a fixed position on the platform. The pointer was used to follow the edges of the horizontal surface with free hand movements. The recorded points were used to reconstruct the shape (see Section 2.5.4.9). Five runs were performed for each ring. The MATLAB algorithm capturing the marker movements was intentionally slowed down for this process so that the computational power was not increased due to high number of captured frames.

2.5.6 Analysis

To evaluate the performance of the system, the following metrics were calculated (Table 2.9): In Set 1.A, the position of each marker was calculated and compared to the actual position. Moreover, the distance between markers were calculated and compared to the actual values. In Set 2.A, only the distance between two markers were evaluated. For Set B and C, the positions of three markers were estimated and their centroid was calculated. Moreover, the orientation of the plane containing these markers was determined as the orientation of the pointer. The tip position was estimated using the centroid position and the pointer orientation. In Set C, the position data was used for shape reconstruction (See 2.5.4.9). For Set A.1 and B.2, the calculations were performed for each camera pair separately and using the camera selection algorithm. For each metric, root-mean square error (RMSE) and standard deviation (STD) were calculated and the boxplot was created to evaluate the precision and the accuracy of the tracking system. The standard deviation (STD) gave information about the repeatability of the measurements and the precision of the results whereas the RMSE and boxplot gave information about the accuracy of the system.

Table 2.8: Experiment structure and variables

Variables	Experiment Set					
	A.1	A.2	B.1	B.2	B.3	C
Tools	2 Boards	1 Board	Pointer	Pointer	Pointer	Pointer and wound
Samples at each point	3x300	1300	3x300	3x300	3x300	5 x 300 for each ring
Points on x-y plane	8	2	1	16	16	2 rings
Height levels (on z axis)	5	-	1	4	1	1
Rotations (vertical)	-	-	3 (0^o,90^o,180^o)	1 (0^o)	1 (0^o)	-
Orientations	-	-	1 (0^o)	1 (0^o)	2 x 2 (16^o,33^o; x,y)	-

Table 2.9: The metrics used in each experiment set

Exp.	Metric	Description
Set A	E_{3d}	Distance of the estimated point to the actual marker position
	E_x (E_y or E_z)	Difference between the x (y or z) coordinates of the estimated and actual marker position
	E_{dist}	Error of the estimated distance between two markers
Set B	C_{3d}	Distance of the estimated centroid to the actual centroid
	C_x (C_y or C_z)	Difference between the x (y or z) coordinate of the estimated and actual centroid position
	T_{3d}	Distance of the estimated tip to the actual tip
	T_x (T_y or T_z)	Difference between the x (y or z) coordinate of the estimated and actual tip position
	E_{dist}	Error of the estimated distance between two markers
	E_{ang}	Angular error of the estimated pointer orientation
Set C	z ,a , b and α	$X = z + \begin{bmatrix} \cos\alpha & -\sin\alpha \\ \sin\alpha & \cos\alpha \end{bmatrix} \begin{bmatrix} a * \cos\theta \\ b * \sin\theta \end{bmatrix}$ with $0 \leq \theta < 2\pi$
	W_{ang}	Angular error of the estimated wound orientation
	W_z	Difference of the z coordinate for the estimated and actual wound position

2.6 Results

2.6.1 Experiment Set A

The initial results without any correction showed that the measurements were repeatable and precise but with low accuracy. In Table 2.10 are RMS and the standard deviation of the marker positions (E_{3d}) for all volume. It can be seen that the Camera Pairs 2&4 and 3&4 had a high RMSE and standard deviation compared to other pairs. Also the pair 1&4 showed slightly higher deviation. On the other hand, the selection algorithm managed to ignore the cases with high inaccuracies and produced results similar to better performing pairs. In Figure 2.40 the uncorrected boxplots of position error (E_{3d}) are given for each camera pair. These figures showed that the deviation and the median error tend to increase with increasing distance to the cameras. Moreover, the measurements at the distance of 1m were with higher error for the camera combinations including the Camera 4.

Table 2.10: The RMSE and standard deviation of the marker position and distances without correction

	E_{3d}		E_{dist}	
Camera Pair	RMSE	STD	RMSE	STD
	(in mm)	*(in mm)*	*(in mm)*	*(in mm)*
1 and 2	67.38	4.37	7.25	2.60
1 and 3	69.43	4.78	7.46	2.40
1 and 4	69.43	6.78	8.73	3.87
2 and 3	67.70	4.45	7.83	2.79
2 and 4	96.43	48.33	85.43	76.82
3 and 4	83.29	24.79	34.76	29.86
Selection	68.97	4.69	6.89	2.55

Although the precision of the system (STD) was satisfactory for most cases, the accuracy (RMSE) was much lower than expected. On the other hand, the distances between markers was calculated with a lower error (E_{dist}) (Table 2.10 and Figure 2.41). The better error for the distances (except for Camera Pairs 2&4 and 3&4) showed that, the measurements of the tracking system were precise, but there were some errors in the alignment of the tracking coordinated to the world coordinates. Again, the average error increased with the increasing distance to the cameras and the combinations with Camera 4 failed to produce reliable results for the distance of 1m.

Table 2.11: The RMSE and standard deviation of the marker position and distances without correction after correction

	E_{3d}		E_{dist}	
Camera Pair	RMSE	STD	RMSE	STD
	(in mm)	*(in mm)*	*(in mm)*	*(in mm)*
1 and 2	5.78	2.32	3.45	2.12
1 and 3	6.03	2.68	3.86	2.19
1 and 4[1]	6.81	2.94	3.75	2.12
2 and 3	6.74	2.63	4.17	2.51
2 and 4	6.32	3.80	3.30	2.31
3 and 4	5.73	3.35	3.52	2.41
Selection	6.46	3.20	3.41	2.01

[1]Excluding the measurements at 1m distance

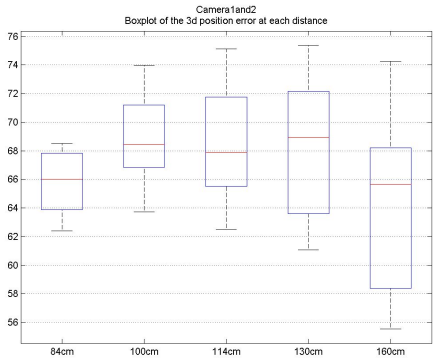

(a) Camera 1 and 2

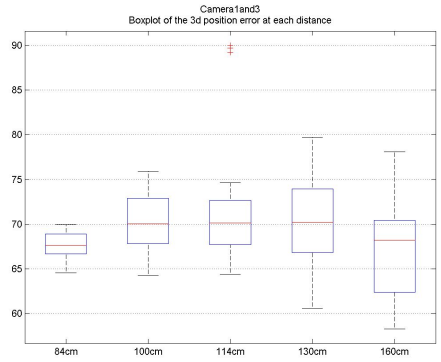

(b) Camera 1 and 3

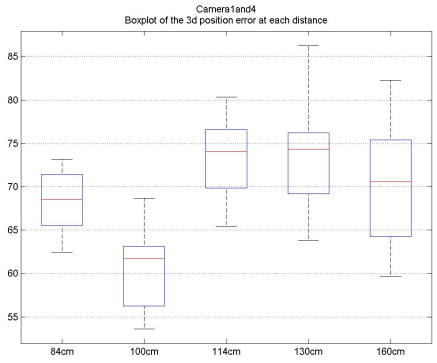

(c) Camera 1 and 4

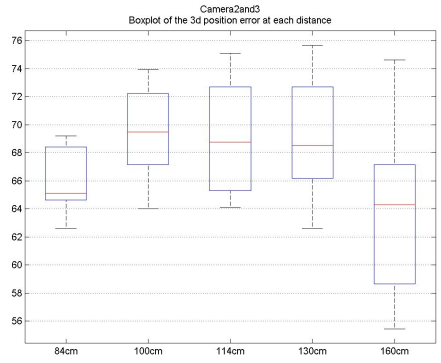

(d) Camera 2 and 3

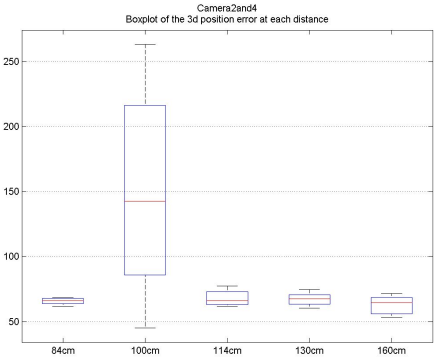

(e) Camera 2 and 4

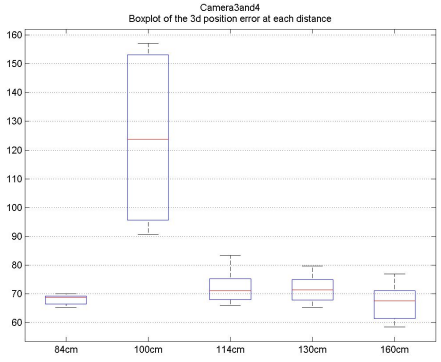

(f) Camera 3 and 4

Figure 2.40: The boxplots of the marker position error E_{3d} before correction for each camera pair at different distances to the camera mount

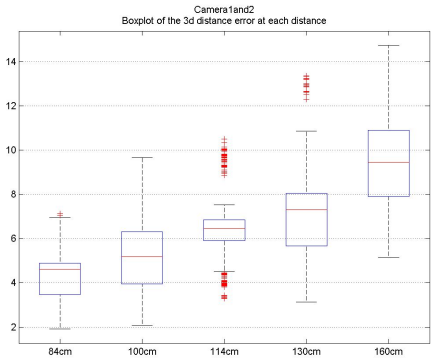

(a) Camera 1 and 2

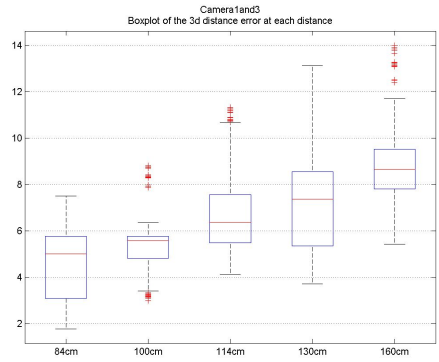

(b) Camera 1 and 3

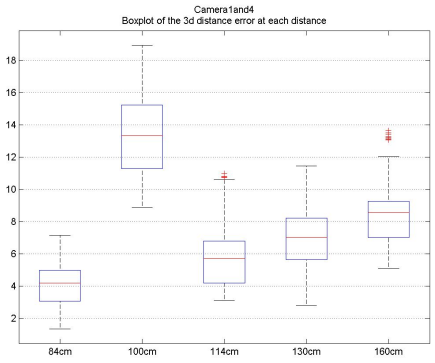

(c) Camera 1 and 4

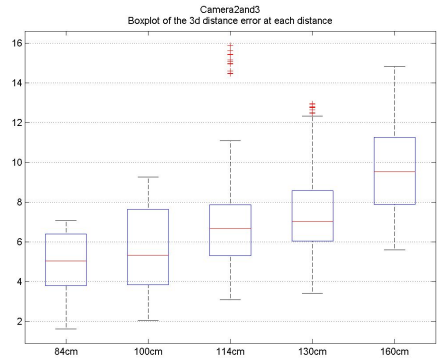

(d) Camera 2 and 3

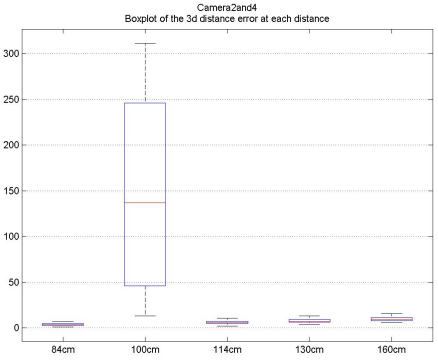

(e) Camera 2 and 4

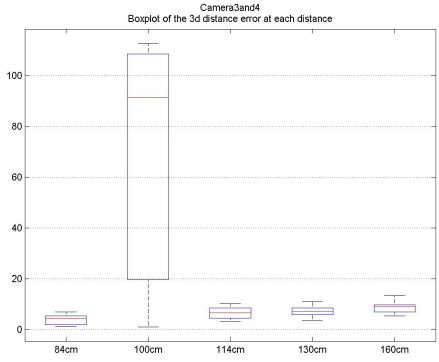

(f) Camera 3 and 4

Figure 2.41: The boxplots of the marker distances error E_{dist} for each camera pair before correction at different distances to the camera mount

After applying the corrections, the extreme errors were eliminated and a more smooth data was obtained (Table 2.11). Figure 2.44 shows again a dependency of the position accuracy on the distance to the cameras, but not necessarily an increasing error with increasing distance. The results at $1m$ distance for the camera pair 1 and 4 were excluded due to results with a very high error at this particular level. For neither any other level nor any other pair a similar behavior was observed. The selection algorithm showed slightly higher RMSE and STD for marker positions. On the contrary of the corrected position results, the marker distances showed increased error with increased distance to the origin (Fig. 2.45). On the other hand, the selection provided superior results for the marker distances. From the histogram of the selected camera pairs in Fig 2.42, it can be concluded that different camera pairs were employed through the process. The Camera Pair 2&3 is never selected.

The overall performance of the camera selection algorithm can be seen in Figure 2.43. In Fig 2.46, the position error produced by the selection algorithm was divided into its axis components. The E_x and E_y were similar, where E_z axis had slightly higher median and deviation. The E_x and E_y errors tended to deviate more with the increasing distance, whereas a similar behavior was not observed for the E_z error.

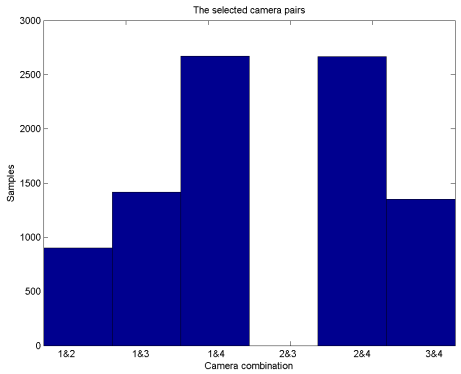

Figure 2.42: The histogram of the selected camera pairs at the Experiment Set A.1.

Besides the static measurements with two fixed boards, one free board was moved in space for dynamic measurements (Exp. A.2). The results for the distance error E_{dist} of two markers can be seen in Figure 2.47. The RMSE is calculated as as 3.26mm with 1217 survived samples (out of 1300). In the histogram it can be seen that the different camera pairs were employed through the process.

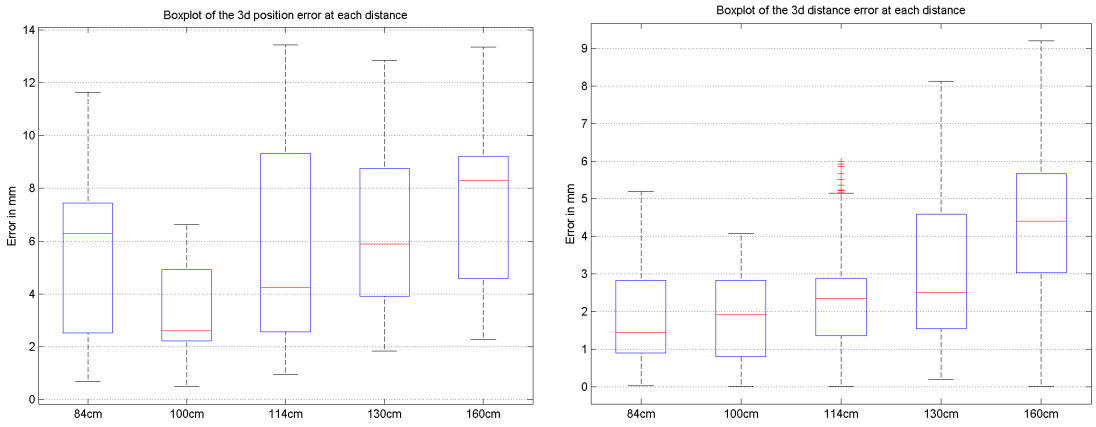

(a) Marker position (b) Marker distances

Figure 2.43: The boxplot of E_{3d} and E_{dist} for the best camera pair selected at each instance according to the epipolar geometry principles

Another series of experiments (Set A.3) were performed to measure the minimum allowable distance between two active markers. It has been found that the minimum allowable distance is 20mm and 40mm, respectively.

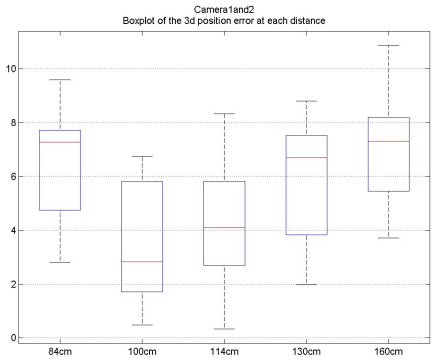

(a) Camera 1 and 2

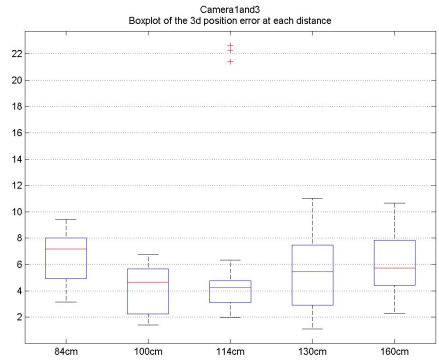

(b) Camera 1 and 3

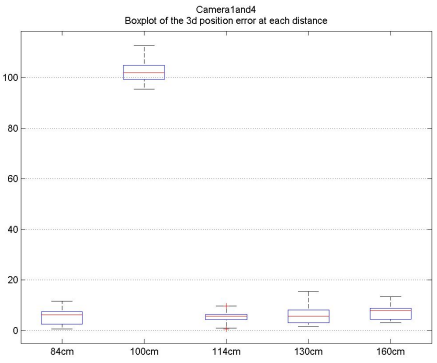

(c) Camera 1 and 4

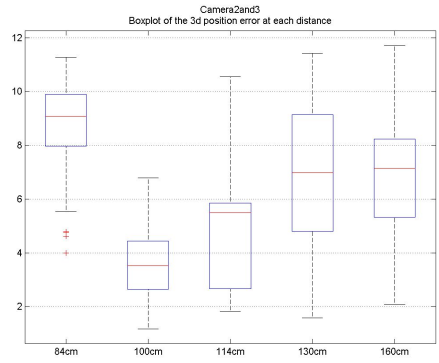

(d) Camera 2 and 3

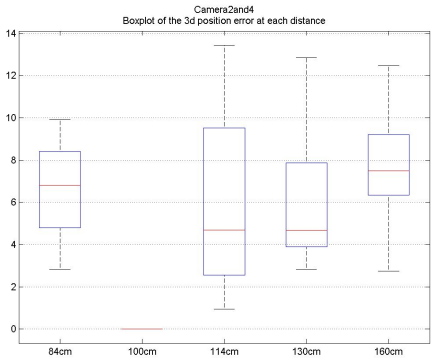

(e) Camera 2 and 4

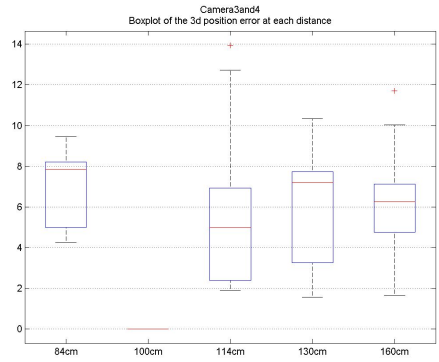

(f) Camera 3 and 4

Figure 2.44: The boxplot of the marker position error E_{3d} for each camera pair after correction at different distances to the camera mount

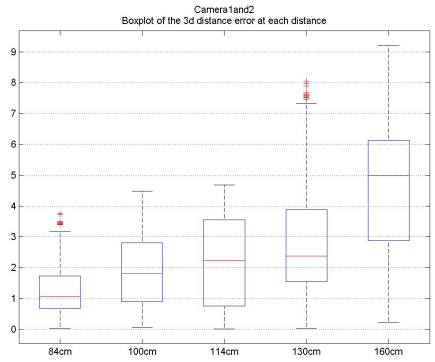

(a) Camera 1 and 2

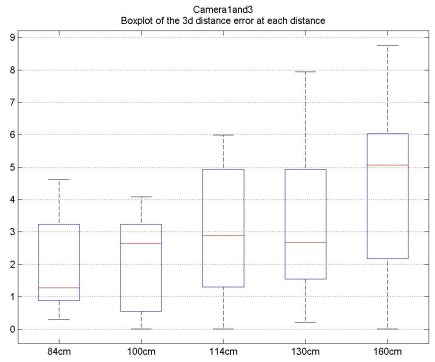

(b) Camera 1 and 3

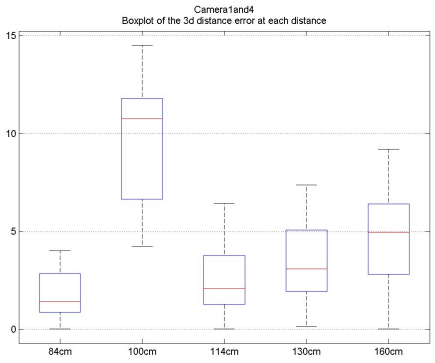

(c) Camera 1 and 4

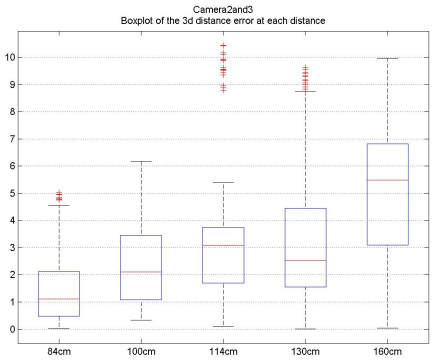

(d) Camera 2 and 3

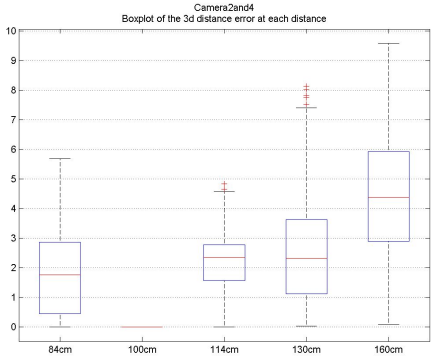

(e) Camera 2 and 4

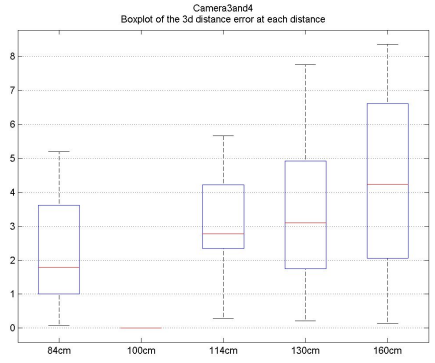

(f) Camera 3 and 4

Figure 2.45: The boxplot of the marker distance error E_{dist} for each camera pair after correction at different distances to the camera mount

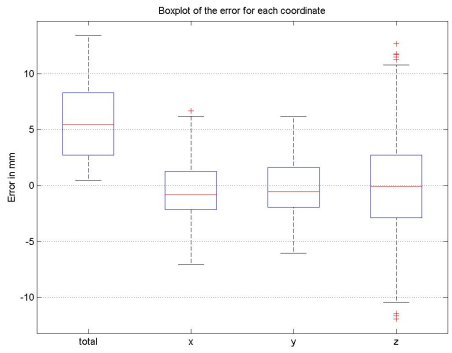

(a) Total Error

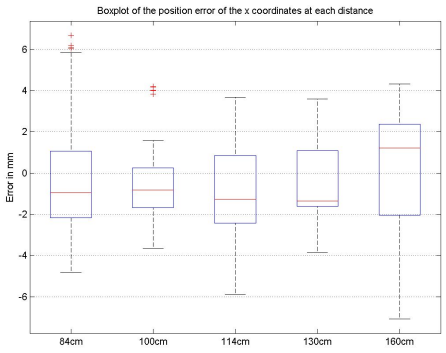

(b) X-error

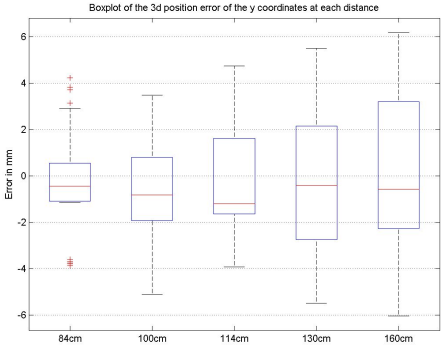

(c) Y-error

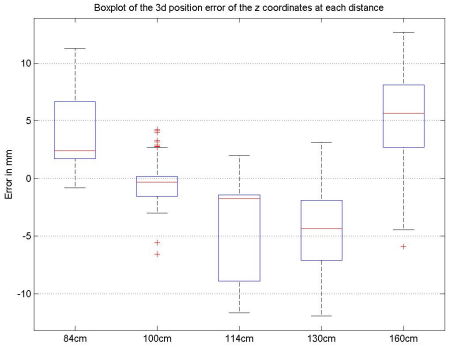

(d) Z-error

Figure 2.46: The boxplot of the position error divided into coordinate components

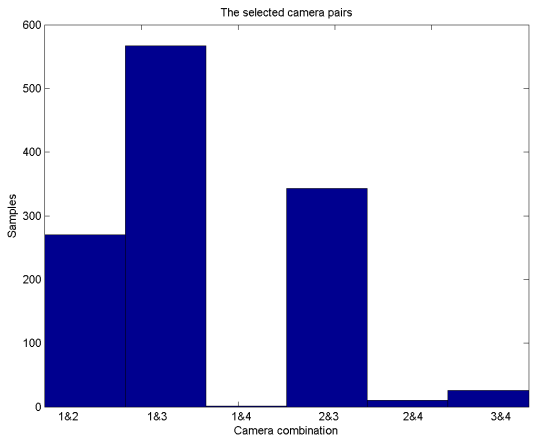

(a) The histogram of the selected camera pairs

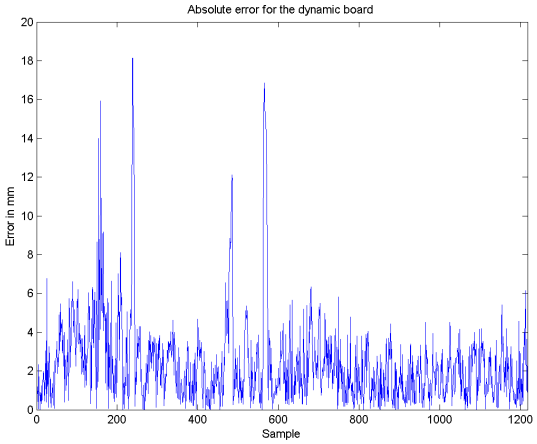

(b) The absolute error for each sample

Figure 2.47: The dynamic measurements with the moving board

.

2.6.2 Experiment Set B

For this set, the previously defined selection algorithm and corrections were applied.Figure 2.49 shows that the results of different rotations were very similar to each other. On the other hand, the median of the error for the tip position was remarkably higher than for the centroid position. The deviation, in other words the size of the boxplots, was small for all cases, but the number of outliers was higher for the tip measurements. Another important measure was the angular error for the orientation of the plane formed by the three markers, which also indicates the lighting direction. For all rotations, the indicated lighting direction was expected to be perpendicular to the horizontal platform. Again, the angular error deviated slightly from expected results, but it showed similar behavior for all rotations (Figure 2.48). This deviations were also reflected to the tip calculations. Another observation was that the tip position was calculated significantly away from the centroid, so that a construction error existed for the model. Moreover, the accuracy was lower than for the dataset used in Set A. A considerable amount of the position error both for the centroid and the tip was due to error in the y-axis.

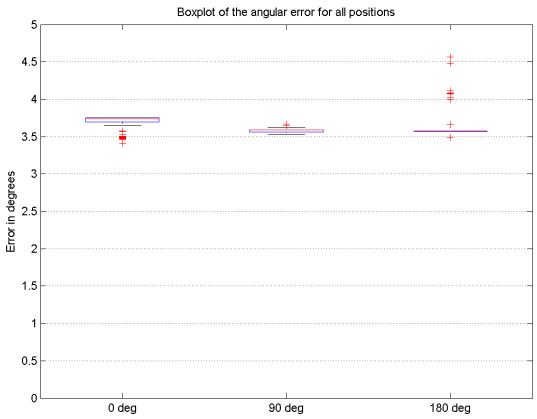

Figure 2.48: The boxplot of the angular error E_{ang} of the plane formed by the three markers.

Set B.2 was conducted to evaluate the pointer at different positions in space. Again, the results from camera pairs and selection algorithm were compared. According to Figure 2.50, the median of C_{3d} and T_{3d} for each camera pair was remarkably different. On the other hand, the relationship between the tip and centroid was similar for all pairs. In Table 2.12 it can be seen that the RMSE and STD for C_{3d} and T_{3d} were highly varying among the camera pairs, especially high values were observed for camera pairs 2&3 and 2&4. On the other hand, the angular orientation errors (E_{ang}) were similar to each other.

Table 2.12: The RMSE and STD of the error for centroid and tip positions and the orientation of the pointer

	RMSE			STD		
	C_{3d}	T_{3d}	E_{ang}	C_{3d}	T_{3d}	E_{ang}
Pair	*mm*	*mm*	*deg*	*mm*	*mm*	*deg*
1&2	10.27	25.40	4.26	4.08	9.93	1.55
1&3	16.88	34.75	5.53	9.50	12.33	1.72
1&4	20.00	31.97	5.30	9.25	10.19	1.54
2&3	47.52	59.22	6.80	22.27	20.06	2.21
2&4	19.32	31.70	4.69	11.35	12.84	1.94
3&4	33.50	47.48	6.09	16.47	15.65	1.35
Selec.	13.23	26.75	4.36	7.93	11.77	1.65

Figure 2.51 shows the results with the selection algorithm. Here, the median error for the

tip position was almost two times larger than the median error for the centroid. Similarly, the deviation of the error was higher for the tip position, even some instances with very high errors (50 to 80 mm) were observed. Furthermore, both RMSE and standard deviation of C_{3d} and T_{3d} were remarkably higher than E_{3d} in Experiment Set A (Table 2.12). On the other hand, the selection algorithm managed to provide results with low RMSE and STD compared to some pairs. Both the centroid and tip position error (C_{3d} and T_{3d})increased slightly with the increasing distance to the cameras. The increase in deviation of the position error was more obvious for the tip. An increase in the median error was not observed for the angular error E_{ang}, but the deviation again increased with increasing distance. In the histogram, it can be seen that the camera pair 1&2 was preferred on the contrary of Set A.

When RMS and STD of the distance error E_dist between the three LED markers are calculated, it was seen that they were comparable to the marker distances in Experiment Set A, except the higher RMSE and STD for camera pair 1 & 4 (Table 2.13).

Table 2.13: The RMSE and standard deviation of the distance between the marker LEDs

Camera Pair	RMSE	STD
1 and 2	4.65 mm	2.10 mm
1 and 3	3.38 mm	2.15 mm
1 and 4	6.38 mm	2.43 mm
2 and 3	4.26 mm	2.15 mm
2 and 4	2.00 mm	1.19 mm
3 and 4	2.98 mm	1.31 mm
Selection	4.62 mm	2.12 mm

Experiment Set B.3 was performed to see the effect of pointer orientation on the target accuracy. As seen in Fig. 2.52, all five rotations (four in the figure and the vertical configuration from Set B.2) provided similar median errors and deviations. For all rotations the total error was dominated by the error in the y-axis. Moreover, some outliers were observed for all cases. Furthermore, the angular error was similar for all rotations (Fig. 2.53. Some rotations provided a slightly higher deviation, but there could not been found a pattern on this behavior. The camera selection histograms showed that the Camera Pair 1&2 was preferred for all orientations (Fig. 2.54). Other cameras were also selected depending on the orientation.

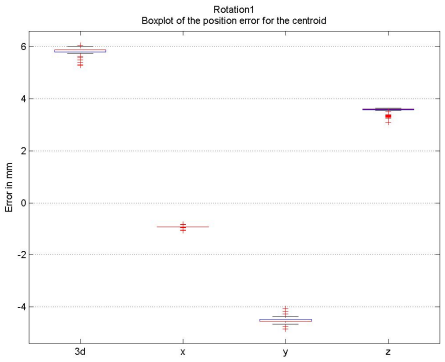

(a) Rotation 1, Centroid

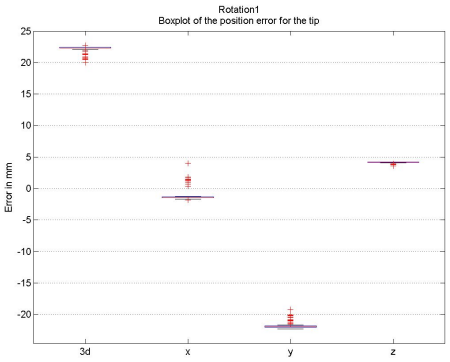

(b) Rotation 1, Tip

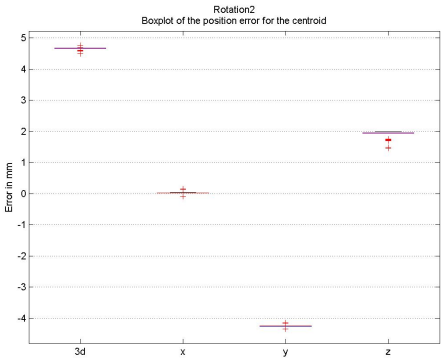

(c) Rotation 2, Centroid

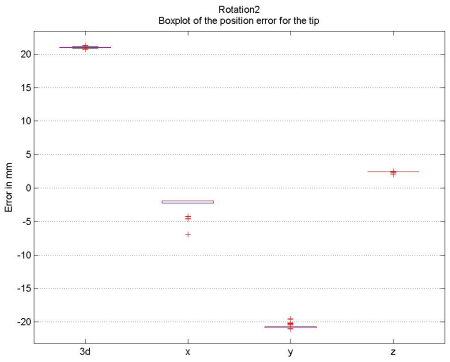

(d) Rotation 1, Tip

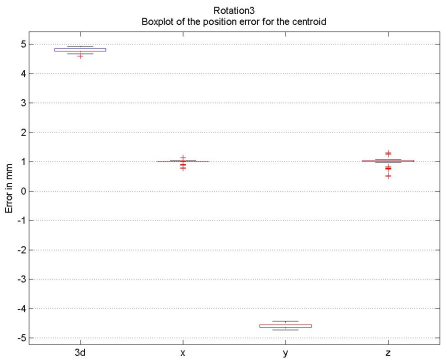

(e) Rotation 3, Centroid

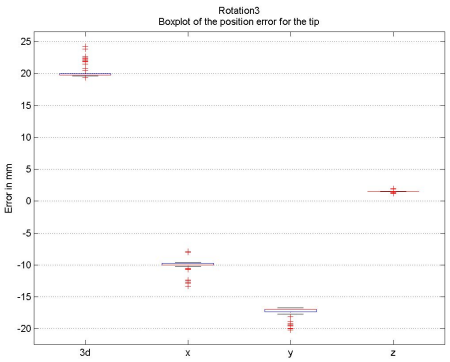

(f) Rotation 3, Tip

Figure 2.49: The boxplots of the C_{3d} and T_{3d} for each rotation, after correction

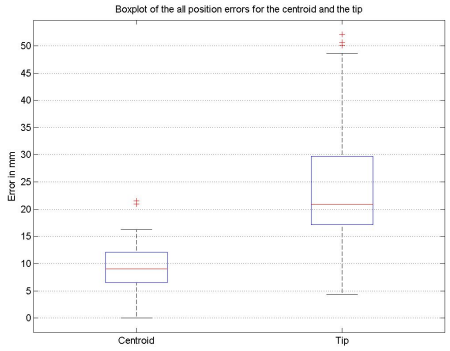

(a) Camera 1 and 2

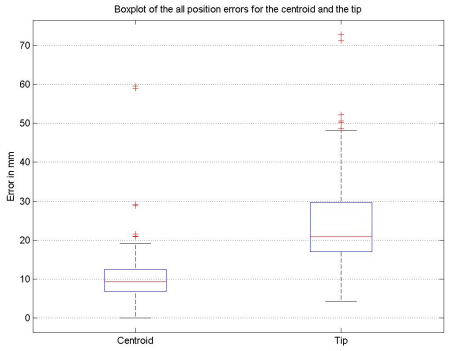

(b) Camera 1 and 3

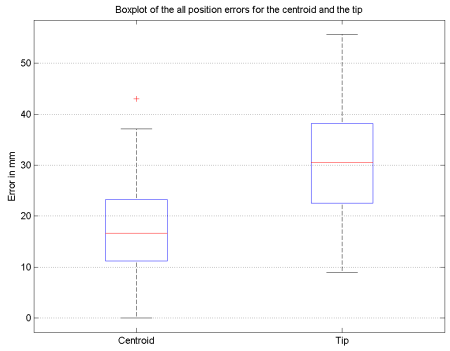

(c) Camera 1 and 4

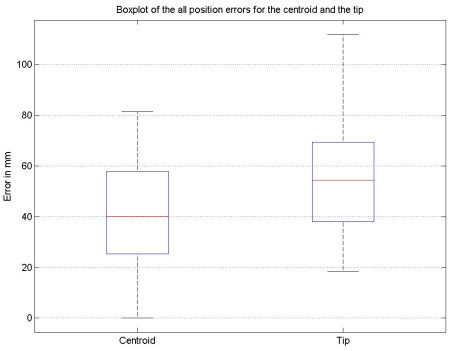

(d) Camera 2 and 3

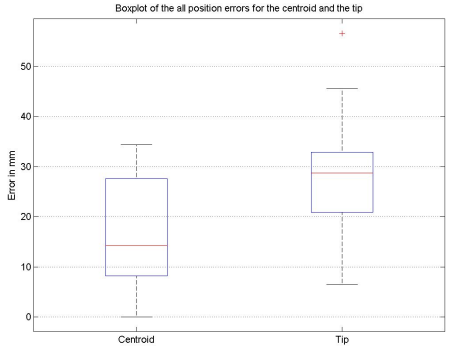

(e) Camera 2 and 4

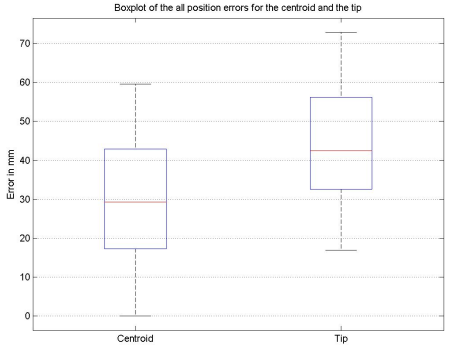

(f) Camera 3 and 4

Figure 2.50: The boxplots of the C_{3d} and T_{3d} for each camera pair

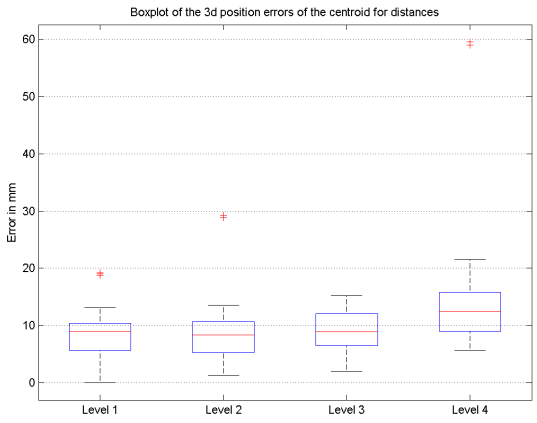

(a) Centroid accuracy

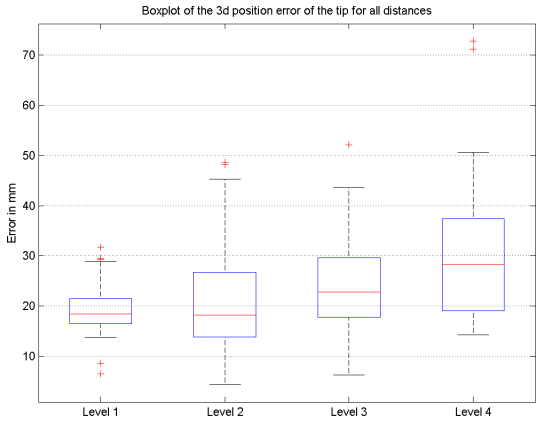

(b) Tip accuracy

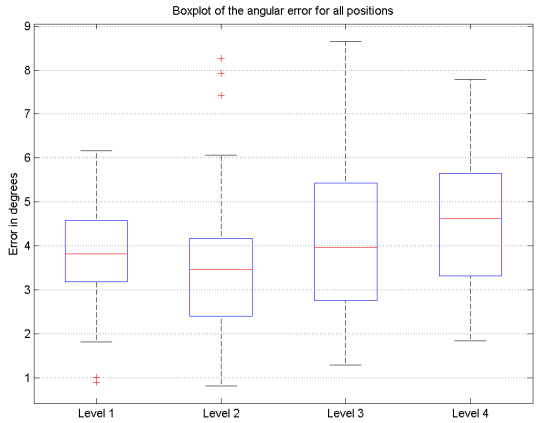

(c) Angular accuracy

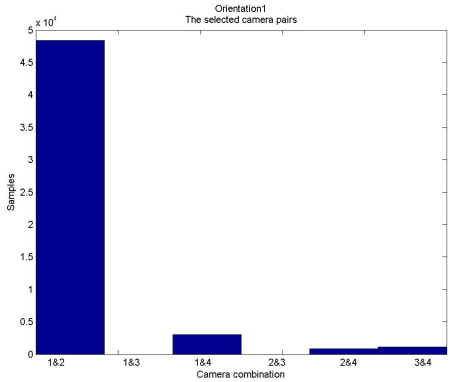

(d) Camera histogram

Figure 2.51: The results with the selection algorithm

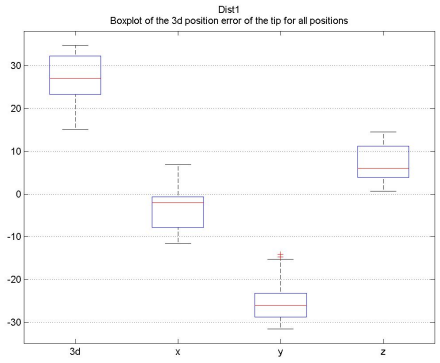

(a) Orientation: 16^o, around x-axis

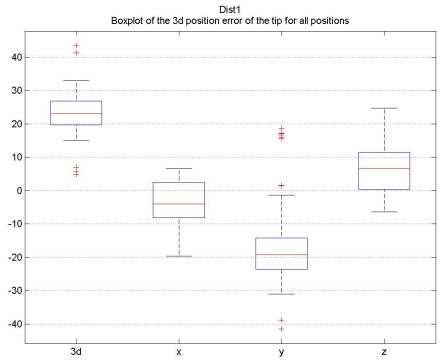

(b) Orientation 16^o, around y-axis

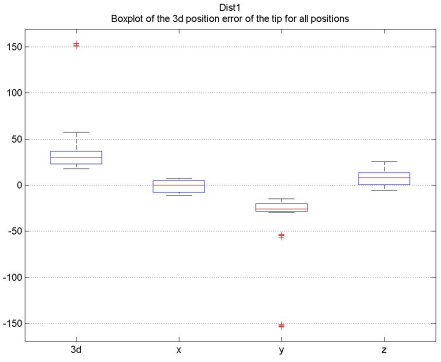

(c) Orientation 33^o, around x-axis

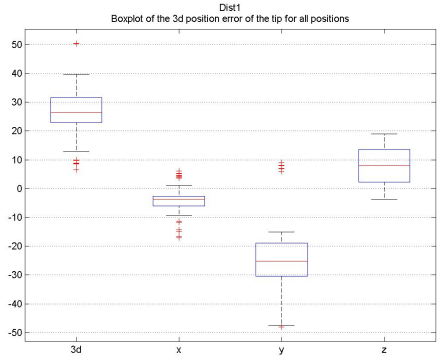

(d) Orientation 33^o, around y-axis

Figure 2.52: The boxplots for the position error (T_{3d}, T_x, T_y and T_z) for the pointer tip.

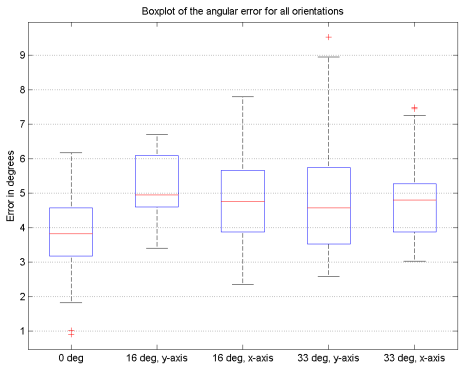

Figure 2.53: Boxplot of the angular error at each orientation.

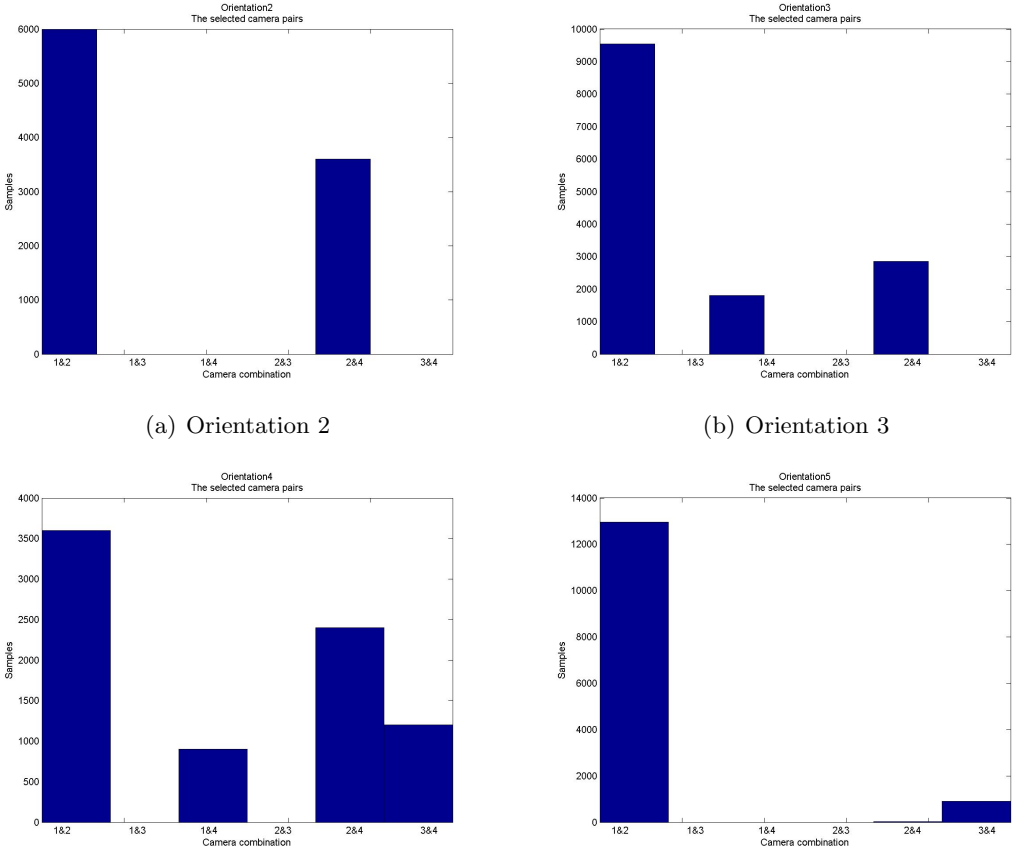

(a) Orientation 2

(b) Orientation 3

(c) Orientation 4

(d) Orientation 5

Figure 2.54: The camera selection histograms for four different orientation of the pointer.

2.6.3 Experiment Set C

In this set, the wound shape reconstruction was investigated. Both of the shapes were (Fig. 2.56 and 2.57) were constructed as an elliptic shape. The larger ring was constructed with a higher number of points and had a more circular shape, whereas the small circle was elliptical. On both figures, the start and end point of the pointer device was recognized with a high number of localized points. All five takes for both shapes was conducted with different pointer speeds. It can be seen in the Fig. 2.56 for "Large circle Take 1" that the dataset with lower speed, in other words with larger number of points provided better reconstruction performance. Less accurate reconstructions tended to form an ellipse instead of a circle, as an expected result for elliptical fit.

Moreover, the position inaccuracy is also observed for the wound construction. The smaller rigs produced a shape close to its actual size but on a different position in space. On the other hand, the reconstruction of the larger circle was both enlarged and dislocated in space.

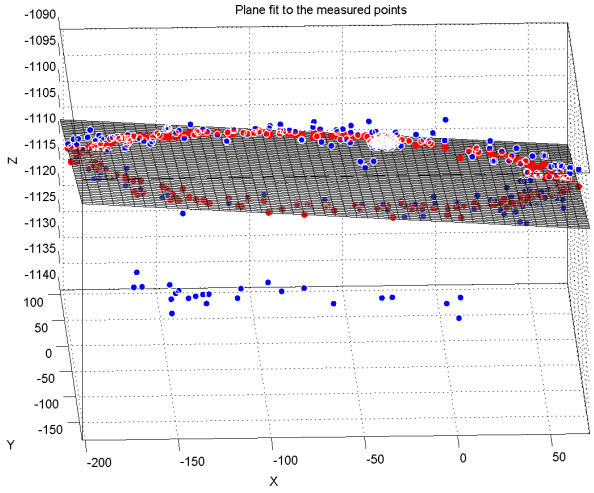

Figure 2.55: An example of the shape data projected on a fitted plane.

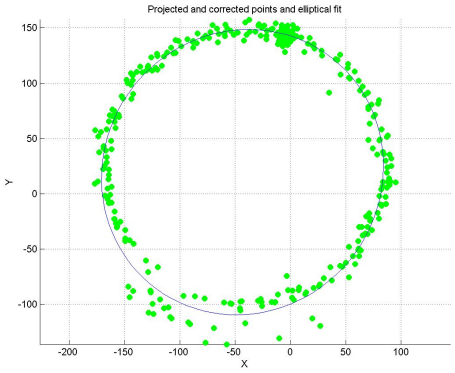

(a) Large circle, Take 1

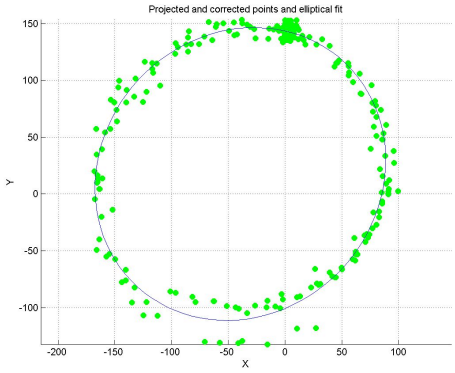

(b) Large circle, Take 2

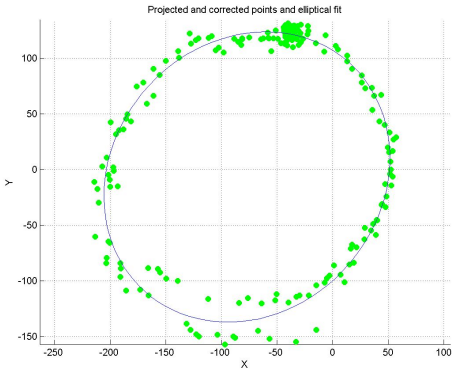

(c) Large circle, Take 3

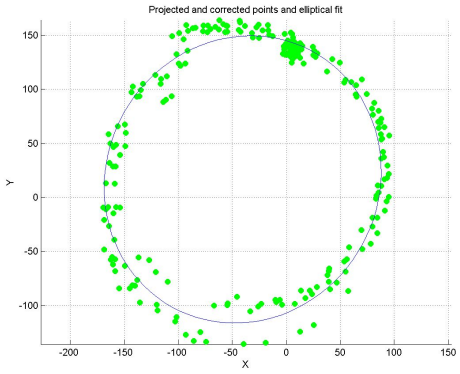

(d) Large circle, Take 4

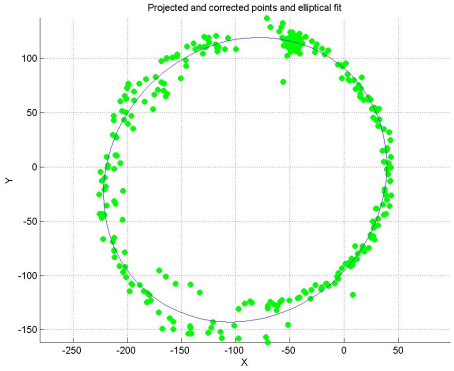

(e) Large circle, Take 5

Figure 2.56: The shape reconstruction with the large circle (220mm diameter)

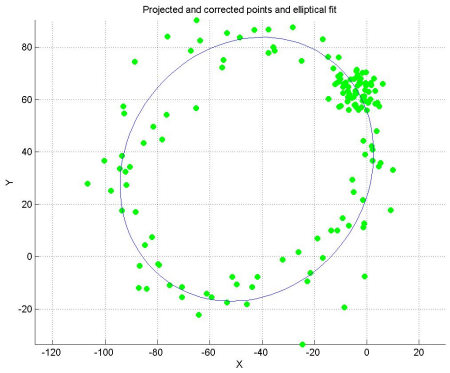

(a) Small circle, Take 1

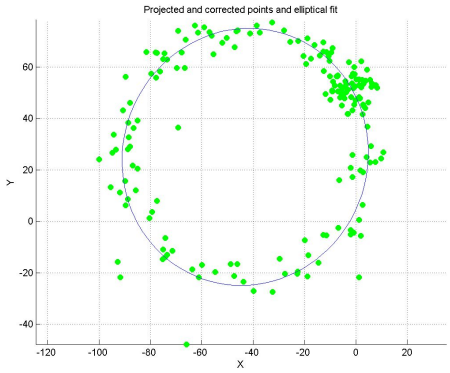

(b) Small circle, Take 2

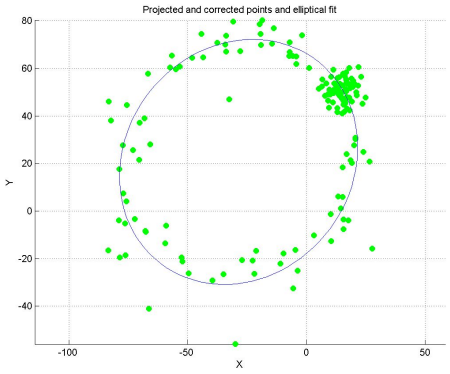

(c) Small circle, Take 3

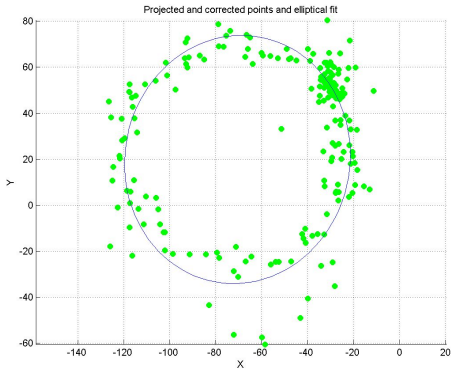

(d) Small circle, Take 4

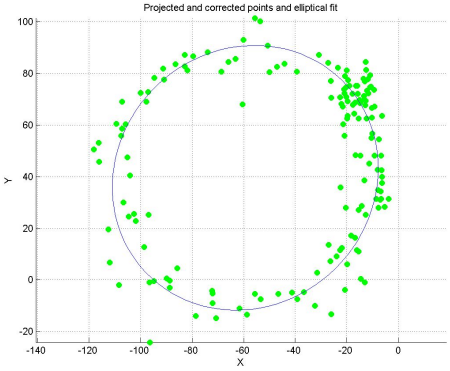

(e) Small circle, Take 5

Figure 2.57: The shape reconstruction with the large circle (220mm diameter)

2.7 Discussion

The results of the Experiment Set A showed that the Wiiremote tracking system gave repeatable and precise results with low standard deviation (between 2 and 3 mm) for errors. The standard deviation of the single position measurements was even lower, less than 1mm in most cases. The error for marker distances $E_{dist_{rms}} = 3.41mm$ was comparable to other studies related to the tracking using Wiimotes [11, 6, 36]. The position error E_{3d} was higher than distance error E_{dist}. On the other hand, it was not possible to compare the position accuracy any other systems, since this value is usually left out and only the RMS error for geometric accuracy is reported.

The uncorrected results were with low accuracy but good precision. Moreover, the error calculations of the distance between the markers was far more successful than the position calculations. Accordingly, it was anticipated that the low position accuracy was due to wrong alignment of the tracking system coordinates to the real world coordinates. The plot of the estimated coordinates relative to the actual coordinates indicated a linear relationship between these two coordinate systems. Thus, linear corrections were created to correct each coordinate relative to the actual coordinates and relative to the z-coordinates. It was also investigated to correct the z coordinate relative to x and y coordinates, but this strategy did not provide satisfactory results. On the other hand, this correction performed poorly for Set B. One strategy to improve this correction step would be to create a correction algorithm which is applied on all coordinates simultaneously instead of sequentially. Another, and more promising, solution is to improve the alignment method during the calibration, such as using a precise grid made of active markers or a calibration object. These strategies were not employed through this project due to their requirements of effort, time and resources, but they are worth to investigate further.

To determine the ideal calibration parameters, several calibration datasets were recorded and run with numerous configuration combinations. It was observed that the calibration dataset plays an important role on the calibration performance, so that the working volume shall be covered throughly while recording the calibration data. Another point is that fast movements were not captured properly and the markers needed to be moved slowly in space. Again, a device with could provide uniform marker movement might be beneficial, but its cost might overcome the benefits.

According to the literature [6], Wiimotes show pinpoint camera behavior with a principal point and focal length close to the therotical values. The results from the calibration were consistent with this information. During the calibration, the tangential distortion parameters was left out since they were found close to zero during prior optimizations. Multiple runs with the same dataset and configuration parameters produced different camera matrices, but their performance were consistent. Another observation was that the configuration parameters effected the time required for the calibration, so that more updates and lower thresholds required longer computation times. With a dataset with high number of outliers, the computational time might take very long and end with the maximum iteration threshold without achieving the minimum error target.

For Set A, the camera combinations including Camera 4 created results with high errors at a distance of 1m to the cameras. When the Camera Pairs 1&4, 2&4 and 3&4 were further investigated, it was seen that this high error was caused by the wrong matching of the corresponding points in two camera views. This failure was related to the principles of the epipolar geometry so that epipolar lines created by the projection of the points in one view did not correspond to the correct points on the other view. This was also a consequence of the calibration parameters. One measure employed to prevent the wrong matching was the global optimization algorithm for point matching, which still failed in a few cases. To eliminate such cases, a correction was applied where the instances with unexpectedly high distance between the markers were eliminated. A similar situation was observed with the camera selection when the markers were missing from the views of one or more cameras. In that case, the camera selection algorithm provided

the available cameras, which might have poor epipolar matching. This resulted in outliers with high errors. To prevent this, a threshold can be defined for point matching cost function.

Besides the inaccuracies occurred due to the calibration process, there were also inaccuracies involved in the triangulation step. The DLT algorithm is suitable for systems with synchronized and correctly aligned cameras, which was our case. The *Optimal algorithm* from Hartley [10] was investigated to correct the inaccuracies, but did not perform as well. Thus, DLT algorithm was employed in further steps due to its simplicity and low computational costs.

The selection algorithm provided satisfactory results by providing low RMS error and standard deviation compared to the single results from camera pairs. On the other hand, some camera pairs seemed to be having better accuracy than the selection, such as Camera Pair 1&2 for Set A.1. When comparing these two outcomes, it shall be kept in mind that selection algorithm also provided results for the cases that the Camera Pair 1&2 failed to gather any data. The effect of the selection algorithm was more obvious for calculation marker distances instead of single marker positions. Especially for the dynamic measurements, the selection algorithm was beneficial for accurate results. In this manner, the line-of-sight or occlusion issues were reduced. For a better performance to prevent occlusions or line-of-sight issues, LED's with higher view angle can be used.

The measurements with the pointer device was with lower accuracy compared to Set A. The Set B included more measurement points and it was expected that the error would increase slightly while employing a dataset rather than the one used for correction, but the increase from 6mm to 20mm and even to 80mm position accuracy was unexpectedly high, whereas the marker distance errors were close to each other. The first reason for this inaccuracy could be a misalignment between the coordinate systems defined for Set A and Set B. This effect was corrected by defining a new origin for each camera pair in Set B. This approach reduced the absolute position error, but still the deviation between the camera pairs was high. Another reason can be inaccuracies during the constructing and measurements with the LED boards. The data resulting from these measurements was used to correct the tracking system, so any existing inaccuracies were also reflected. Similarly, the model construction included errors, such as the pointing rod being not perfectly straight or the difficulties to place the model in a certain position. These aspects can be improved by employing a more accurate elements for the experiment setup.

Another cause of the inaccuracies can be due to camera limitations of the Wiiremotes and the synchronization of the for cameras. The communication between the host computer and four Wiimotes was done via Bluetooth, which works with *information packages*. It was very likely that these packages from each of the Wiiremote arrive to the computer with a slight time delay in between, so that the captured views were not exactly simultaneous. The implementation of a time stamp for this purpose was tried out, but it did not provide meaningful results. Moreover, the Wiiremote's have their own processor for image processing, which expected to include inaccuracies.

On the other hand, it was shown that the pointer device was useful to indicate the lighting direction and the wound shape. The measurements in Set B.2 and B.3 had an low angular error around 6 degrees even including the inaccuracies due to the pointer and holder construction. The wound reconstruction was successful considering the shift due to position inaccuries. During the "free hand" movements to indicate the wound, the orientation of the pointer was constantly changing, which resulted in selection of different camera pairs. According to the results from Set B, the results from these pairs introduces position error to the measurements. Moreover, for such an operation with the pointer device, the time required is an important parameter. A high number of samples provide more accurate results, but they require longer sampling and computational time. Thus, a balance between the required samples per second and the pointing duration shall be investigated and defined.

2.8 Conclusion

The purpose of this study was to investigate the use of a low-cost tracking system to provide the required parameters for surgical lighting control. The relevant parameters were defined as: Wound position, indicated lighting direction, working depth and the wound dimensions and shape. A handheld pointer device was designed for the surgeon to indicate these parameters during surgery. A tracking system was constructed using four Wiimotes considering the operation room environment. The working principles of the designed device was tested using this tracking system. A set of experiments showed that the developed Wiiremote tracking system was promising (($E_{dist_{rms}} = 3.41mm$) and ($E_{dist_{std}} = 2.01mm$)) but it requires further improvements especially in the alignment of the tracking system coordinates to the world coordinates. The data collection with the pointer device was achieved for the tip position, orientation and shape reconstruction with errors larger than expected. For future work, it would be beneficial to implement an actuated lighting system to investigate the user-lighting unit interaction further.

Bibliography

[1] Brechtold . Chromophare e series surgical lighting. Product Brochure, 29.12.2010.

[2] Amkay Products Pvt. Ltd. . Surgical drapes. Website, 13.01.2011. `http://trade.indiamart.com/details.mp?offer=1452565`.

[3] Apothecaries Sundries Mfg. Co. . Operation tables. Website, 13.01.2011. `http://www.operation-tables.com`.

[4] A.R.T. GmbH . Infrared optical tracking systems. Website, 01.08.2011. `http://www.ar-tracking.de`.

[5] Beck W. Operating room illumination: the current state of the art. *Bulletin of the American College of Surgeons*, 66(5):10–5, 1981.

[6] De Amici D, Sanna A, Lamberti F, and Pralio B. A wii remote based infrared-optical tracking system. *Entertainment Computing*, 1(3-4):119 – 124, 2010.

[7] gl.tter . WiiYourself! Native C++ Wiimote Library v1.15 RC3, 2007-2011. `http://wiiyourself.gl.tter.org`.

[8] Gregory M. Surgical lights: Making a purchase decision. *AORN Journal*, 46(5):904–907, 1987.

[9] Hartley R and Sturm P. Triangulation. *Computer Vision and Image Understanding*, 68(2):146 – 157, 1997.

[10] Hartley R and Zisserman A. *Multiple View Geometry in Computer Vision*. Cambridge University Press, ISBN: 0521540518, second edition, 2004.

[11] Hay S, Newman J, and Harle R. Optical tracking using commodity hardware. In *Proceedings of the 7th IEEE/ACM International Symposium on Mixed and Augmented Reality*, ISMAR '08, pages 159–160, Washington, DC, USA, 2008. IEEE Computer Society.

[12] Horgmo O. Medical photographer in university of oslo institute of clinical medicine. Website, 29.12.2010. `http://sterileeye.com/2008/01/07/darkness-on-the-edge-of-wound`.

[13] Illuminating Engineering Society . Lighting for hospitals and health care facilities. Manual, 1995.

[14] Jansen C, Steinicke F, Hinrichs K, Vahrenhold J, and Schwald B. Performance improvement for optical tracking by adapting marker arrangements. In Zachmann G, editor, *VR Workshop on Trends and Issues in Tracking for Virtual Environments*, pages 28–33. IEEE, Shaker-Verlag, 2007.

[15] Jesurun D. Led technology provides enlightening solution for surgical areas. *Emlen Publications, Inc.*, 6(1), 2008.

[16] Jireh Design . Eye anatomy. Website, 24.03.2010. http://www.maculacenter.com/EyeAnatomy.htm.

[17] Jolly Medical . Electrosurgical pencil. Website, 05.08.2011. http://jolly-medical.com/doc/4/Eletrosurgical_pencil.htm.

[18] Joystiq . Kinect: The company behind the tech explains how it works. Website, 15.07.2010. http://www.joystiq.com/2010/06/19/kinect-how-it-works-from-the-company-behind-the-tech.

[19] Knulst A. Prestatiemetingen aan led-operatielampen. Delft University of Technologyi Department of Biomechanical Engineering Internal report, 2008.

[20] Knulst A, Mooijweer R, Jansen F, Stassen L, and Dankelman J. Indicating shortcomings in surgical lighting systems. *Minimally Invasive Therapy & Allied Technologies*, 0(0):1–9, 0.

[21] Manintveld B and Hogerwerf E. Nintendo wiimote 3d tracking using reflective optical markers. TU Delft Haptics Lab, Biomedical Engineering Minor final assignment, 2010.

[22] Maquet . Prismalix surgical light. Product Brochure, 29.12.2010.

[23] Martinec D and Pajdla T. Structure from many perspective images with occlusions. In *Proceedings of the 7th European Conference on Computer Vision-Part II*, ECCV '02, pages 355–369, London, UK, UK, 2002. Springer-Verlag.

[24] Matern U and Koneczny S. Safety, hazards and ergonomics in the operating room. *Surgical Endoscopy*, 21:1965–1969, 2007.

[25] medGadget . marLED surgical lights from kls martin. Website, 29.12.2010. http://medgadget.com/archives/2010/03/marled_surgical_lights_from_kls_martin.html.

[26] Nintendo . Wii remote controller. Website, 01.08.2011. http://www.nintendo.com/.

[27] Northern Digital Inc . Polaris. Website, 08.01.2011. http://www.ndigital.com/.

[28] Overstockme.com . Figure: Lighting unit. Website, 15.12.2010. http://www.overstockme.com/Merchant2/nuov-surgical-major-surgical-lights-click-image-details-brochure-pi-190.html.

[29] Pintaric T and Kaufmann H. A rigid-body target design methodology for optical pose-tracking systems. In *Proceedings of the 2008 ACM symposium on Virtual reality software and technology*, VRST '08, pages 73–76, New York, NY, USA, 2008. ACM.

[30] PrimeSense Ltd. . Natural interaction. Website, 21.07.2010. http://www.primesense.com.

[31] Scott C, Sanderson J, and Guthrie T. Choice of ventilation system for operating-theatres. comparison of turbulent versus laminar-linear flow systems in operating-rooms and industrial clean rooms. *Lancet*, 1(7712):1288–91, 1971.

[32] Shree Hospital Equipments . Operation tables. Website, 13.01.2011. http://www.shriequipment.com/ot-tables.php.

[33] Stefan D. F, Kirsch S. R, and Wiles A. D. Specifying 3d tracking system accuracy one manufacturer's views, 2004.

[34] Sturm P and Triggs B. A factorization based algorithm for multi-image projective structure and motion. In Buxton B and Cipolla R, editors, *Computer Vision ECCV '96*, volume 1065 of *Lecture Notes in Computer Science*, pages 709–720. Springer Berlin / Heidelberg, 1996.

[35] Svoboda T, Martinec D, and Pajdla T. A convenient multi-camera self-calibration for virtual environments. *Teleoperators and Virtual Environments*, 14(4):407–422, August 2005.

[36] Vader M, Chadda A, Zhu W, Leu M, Liu X, and Vance J. An integrated calibration technique for multi-camera vision systems. *ASME Conference Proceedings*, 2010(49088):267–274, 2010.

[37] Vishay Semiconductors . Tsal6400. Website, 04.08.2011. `http://www.vishay.com/`.

[38] Zhang Z. A flexible new technique for camera calibration. *IEEE Transactions on Pattern Analysis and Machine Intelligence*, 22:1330–1334, 2000.

Appendices

Appendix A

Technical drawings for the experiment setup

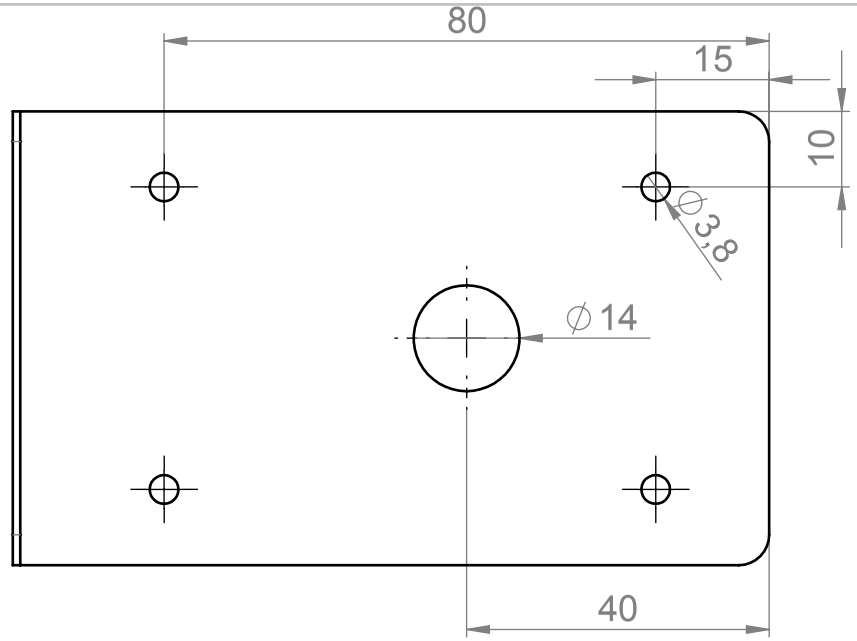

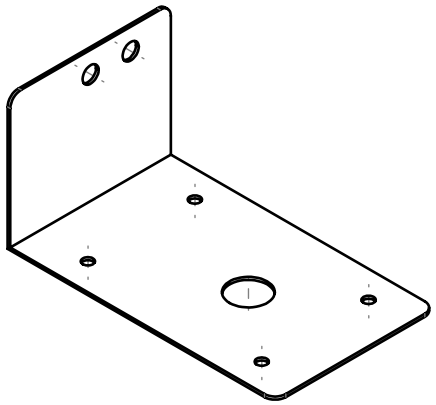

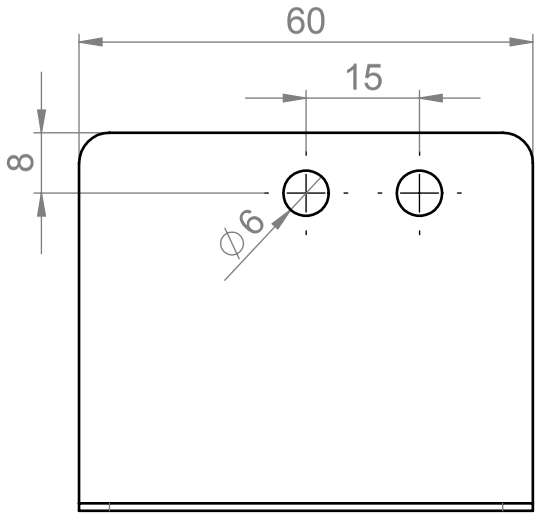

TU Delft Industrial Design Engineering	benaming **Wiiconnect**	datum 05.04.2011	maateenheid mm
	schaal 1:1	groep <<groep>>	formaat A4
	getekend Eda Emirdag		tekeningnummer 1

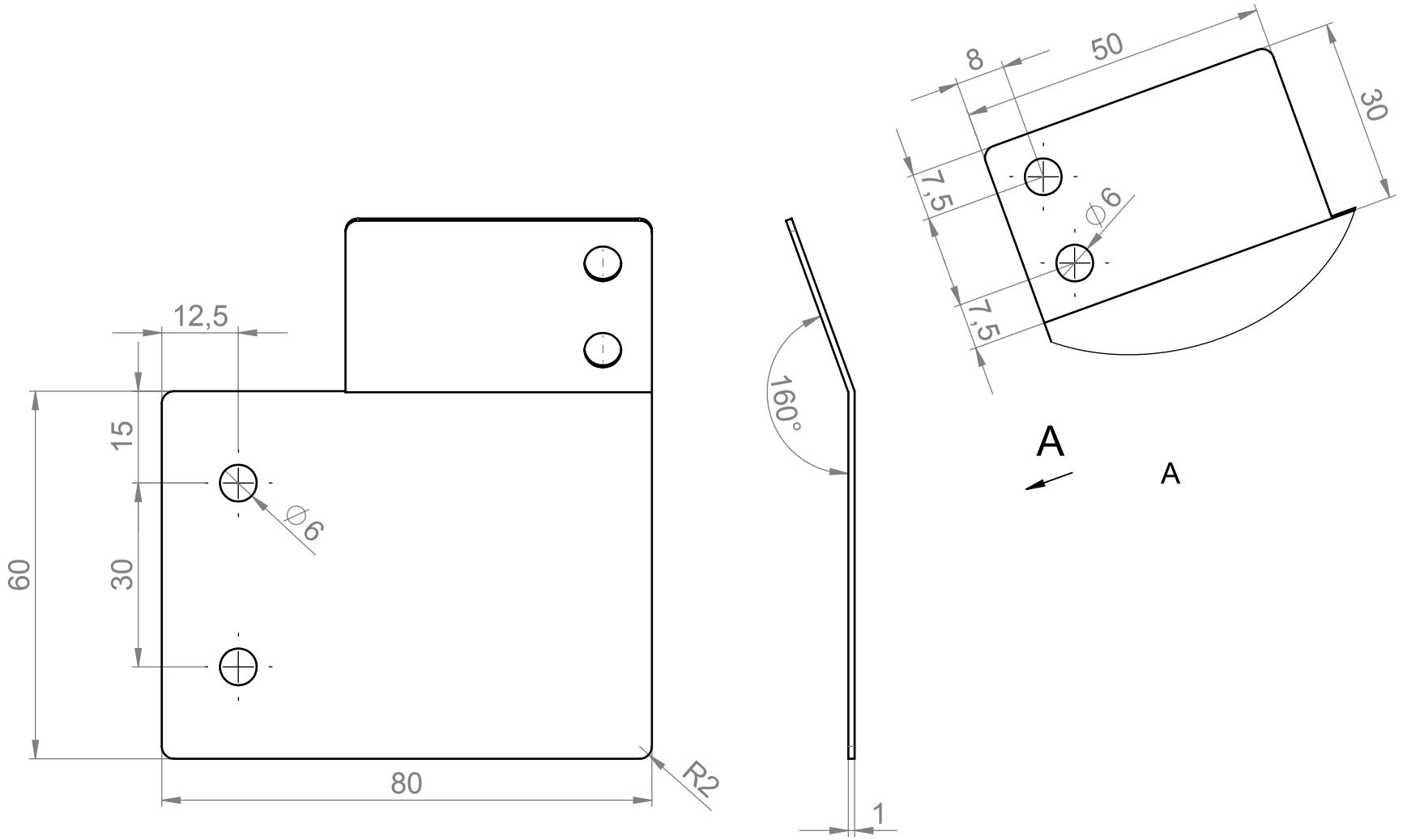

TU Delft Industrial Design Engineering	benaming **Wiiara**		datum 05.04.2011	maateenheid mm
		schaal 1:1	groep <<groep>>	formaat **A4**
		getekend Eda Emirdag		tekeningnummer 1

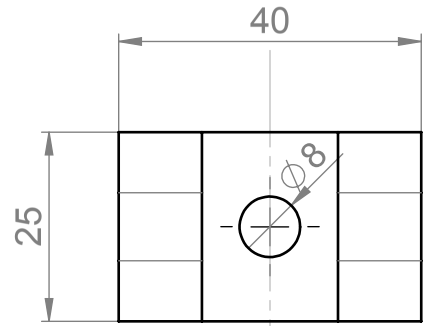

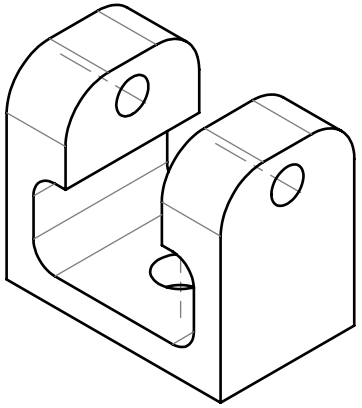

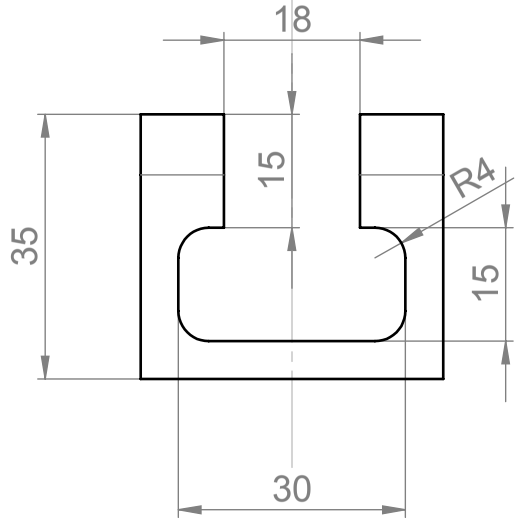

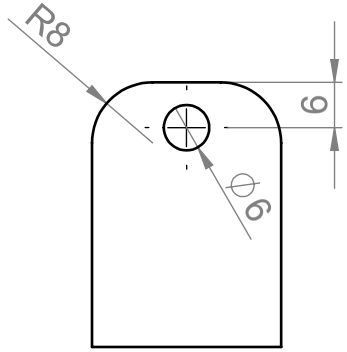

TU Delft Industrial Design Engineering	benaming **Bag2**		datum 03.04.2011	maateenheid <<mm>>
		schaal 1:1	groep <<groep>>	formaat **A4**
		getekend Eda Emirdag		tekeningnummer 2

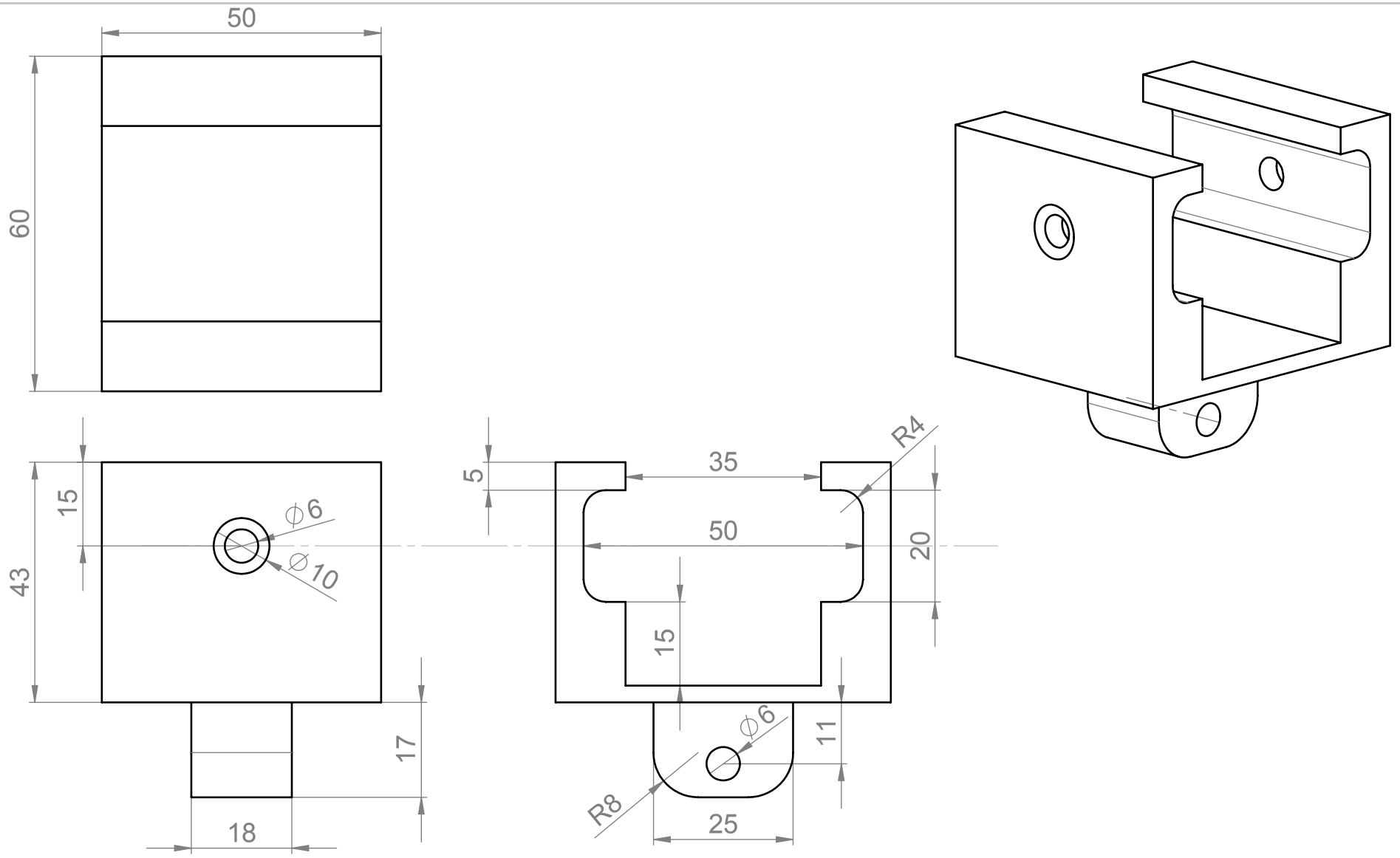

TU Delft Industrial Design Engineering	benaming **Bag1**	datum 03.04.2011	maateenheid mm
		schaal 1:1 / groep <<groep>> / formaat **A4**	tekeningnummer 2
		getekend Eda Emirdag	

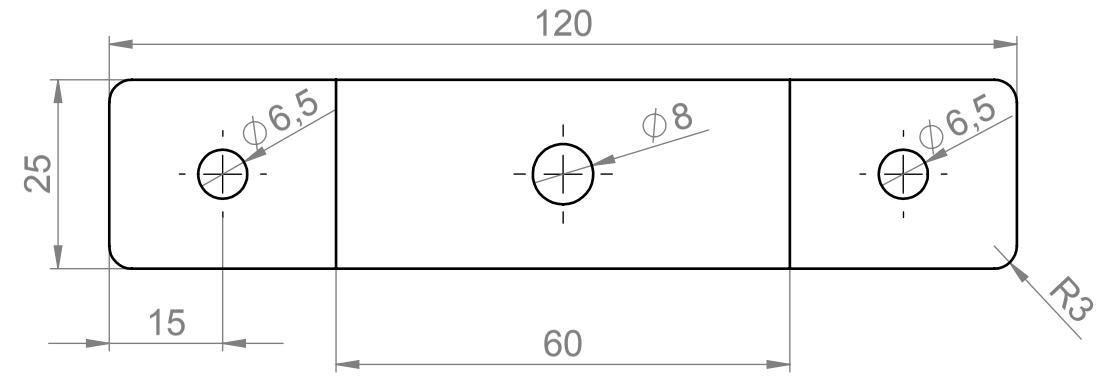

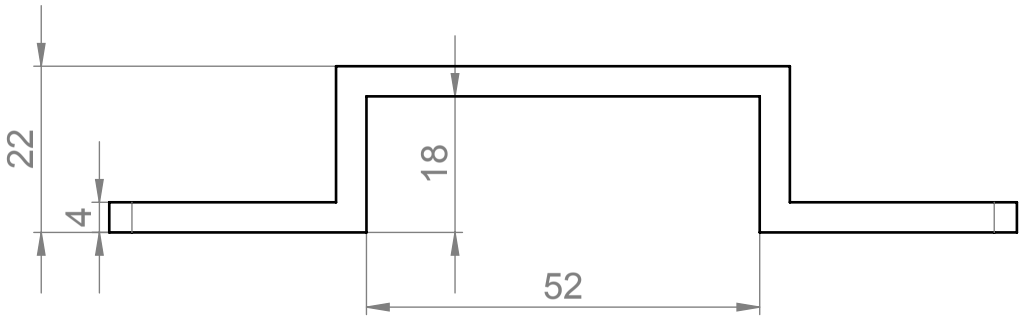

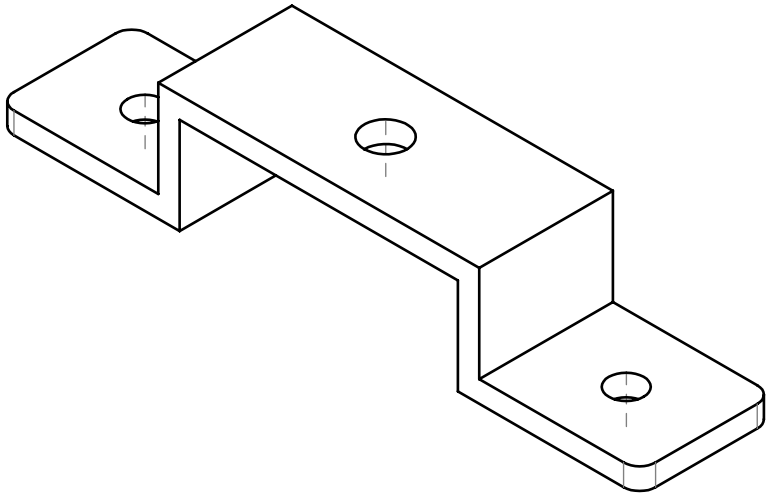

TU Delft Industrial Design Engineering	benaming **Bag3**	datum 03.04.2011	maateenheid mm
		schaal 1:1 / groep <<groep>> / formaat **A4**	tekeningnummer 2
		getekend Eda Emirdag	

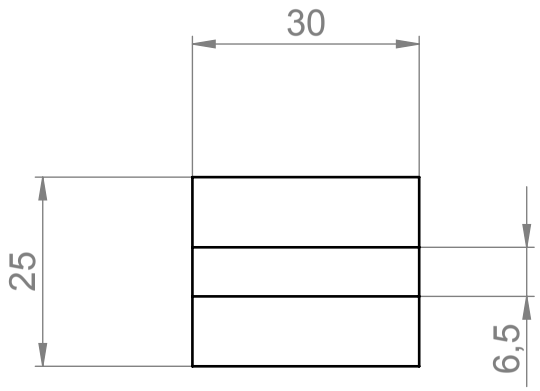

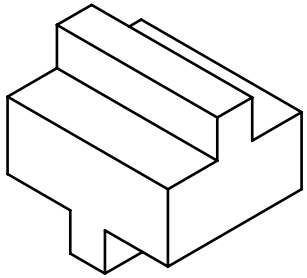

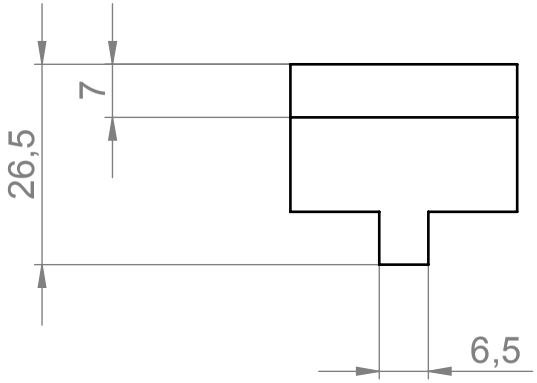

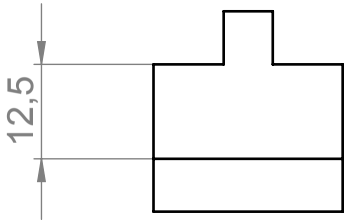

TU Delft Industrial Design Engineering	benaming **Alum_bag**		datum 28.03.2011	maateenheid mm
		schaal 1:1	groep Env	formaat **A4**
		getekend Eda Emirdag		tekeningnummer 1

Appendix B

Tracking area calculations

The basic geometry of the tracking area was given below in Figure B.1. The aim was to achieve the maximum hatched area with a sufficient portion above 1m line. The optimal mounting angle x was found by calculating the maximum hatched area A.

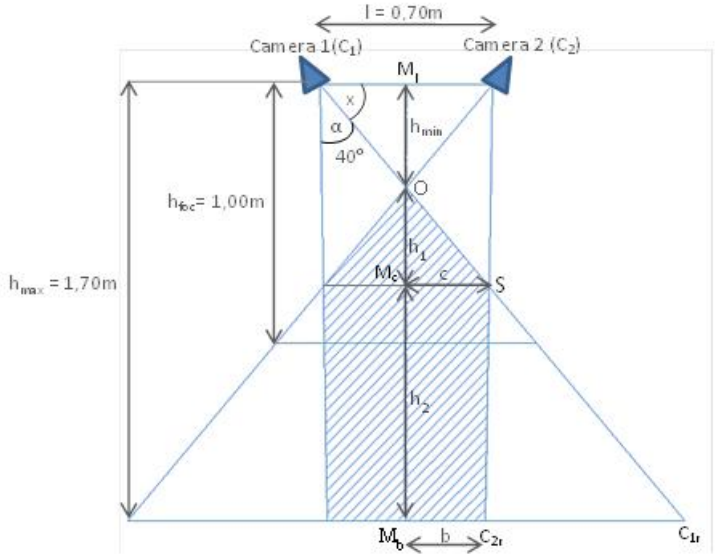

Figure B.1: Camera positioning and orientation

The hatched area consisted of a triangle and a trapezoid and was formulated as following using the dimensions mentioned in the Figure B.1:

$$A = 2 \cdot \left(\frac{c \cdot h_1}{2} + \frac{b + c}{2} \cdot h_2 \right) \tag{B.0.1}$$

where b was the distance to the midline from the cross-section of the base and the right border of the Camera 2 view field (Point C_{2r}), c was the distance to the midline from the cross-section of the right borders of the Camera 1 and Camera 2 view fields (Point S), h_1 was the distance from the start of the tracking area (Point O) to Line c and the h_2 was the distance from Line c to Line b. Line c formed the base of the triangle and h_1 was the height of the triangle. The height of the trapezoid was given as h_2 and the two parallel edges are c and b. The values for c, b, h_1 and h_2 was calculated using the theory of similar triangles. It was assumed that the midline M and the borders of the view field of one camera (e.g. Camera 2) coincided in two points: Point O and Point P, which was not shown in Figure B.1. For this geometry, the

following relationships were valid:

$$\triangle M_l C_2 P \sim \triangle M_c S P \sim \triangle M_b C_{2r} P \quad \text{and} \quad \triangle M_l C_2 O \sim \triangle M_c S O \tag{B.0.2}$$

The unknown parameters in Equation B.0.1 were calculated triangular similarities and trigonometric relations. These relations are expressed as below in terms of the mounting angle x:

$$\tan\alpha + x = \frac{M_l P}{l/2} \quad \Rightarrow \quad M_l P = \frac{\tan\alpha + x \cdot l}{2} \tag{B.0.3}$$

$$\frac{l/2}{b} = \frac{M_l P}{M_l P - h_{max}} \quad \Rightarrow \quad b = \frac{l/2 \cdot (M_l P - h_{max})}{2} \tag{B.0.4}$$

$$\tan x = \frac{h_{min}}{l/2} \quad \Rightarrow \quad h_{min} = \frac{\tan x \cdot l}{2} \tag{B.0.5}$$

$$\frac{h_{min}}{h_1} = \frac{l/2}{c} \quad \Rightarrow \quad c = \frac{l/2 \cdot h_1}{h_m in} \tag{B.0.6}$$

$$\frac{(M_l P - h_{max}) + h_2}{M_l P - h_{max}} = \frac{c}{b} \quad \Rightarrow \quad h_2 = \frac{(M_l P - h_{max}) \cdot (c - b)}{b} \tag{B.0.7}$$

$$h_1 \quad = \quad h_{max} - h_{min} - h_2 \tag{B.0.8}$$

When the the known parameters was set this equation, the area could be optimized by changing the mounting angle.

Appendix C

Camera calibration results

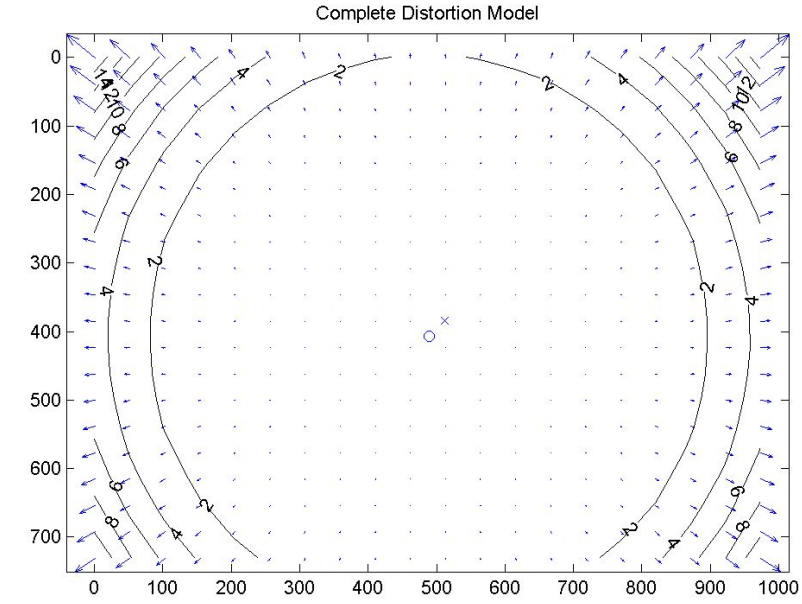

Pixel error	= [0.7343, 0.6703]	
Focal Length	= (1401.38, 1402.14)	+/- [4.505, 4.194]
Principal Point	= (488.649, 406.373)	+/- [7.487, 6.899]
Skew	= 0	+/- 0
Radial coefficients	= (0, 0.6599, 0)	+/- [0, 0.2979, 0]
Tangential coefficients	= (0, 0)	+/- [0, 0]

Figure C.1: Camera 1

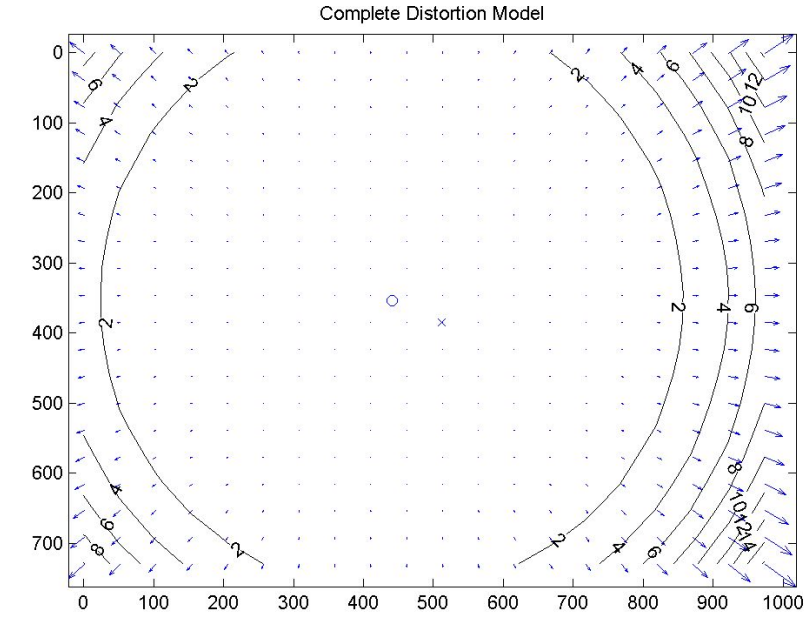

Pixel error	= [0.7804, 0.7525]	
Focal Length	= (1381.56, 1383.3)	+/- [4.966, 4.614]
Principal Point	= (440.169, 352.591)	+/- [9.091, 7.483]
Skew	= 0	+/- 0
Radial coefficients	= (0, 0.5627, 0)	+/- [0, 0.2854, 0]
Tangential coefficients	= (0, 0)	+/- [0, 0]

Figure C.2: Camera 2

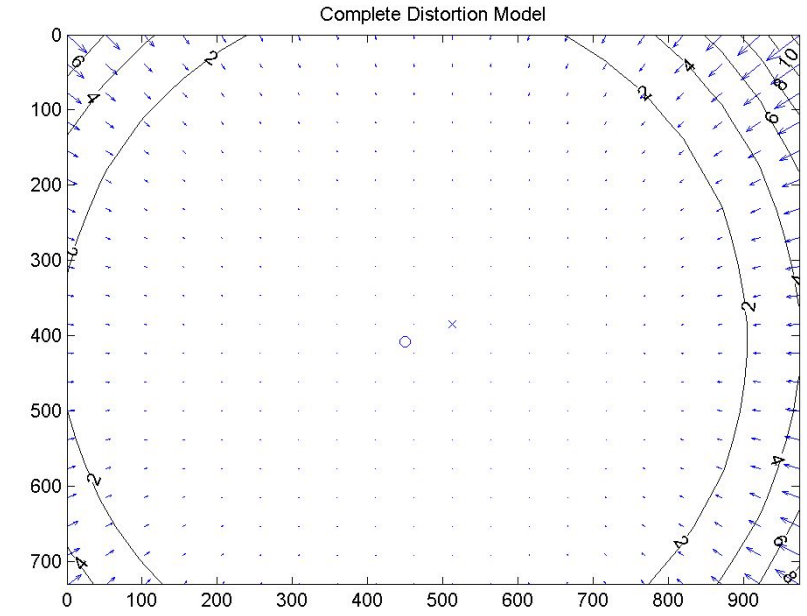

Pixel error	= [0.6689, 0.8595]	
Focal Length	= (1380.96, 1381.85)	+/- [4.212, 3.921]
Principal Point	= (449.241, 406.624)	+/- [8.313, 8.795]
Skew	= 0	+/- 0
Radial coefficients	= (0, -0.3615, 0)	+/- [0, 0.3624, 0]
Tangential coefficients	= (0, 0)	+/- [0, 0]

Figure C.3: Camera 3

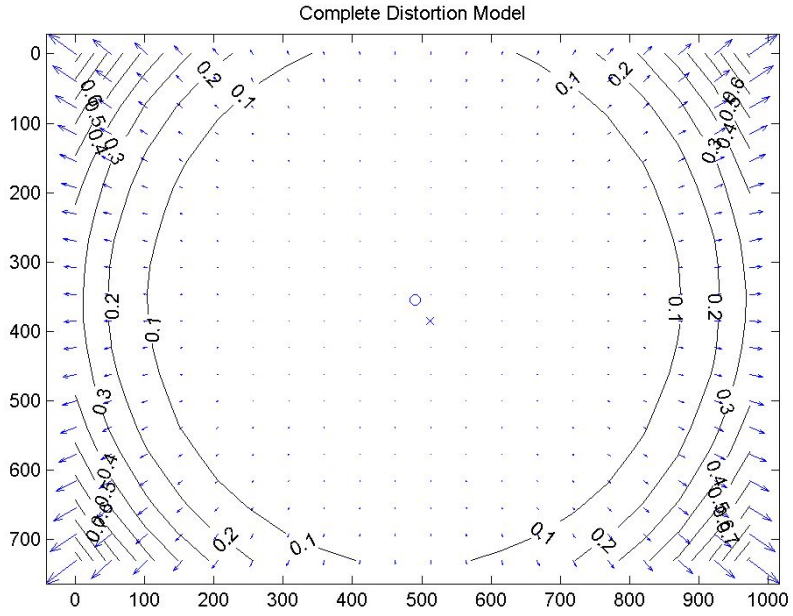

Pixel error	= [0.7332, 0.8998]	
Focal Length	= (1395.37, 1394.4)	+/- [5.811, 5.44]
Principal Point	= (488.848, 354.222)	+/- [9.865, 10.12]
Skew	= 0	+/- 0
Radial coefficients	= (0, 0.04471, 0)	+/- [0, 0.2361, 0]
Tangential coefficients	= (0, 0)	+/- [0, 0]

Figure C.4: Camera 4

Appendix D

Correction parameters

Table D.1: The linear coefficients for correcting the x-coordinates relative to the actual x-coordinates.)

	Linear Coefficients $x_c = ax + b$	
Camera Pair	a	b
1 and 2	1.06911033007770	-0.676541031202954
1 and 3	1.07809067425456	-1.63376829603824
1 and 4	1.06275209829665	-2.20078507189001
2 and 3	1.08072808811265	-1.08915016197089
2 and 4	1.07398811536549	-0.966317102771732
3 and 4	1.07398811536549	-0.966317102771732

Table D.2: The linear coefficients for correcting the y-coordinates relative to the actual y-coordinates.)

	Linear Coefficients $y_c = ay + b$	
Camera Pair	a	b
1 and 2	1.03266813033205	42.1746041777707
1 and 3	1.02214177546407	43.1651718733777
1 and 4	1.02020193738985	43.4261913882466
2 and 3	1.02500589348927	42.4434089788496
2 and 4	1.03389309025149	42.5427433653500
3 and 4	1.01768762536339	43.8135804253921

Table D.3: The linear coefficients for correcting the z-coordinates relative to the actual z-coordinates.)

	Linear Coefficients $z_c = az + b$	
Camera Pair	a	b
1 and 2	1.04295981938698	103.458930552713
1 and 3	1.04036894134377	103.167735407350
1 and 4	1.03020520438846	92.9383727208753
2 and 3	1.04689929425193	109.320720539420
2 and 4	1.04331281235387	103.585570663918
3 and 4	1.03932372936678	103.453945447052

Table D.4: The linear coefficients for correcting the x-coordinates relative to the actual z-coordinates.)

	Linear Coefficients $x_{c2} = x_c + az + b$	
Camera Pair	a	b
1 and 2	-0.00789993843050433	-9.40573539046216
1 and 3	-0.00668814639495503	-8.17575229007355
1 and 4	-0.00957971902016974	-11.6872572046084
2 and 3	0.00675938301394026	-8.26283366007031
2 and 4	-0.00831140092761169	-10.3134438763334
3 and 4	-0.00625580505454361	-7.95645724344285

Table D.5: The linear coefficients for correcting the y-coordinates relative to the actual z-coordinates.)

	Linear Coefficients $y_{c2} = y_c + az + b$	
Camera Pair	a	b
1 and 2	0.0369733140287375	44.0207491896945
1 and 3	0.0374714109170032	45.8059611027844
1 and 4	0.0367973461062779	44.8927622496486
2 and 3	0.0374562057714901	45.7873739643018
2 and 4	0.0374562057714901	45.7873739643018
3 and 4	0.0374562057714901	45.7873739643018